

Improving the Estimation of Site-Specific Effects and their Distribution in Multisite Trials

JoonHo Lee^{*1}, Jonathan Che², Sophia Rabe-Hesketh³, Avi Feller³, and Luke Miratrix²

¹The University of Alabama

²Harvard University

³University of California, Berkeley

August 15, 2023

Abstract

In multisite trials, statistical goals often include obtaining individual site-specific treatment effects, determining their rankings, and examining their distribution across multiple sites. A standard Bayesian approach employs Gaussian distributional assumptions and uses posterior means (PM) to estimate these site-level effects. In this paper, we explore two strategies for improving inferences related to site-specific effects: (a) semiparametric modeling of the prior distribution using Dirichlet process mixture (DPM) models to relax the normality assumption, and (b) using estimators other than the PM estimator, such as the constrained Bayes (CB) or triple-goal (GR) estimators, to summarize the posterior. To do so, we conduct a large-scale simulation study, calibrated to multisite trials common in education research. We then explore the conditions and degrees to which these strategies and their combinations succeed or falter in the limited data environments typically encountered in multisite

*jlee296@ua.edu

trials. We found that the average reliability of observed within-site effect estimates is crucial for determining the most effective estimation strategies, as it governs overall data informativeness and drives performance for all inferential goals. In settings with low-to-moderate data informativeness, flexible DPM models perform no better than the simple parametric Gaussian model coupled with a posterior summary method tailored to a specific inferential goal. DPM models outperform Gaussian models only in select high-information settings, indicating considerable sensitivity to the level of cross-site information available in the data. We apply these insights to estimate the cross-site distribution of treatment effects in an evaluation of Conditional Cash Transfers in Colombia. We discuss the implications of our findings for balancing trade-offs associated with shrinkage for the design and analysis of future multisite randomized experiments.

Keywords: multisite trials; site-specific effects; finite-population estimand; Dirichlet process mixture; constrained Bayes; triple-goal estimator

1 Introduction

Multisite trials, which conduct (nearly) identical randomized experiments simultaneously at multiple sites, have become increasingly prevalent as an experimental design in education (Spybrook and Raudenbush, 2009; Spybrook, 2014; Raudenbush and Bloom, 2015). Multisite trials can be viewed as a form of planned meta-analysis (Bloom et al., 2017). By synthesizing evidence from multiple contexts to estimate the average treatment effect, multisite trials can establish a more robust foundation for general policy recommendations (Meager, 2019). Understanding the extent of treatment effect variation also allows researchers to determine how an intervention may perform in diverse contexts (Weiss et al., 2017). Recently, the analysis of multisite trial data has put greater emphasis not only on estimating the overall average treatment effect but also on the variance parameters of the cross-site population distribution of program effects (e.g., Padilla, 2020; Sabol et al., 2022; Schochet and Padilla, 2022).

Expanding on such meta-analytic objectives of multisite trials, researchers occasionally direct their attention to the sites in the sample itself. This approach pursues several inferential goals, including (a) estimating site-specific treatment effects, (b) ranking the sites, and (c) analyzing the distribution of site-specific effects. Institutional performance evaluation studies have pioneered the examination of such fine-grained, site-specific parameters. For instance, school or teacher effectiveness studies directly aim to estimate individual school- or teacher-specific effect parameters (Angrist et al., 2017; Chetty et al., 2014a,b; Harris and Sass, 2014; Mountjoy and Hickman, 2021). There has also been a sustained interest in generating rankings or league tables based on estimated effectiveness for schools or other service providers (Goldstein and Spiegelhalter, 1996; Lockwood et al., 2002; Mogstad et al., 2020; Normand et al., 2016). Performance evaluation objectives also include estimating empirical distribution functions (EDFs) (Kline et al., 2022) or histograms

of site-specific parameters (Marshall and Spiegelhalter, 1998), identifying outliers or hot spots (Ohlssen et al., 2007; Marshall and Spiegelhalter, 2007), and determining the proportion of sites with effects surpassing a threshold (Conlon and Louis, 1999; Gu and Koenker, 2023). These practices can be effectively adapted to contexts that investigate site-specific treatment effects in multisite trial settings.

In this paper, we conduct a comprehensive simulation study to examine how applying different analytic strategies can improve the estimation of site-specific effects and their empirical distribution under a range of conditions. As we cannot directly observe the true individual site-specific effects, we must model them using observed data. Standard modeling approaches depend on parametric distributional assumptions in random-effect multilevel models. Generally, random effects are assumed to follow a normal distribution, and empirical Bayes (EB) estimates are used for the random effects themselves (e.g., Raudenbush and Bloom, 2015). EB estimates are conditional posterior means, with estimates plugged in for model parameters. When adopting a fully Bayesian approach, empirical Bayes is replaced by the marginal posterior means (PM) of the random effects, which are derived from the joint posterior distribution of the random effects and model parameters.

Assuming a normal distribution for random effects can be problematic when the true distribution is far from normal. For instance, McCulloch and Neuhaus (2011) discovered that when the true distribution is multi-modal or long-tailed, the shape of the empirical Bayes (EB) predictions may reflect the assumed Gaussian distribution rather than the true distribution of effects. To address this issue, researchers have proposed more flexible distributional assumptions for random effects. These alternatives encompass continuous parametric non-Gaussian distributions, such as Student’s t (Pinheiro et al., 2001) and skewed parametric families (Liu and Dey, 2008); arbitrary discrete distributions obtained using nonparametric maximum likelihood estimation (NPMLE, Rabe-Hesketh et al., 2003) or smoothing by roughening (Shen and Louis, 1999); and mixture distributions, including

finite mixtures of Gaussians (Verbeke and Lesaffre, 1996), penalized Gaussian mixtures (Ghidey et al., 2004), or Dirichlet process mixtures (Antonelli et al., 2016; Paddock et al., 2006). These studies advocate for employing flexible distributional assumptions to safeguard against model misspecification while maintaining efficiency.

Instead of relaxing the normality assumption, some approaches replace EB or PM estimators with alternative posterior summaries, such as constrained Bayes (CB, Louis, 1984) and triple-goal (GR, Shen and Louis, 1998) estimators, which are designed to correct shrinkage-induced underdispersion in PM estimates. These alternative methods modify the loss function minimized by the estimator to target specific inferential goals. For example, the triple-goal estimator aims to optimize the estimation of the empirical distribution and ranks of site-specific parameters, with a minor trade-off in the optimality of site-specific parameter estimates (Shen and Louis, 1998). These strategies have received less attention compared to flexible modeling of the random-effects distribution.

In practice, the joint application of these two strategies has been relatively rare, with only a few notable exceptions (e.g., Paddock et al., 2006; Lockwood et al., 2018). The costs and benefits of these strategies have not been systematically compared under varying conditions in previous simulation studies exploring similar topics (e.g., Kontopantelis and Reeves, 2012; Paddock et al., 2006; Rubio-Aparicio et al., 2018). For instance, if the true distribution is not Gaussian and the inferential goal is to estimate the empirical distribution of site-specific effects, a question arises about which approach performs better: (a) combining the misspecified Gaussian model for random effects with a targeted posterior summary method (CB or GR), or (b) utilizing the flexible semiparametric model in conjunction with the misselected posterior mean estimator that solely aims at the optimal estimation of individual site-specific effects. To our knowledge, no prior studies have compared these two strategies within the context of multisite trials, thereby revealing an unexplored area in the literature that warrants further investigation.

This paper offers four important contributions. First, our simulations focus on educational applications, often characterized by small sample sizes. Beyond the standard relative comparisons between methods, we offer practical guidelines for practitioners in these low-data settings, acknowledging that even the best method may deliver suboptimal results. Second, we bring attention to the frequently overlooked distinction between super population and finite-population estimands, which serves to frame and motivate different estimators. Third, rather than solely focusing on one strategy, we examine the effects of combining flexible random-effects distributions with alternative posterior summaries. Finally, we apply insights gleaned from our simulation to real-world multisite trial data, thereby emphasizing how the selection of analytic strategies can considerably influence site-specific estimates.

This paper is structured as follows. First, we introduce standard approaches for modeling super population and finite-population effects. Next, we discuss inferential goals, potential threats to inferences for site-specific effects, and outline two strategies to improve these inferences. We then provide a comprehensive description of our simulation study's design and results, followed by a real-data example that demonstrates the application of these strategies. Finally, we summarize our findings, consider their practical implications, and propose future research directions in this area.

2 Standard approaches to modeling site-specific effects

2.1 Basic setup: the Rubin (1981) model

Multisite trials generate multilevel or clustered data because individuals are randomly assigned to a treatment or control group within each site. While numerous generalized

linear mixed models are available to analyze such multilevel data, this paper focuses on the [Rubin \(1981\)](#) model for parallel randomized experiments, also known as a random-effects (or empirical Bayes) meta-analysis ([DerSimonian and Laird, 1986](#); [Raudenbush and Bryk, 1985](#)). Suppose a multisite trial comprises J sites indexed by $j = 1, \dots, J$, where identical treatments are administered. Since site-specific true effects, τ_j , are unobservable, researchers can only access the observed or estimated effects $\hat{\tau}_j$ from each of the J sites, along with their corresponding squared standard errors $\hat{s}e_j^2$. The $\hat{\tau}_j$ and $\hat{s}e_j^2$ values are obtained through maximum likelihood (ML) estimation using data exclusively from site j . The first stage of the hierarchical model describes the relationship between the observed statistics $\hat{\tau}_j$ and the latent parameter τ_j :

$$\hat{\tau}_j \mid \tau_j, \hat{s}e_j^2 \sim N(\tau_j, \hat{s}e_j^2) \quad j = 1, \dots, J. \quad (1)$$

The second stage assumes that τ_j are independent and identically distributed (*i.i.d.*) with a specific prior distribution G ,

$$\tau_j \mid \tau, \sigma^2 \sim G \equiv N(\tau, \sigma^2) \quad j = 1, \dots, J. \quad (2)$$

The prior distribution G is generally unknown, but is classically specified G as a Gaussian distribution with two hyperparameters: τ , the average treatment effect across the sites, and σ^2 , the variance in true site-specific effects τ_j across sites, both defined at the super population level.

Critically, the observed variation in estimated site-specific effects, $\text{var}(\hat{\tau}_j)$, arises from two sources: (1) genuine heterogeneity in true effects τ_j between sites (σ^2), and (2) the sampling variation of each $\hat{\tau}_j$ around its τ_j within sites ($\hat{s}e_j^2$). When site sample sizes are small, the ML estimates of site-specific effects $\hat{\tau}_j$ may exhibit large sampling error variances $\hat{s}e_j^2$. As a result, the $\hat{\tau}_j$ values could be overdispersed compared to true τ_j values. Further-

more, the rank order of effects for different sites might be misrepresented, as sites with smaller samples might also have the most extreme estimates due to large \widehat{se}_j^2 (Raudenbush and Bloom, 2015). The Bayesian hierarchical framework plays a vital role in removing the influence of sampling error within sites, allowing estimation of the true heterogeneity in treatment effects across sites (Meager, 2019).

2.2 Site-specific parameter estimation

In the special case of the normality assumption for G , the conditional posterior distribution of τ_j given the hyperparameters τ and σ^2 is normal and the corresponding conditional posterior mean and variance of τ_j have simple closed-form expressions that are well-known from the empirical Bayes literature (see also Gelman et al., 2013):

$$\tau_j \mid \tau, \sigma^2, \widehat{\tau}_j \sim N(\tau_j^*, V_j) \quad j = 1, \dots, J,$$

where

$$\tau_j^* = \frac{\frac{1}{\sigma^2} \cdot \tau + \frac{1}{\widehat{se}_j^2} \cdot \widehat{\tau}_j}{\frac{1}{\sigma^2} + \frac{1}{\widehat{se}_j^2}}, \quad V_j = \frac{1}{\sigma^2 + \frac{1}{\widehat{se}_j^2}}. \quad (3)$$

The inverses of σ^2 and \widehat{se}_j^2 , known as *precisions*, serve a critical role in determining the conditional posterior mean τ_j^* and variance V_j . The conditional posterior mean effect is a precision-weighted average of the population mean effect τ and the observed effect for the site, $\widehat{\tau}_j$. When maximum likelihood or restricted maximum likelihood estimates for the hyperparameters τ and σ^2 are used in the above, τ_j^* becomes an empirical Bayes estimate.

The posterior mean effect, τ_j^* , can be expressed as the observed mean effect, $\widehat{\tau}_j$, shrunk toward the prior mean effect, τ :

$$\tau_j^* = \tau + (\hat{\tau}_j - \tau) \cdot \frac{\sigma^2}{\sigma^2 + \hat{s}e_j^2}. \quad (4)$$

The weight $S_j = \sigma^2 / (\sigma^2 + \hat{s}e_j^2)$ can be interpreted as the reliability of the ML estimator of $\hat{\tau}_j$, defined as the proportion of the variance of the ML estimator attributable to genuine underlying heterogeneity across sites (Rabe-Hesketh and Skrondal, 2022). If $\hat{s}e_j^2 = 0$, the ML estimator of $\hat{\tau}_j$ is perfectly precise or reliable, and the posterior mean and the ML estimator are identical ($\tau_j^* = \hat{\tau}_j$). A large $\hat{s}e_j^2$ indicates the data is less informative about τ_j than the prior distribution for τ , resulting in the posterior mean effect, τ_j^* , being more significantly shrunk toward the prior mean effect, τ . To assess the magnitude of σ^2 in comparison to the site-specific sampling error $\hat{s}e_j^2$, we use the weight, S_j , often termed the *shrinkage factor*. This weight ranges between 0 and 1, providing a direct measure for each site. For a comprehensive evaluation over all J sites, we calculate the geometric mean¹ of $\hat{s}e_j^2$, thereby deriving an average measure of reliability for the ML estimator of $\hat{\tau}_j$:

$$I = \frac{\sigma^2}{\sigma^2 + \exp\left(\frac{1}{J} \sum_{j=1}^J \ln(\hat{s}e_j^2)\right)}. \quad (5)$$

Higher values of I indicate greater average informativeness of the within-site data about the τ_j 's compared to lower values.

2.3 Super population vs. finite-population estimands

The Rubin model highlights two estimands of interest: the super population distribution of site-specific effects, G , and the finite-population distribution, $\{\tau_j\}_{j=1}^J$, for the J sites in the experiment. These two estimands correspond to distinct research objectives. Super population inference aims to recover G , the effect distribution for the broader population of

¹In this context, the geometric mean is preferred to the arithmetic mean due to its lessened susceptibility to skewness from extreme $\hat{s}e_j^2$ values. This is particularly important when dealing with smaller site sizes, where such extreme values can be more prevalent.

sites from which the J experimental sites were sampled. This task is referred to as a *Bayes deconvolution problem*, wherein the observed, noisy sample estimates $\{\widehat{\tau}_j, \widehat{se}_j^2\}_{j=1}^J$ are used to compute an estimate \widehat{G} of G (Efron, 2016). Performance evaluation studies typically focus on this research objective, as they often have sufficiently large J (e.g., Gilraine et al., 2020)². In contrast, finite-population inference examines the distribution of the true site-effect parameters of the given J sites, proceeding under the assumption that the specific sites included in the study represent the entirety of the finite population of interest.

Recovering the super population estimand G might not be feasible in multisite trial settings without assumptions about the form of G . In the normal model of G , deconvolution requires estimating only two hyperparameters: τ and σ^2 . However, when the prior G is unknown, the performance of deconvolution estimators depends heavily on the shape of the underlying G and the number of sites J (McCulloch and Neuhaus, 2011). Specifically, the mathematical guarantees of flexible estimators are typically asymptotic in nature, necessitating a large J (Jiang and Zhang, 2009). In the context of multisite trials, J is often small to moderate (Weiss et al., 2017), rendering asymptotics potentially inapplicable in such cases. Furthermore, in many multisite trials, it may be unreasonable to assume that the experimental sites are adequately representative of the super population (Stuart et al., 2011; Tipton and Olsen, 2018). For example, Tipton et al. (2021) noted that schools participating in IES-funded grants were predominantly located in large urban districts, geographically close to one another and to the study’s principal investigators.

In this paper, we focus on finite-population estimands, represented by $\{\tau_j\}_{j=1}^J$. This approach helps us circumvent the risks associated with generalizing treatment effect estimates from a sample of sites to a super population when systematic discrepancies exist between them. Finite-population estimands also enable more targeted and context-specific

²Assuming J is large, various computational methods have been proposed for estimating G , including the EM algorithm (Laird, 1978), interior point algorithm (Koenker and Mizera, 2014), Efron’s logspline (Efron, 2014), and nonparametric maximum likelihood estimation (Gilraine et al., 2020).

investigations, which are essential in certain research scenarios. [Miratrix et al. \(2021\)](#) highlighted cases where sites are purposefully selected based on specific site-level characteristics. When these characteristics serve as theoretically plausible site-level effect moderators, researchers can achieve causal generalization without relying on statistical random sampling. If site selection criteria involve less-than-ideal or worst-case scenarios, finite-population estimands can provide valuable insights into an intervention’s resilience under such challenging conditions. Moreover, concentrating on a finite-population of sites typically results in more precise estimated effects compared to situations where researchers aim to generalize to a super population. This approach is statistically less demanding, allowing for more relevant recommendations in low-data settings for multisite trials.

3 Improving inferences for site-specific effects

3.1 Inferential goals and threats to inferences for τ_j

[Shen and Louis \(1998\)](#) identify three common finite-population inferential goals: (1) estimating the individual site-specific effect parameters, τ_j , (2) ranking the sites based on τ_j , and (3) estimating the empirical distribution function (EDF) of the τ_j ’s. Each of these three goals can be associated with a different loss function, which may be minimized by a distinct estimator. In this setting, we are concerned with the collective performance-estimators for the vector $\tau = (\tau_1, \dots, \tau_J)$ that exhibit good performance as a whole. This is known as a *compound decision problem* ([Robbins, 1951](#)), in contrast to a simple decision problem, which would ignore the ensemble of J problems and construct estimators for τ_j individually.

The loss function typically associated with the first goal is the finite-population mean-squared error loss (MSEL):

$$\text{MSEL} = \frac{1}{J} \cdot \sum_{j=1}^J (a_j - \tau_j)^2 \quad (6)$$

where a_j is the estimate of τ_j generated by a candidate estimator. In practice, we will work with root-mean-squared error, $\text{RMSE} = \sqrt{\text{MSEL}}$, since it preserves the scale of the τ_j values, making it more interpretable and less sensitive to extreme values. The theoretical posterior means (PMs) of τ_j , $a_j = \text{E}[\tau_j | \hat{\tau}_j]$ for $j = 1, \dots, J$, minimize the expected MSEL and RMSE. For example, when the τ_j values are indeed Normally distributed, setting $a_j = \tau_j^*$ from equation (4) minimizes the MSEL and RMSE.

For the second inferential goal, we can choose an estimator for the vector of ranks of τ_j that minimizes the finite-population mean squared error loss of the ranks (MSELR),

$$\text{MSELR} = \frac{1}{J} \cdot \sum_{j=1}^J (A_j - R_j)^2 \quad (7)$$

where $I(\cdot)$ is the indicator function, $R_j = \sum_{i=1}^J I(\tau_i \leq \tau_j)$ is the true rank of τ_j , and A_j is an estimated rank. In practice, we measure the finite-population mean squared error loss of the percentiles (MSELP),

$$\text{MSELP} = \frac{1}{J} \cdot \sum_{j=1}^J \left(\frac{A_j}{J} - \frac{R_j}{J} \right)^2 = \frac{1}{J^2} \cdot \text{MSELR}, \quad (8)$$

where A_j/J and R_j/J correspond to the estimated and true percentiles in decimal form, respectively. The MSELP is less sensitive to changes in J , so may be compared across settings with different numbers of sites. The theoretical expected posterior percentiles in decimal form $A_j/J = \text{E}[R_j/J | \hat{\tau}_j]$ minimize expected MSELP. These expected posterior percentiles may not correspond to the percentiles based on the posterior means, and indeed, [Goldstein and Spiegelhalter \(1996\)](#) show that ranks based on posterior means can be suboptimal in general.

For the third inferential goal, [Shen and Louis \(1998\)](#) suggest minimizing the integrated squared-error loss (ISEL):

$$\text{ISEL}(A, G_J) = \int \{A(t) - G_J(t)\}^2 dt \quad (9)$$

where $G_J(t) = J^{-1} \cdot \sum I_{\{\tau_j \leq t\}}$ is the true EDF and $A(t)$ is an estimated EDF, $-\infty < t < \infty$. They show that $\bar{G}_J(t) = J^{-1} \cdot \sum_{j=1}^J \Pr(\tau_j \leq t \mid \hat{\tau}_j)$ minimizes the expected ISEL. The third inferential goal is related to the deconvolution problem, where the goal is to use observed data to recover an unknown prior density G ([Laird, 1978](#); [Stefanski and Carroll, 1990](#); [Efron, 2016](#)). We focus on finite-population inference in this paper, so our goal is to use the observed $\hat{\tau}_j$ values to infer the EDF of the true τ_j values.

The three inferential goals, their associated loss functions, and optimal estimators reveal two primary challenges in achieving valid finite-population estimation. The first challenge is model misspecification, which arises when we assume an incorrect parametric form for the super population distribution G . If the true distribution G is not Gaussian, assuming normality may result in insensitivity to skewness, long tails, multimodality, and other complexities in the EDF of the τ_j 's ([McCulloch and Neuhaus, 2011](#)). Consequently, the standard Rubin model becomes unreliable, especially for the third inferential goal. The second challenge emerges when an unsuitable estimator is chosen, even when the prior distribution G is accurately specified in a model. The optimal estimator is contingent upon the chosen loss function or inferential goal. However, practitioners often use the same set of posterior mean effect estimates for all three goals, leading to suboptimal outcomes. For instance, the EDF of posterior mean effect estimates will tend to be underdispersed compared to the EDF of τ_j due to shrinkage towards the prior mean effect τ . Conversely, the EDF of raw observed ML effect estimates $\hat{\tau}_j$ is overdispersed because of sampling errors ([Mislevy et al., 1992](#)).

3.2 Strategies to improve inferences for the distribution of τ_j

To address the threats outlined in the previous section, two strategies can be employed. The first strategy entails adopting flexible semiparametric or nonparametric specifications for the prior distribution G to protect against model misspecification (Paddock et al., 2006). One prominent Bayesian nonparametric specification is the Dirichlet process (DP) prior, which has gained widespread use in the literature (Lockwood et al., 2018; Paganin et al., 2022). The second strategy focuses on employing posterior summary methods, such as the constrained Bayes (CB, Louis, 1984; Ghosh, 1992) or the triple-goal (GR, Shen and Louis, 1998) estimators. These estimators are designed to directly target the loss functions associated with specific inferential goals. The following sections delve into a comprehensive examination of these two strategies and their implications for addressing the challenges in finite-population estimation.

3.3 Posterior summary methods: Constrained Bayes and triple-goal estimators

In this section, we discuss two posterior summary methods specifically designed to address the underdispersion of posterior means: the constrained Bayes (CB) and triple-goal (GR) estimators. Our primary target of interest is $\{\tau_j\}_{j=1}^J$, representing the EDF of the τ_j 's. Both CB and GR generate estimates of the τ_j that are not as overly shrunk as the simple posterior means.

The CB estimator directly modifies the posterior mean estimates to avoid underdispersion. This is accomplished by rescaling the posterior mean estimates τ_j^* , thereby ensuring the estimated variance of site-specific effect estimates aligns with the estimated marginal variance of the latent parameters τ_j . In equation (4), the posterior mean of τ_j is denoted as $\tau_j^* \equiv E(\tau_j|\hat{\tau}_j)$, and the posterior variance of τ_j as $V_j \equiv \text{Var}(\tau_j|\hat{\tau}_j)$. We introduce

$\bar{\tau} \equiv J^{-1} \sum \tau_j^*$ to represent the finite-population mean of the posterior means. The CB estimates, indicated as τ_j^{CB} , are then estimated as follows (Ghosh, 1992):

$$\tau_j^{\text{CB}} = \bar{\tau} + (\hat{\tau}_j - \bar{\tau}) \cdot S_j \cdot \frac{\sigma}{\sqrt{V_j}}. \quad (10)$$

Here, S_j is the shrinkage factor, defined in equation (4) as $\sigma^2/(\sigma^2 + \hat{s}e_j^2)$. The cross-site impact standard deviation (σ), and the posterior variance of τ_j^* (V_j) can be estimated as:

$$\sigma = \sqrt{\frac{\sum V_j}{J} + V_j}, \quad V_j = \frac{\sum (\tau_j^* - \bar{\tau})^2}{J - 1}. \quad (11)$$

Posterior mean estimates tend to be under-dispersed because their variance V_j is always less than the marginal variance σ^2 , as demonstrated in equation (11). By incorporating the term $\sigma/\sqrt{V_j}$, the CB estimator in equation (10) essentially “reverses” the shrinkage towards the finite-poulation prior mean effect $\bar{\tau}$ driven by S_j . This adjustment expands the gap between τ_j^* and $\bar{\tau}$ because $(\hat{\tau}_j - \bar{\tau}) \cdot S_j$ is equal to $\tau_j^* - \bar{\tau}$. Details behind the choice of rescaling can be found in Appendix A.1. An empirical Bayes version of the CB estimator was also introduced by Bloom et al. (2017).

In contrast, the GR estimator employs evenly spaced percentiles of the estimated G to generate its estimates. The GR estimator is constructed via a three-stage process. In the first stage, an estimate of the distribution function that minimizes ISEL is constructed as

$$\bar{G}_J(t) = J^{-1} \cdot \sum_{j=1}^J \Pr(\tau_j \leq t \mid \hat{\tau}_j) \quad (12)$$

The smooth function $\bar{G}_J(t)$ is then discretized to an EDF that places a mass of $1/J$ at J evenly spaced discrete points $\hat{U}_k = \bar{G}_J^{-1}(\frac{2k-1}{2J})$ for $k = 1, \dots, J$. In the second stage, a rank for each site j is computed as

$$\bar{R}_j = \sum_{k=1}^J \Pr(\tau_j \leq \tau_k | \hat{\boldsymbol{\tau}}). \quad (13)$$

The generally non-integer-valued ranks \bar{R}_j are then discretized to integer-valued ranks as $\hat{R}_j = \text{rank}(\bar{R}_j)$. In the final stage, the GR estimate τ_j^{GR} for each site j is computed as $\tau_j^{\text{GR}} = \hat{U}_{\hat{R}_j}$. Intuitively, the GR estimator first finds a good estimate $\bar{G}_J(t)$ of the full distribution of τ_j values and then produces estimates for the J sites as J evenly spaced quantiles of $\bar{G}_J(t)$, in an appropriate order. The details behind the choices made in the procedure can be found in Appendix [A.2](#).

3.4 Relaxing the distributional assumption for the prior G : Dirichlet process mixture

Instead of presupposing a known parametric form for the prior distribution G in equation (2), a Dirichlet process (DP) can be employed as the prior for G to accommodate uncertainty regarding its shape. The DP prior is characterized by two hyperparameters: a base distribution G_0 and a precision parameter α ([Antoniak, 1974](#); [Congdon, 2020](#)). A two-stage hierarchical model, incorporating the DP prior, can be formulated as follows:

$$\begin{aligned} \hat{\tau}_j | \tau_j, \hat{s}e_j^2 &\sim N(\tau_j, \hat{s}e_j^2), \quad j = 1, \dots, J, \\ \tau_j | G &\stackrel{\text{i.i.d.}}{\sim} G, \\ G | \alpha, G_0 &\sim \text{DP}(\alpha, G_0). \end{aligned} \quad (14)$$

This model’s semiparametric nature stems from the combination of a parametric first-stage model for $\hat{\tau}_j$ with a Gaussian error distribution and a nonparametric second-stage model for τ_j that employs a DP prior. Conceptually, the DP model can be viewed as an infinite mixture model in which both the priors and the data contribute to determining the number of mixture components.

To finalize the model specification, we must define the base distribution G_0 and establish a hyperprior for the parameter α . G_0 serves as the initial best guess for the shape of the prior distribution G . Typically, we assume G_0 follows a Gaussian distribution with mean τ and variance σ^2 . For computational convenience, the base distribution G_0 is typically constructed as the product of conjugate distributions, such as a normal distribution for the mean parameter τ and an inverse-gamma distribution for the variance parameter σ^2 (Paganin et al., 2022).

The precision hyperparameter, denoted as α , controls the degree to which G converges toward G_0 . A larger α promotes a more diverse set of τ_j values, commonly termed as the distinct count of *clusters* K derived from the DP. It is worth noting that K does not always precisely correspond to the number of mixture components, C , which represent latent subpopulations with substantive meaning as defined in finite mixture models. However, K can be reasonably regarded as an upper limit for C (Ishwaran and Zarepour, 2000).

The hyperprior for α plays a pivotal role in determining K , which in turn shapes the posterior distribution over clusters. Using a Gamma distribution — with a as the shape parameter and b as the rate parameter — as a hyperprior for α is common practice, attributable to its computational advantages (Escobar and West, 1995). Nonetheless, the choices of a and b could significantly influence the posterior distribution of α , thus affecting the clustering behavior.

The topic of hyperprior selection, however, remains subject to debate. Some studies assert that the data are usually informative enough to yield a concentrated posterior, thus reducing the influence of the hyperprior, even when employing a high-variance prior for α (Leslie et al., 2007; Gelman et al., 2013). In contrast, other research highlights that the selection of hyperpriors, and more generally the strategies employed for determining α , can significantly sway the estimation or inference process (Dorazio, 2009; Paddock et al., 2006; Murugiah and Sweeting, 2012).

Our objective is to assess the sensitivity under two distinct hyperprior options for α , particularly in the context of varying levels of data informativeness. The first hyperprior, explored by [Antonelli et al. \(2016\)](#), is relatively diffuse, allowing for numerous clusters. This strategy, which we refer to as the DP-diffuse model, is applicable when prior knowledge about K is absent. DP-diffuse model chooses values of a and b such that α is centered between 1 and J with a large variance to assign a priori mass to wide range of α values. For instance, with $J = 50$, we might set the mean of the α distribution to 25 and its variance to 250, ten times the mean. With these initial values, we can use the moments of a Gamma distribution to derive the corresponding hyperparameters $a = 2.5$ and $b = 0.1$, based on the formulas $E(\alpha | a, b) = a/b$ and $\text{Var}(\alpha | a, b) = a/b^2$.

This research proposes a novel approach, employing a χ^2 distribution to formulate an informative hyperprior for α . Assume we have $\text{Pr}(K)$, a prior that encapsulates our knowledge of the distribution of K . [Dorazio \(2009\)](#) provides an expression for $\text{Pr}(K | J, a, b)$, the probability mass function for the prior distribution K induced by a $\text{Gamma}(a, b)$ prior for α and J (see equation (A.7) in Appendix A.3). We can then obtain optimal values for a and b by minimizing the discrepancy between the encoded prior $\text{Pr}(K)$ and the α -induced prior $\text{Pr}(K | J, a, b)$ using the Kullback-Leibler divergence measure.

Our proposal involves setting $\text{Pr}(K) \sim \chi^2(\text{df} = u)$ to more intuitively encapsulate our prior knowledge on K and its inherent uncertainty. This strategy is primarily motivated by the fact that the χ^2 distribution has a mean and variance of u and $2u$, respectively. For instance, if we regard five clusters ($K = 5$) among 50 sites as a reasonable approximation of the underlying distribution, we could assume that $\text{Pr}(K)$ follows a $\chi^2(5)$ distribution and specify a $\text{Gamma}(a, b)$ that closely matches $\chi^2(5)$. In this case, the appropriate Gamma distribution would have parameters $(a, b) = (1.60, 1.22)$ (see Figure A.1 in Appendix A.3). This approach, which we term the DP-inform model, is particularly effective for crafting an informative prior for K , especially when aiming to impose near-zero probabilities beyond

The probability mass function for the expected number of clusters (K)
 The prior of K induced by the diffuse Gamma(2.5, 0.1) prior for α vs. the informative $\chi^2(5)$

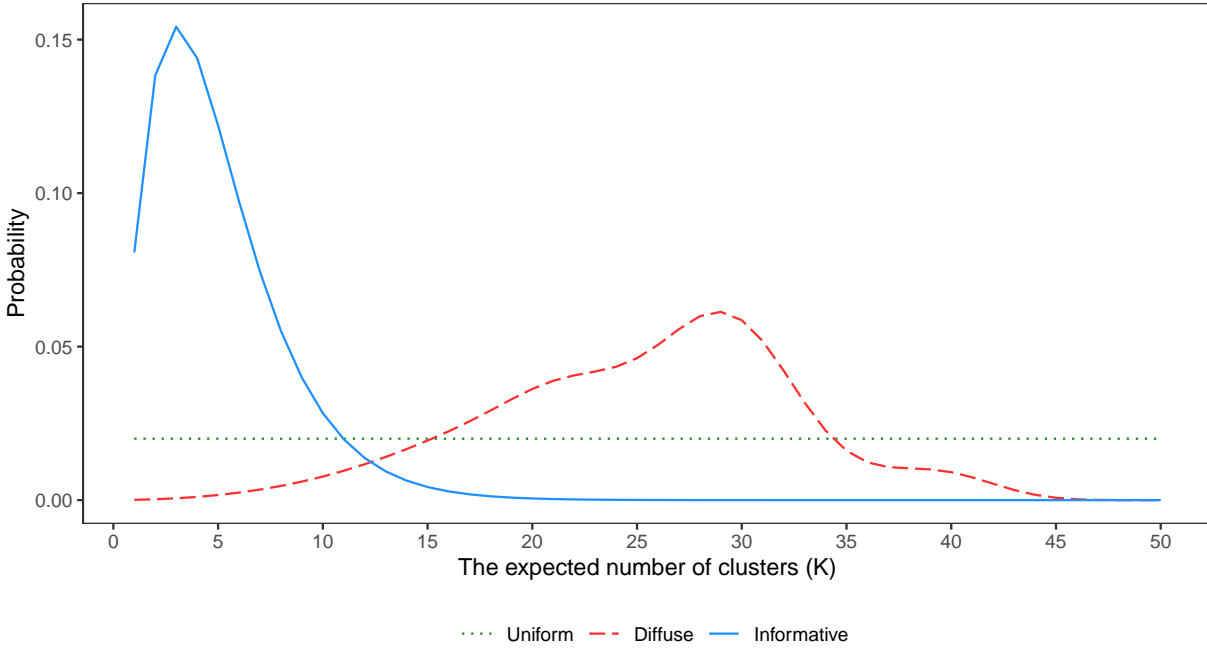


Figure 1: The distributions of the expected number of clusters K for the DP-diffuse and DP-inform models ($J = 50$)

a certain threshold (e.g., $K = 25$ as shown in Figure 1) and to clarify the prior mean and variance of K .

In Figure 1, we observe that the two DPM models represent contrasting beliefs regarding K . The DP-diffuse model favors a smoother G with approximately 25-30 clusters for 50 sites, while the DP-inform model, based on $\chi^2(5)$, is more favorable to a more uneven and multimodal G , assuming that about five clusters are needed for 50 sites. Further details about the choices of hyperpriors and their implementations can be found in Appendix A.3.

4 A simulation study

4.1 Simulation design

To compare the performance of different models and posterior summary methods, we conduct a comprehensive Monte Carlo simulation. We generate data by systematically varying five factors: (a) the number of sites (J), (b) the average number of observations per site (\bar{n}_j), (c) the coefficient of variation in site sizes (CV), (d) the true cross-site population distribution (G) of τ_j , and (e) the true cross-site population standard deviation of impacts (σ). We calibrate our simulated datasets to mirror typical data settings for multisite trials in education, as described by [Weiss et al. \(2017\)](#), which reports values of J , \bar{n}_j , and σ observed in 16 different multisite trials across a range of educational levels.

We consider five values for the number of sites in our study: $J = 25, 50, 75, 100$, and 300. The number of random assignment blocks reported in the 16 studies from [Weiss et al. \(2017\)](#) ranged from 20 to 356, with a median of 78. Although multisite trials typically involve a small to moderate numbers of sites, we also wanted to investigate model performance for larger multisite trials, such as the Head Start Impact Study (e.g., [Bloom and Weiland, 2015](#); [Padilla, 2020](#); [Schochet and Padilla, 2022](#)).

We vary the average number of observations per site in our study as $\bar{n}_j = 10, 20, 40, 80$, and 160. [Weiss et al. \(2017\)](#) reported a range of mean site sizes, from 11 in the Head Start Impact Study to 1,176 in the Welfare-to-Work Program, with the 25th and 75th percentiles at 75 and 163, respectively. We note that multisite trials often have relatively small site sizes, due in part to design choices and logistical constraints ([Sabol et al., 2022](#); [Weiss et al., 2017](#)).

We control the variation in site sizes by setting the coefficient of variation $\frac{sd(n_j)}{\bar{n}_j}$ of the site sizes to be $CV = 0.00, 0.25, 0.50, 0.75$ by sampling n_j from a gamma distribution with

a mean of \bar{n}_j and a standard deviation of $\bar{n}_j \cdot \text{CV}$. We then truncate n_j at the lower limit of $n_j = 5$. Finally, we compute the within-site sampling variances as: $\widehat{se}_j^2 = 4/n_j$ (See Appendix B.1 for details).

We vary the cross-site impact standard deviation as $\sigma = 0.05, 0.10, 0.15, 0.20$, and 0.25 in effect size units. Weiss et al. (2017) report that the cross-site standard deviation of program impact, in effect size units, ranges between 0.00 and 0.35 , with the majority of values falling between 0.10 and 0.25 . They define 0.05 , 0.15 , and 0.25 as having a modest, moderate, and substantial impact variation, respectively. In conjunction with the range of \widehat{se}_j^2 determined by our selection of \bar{n}_j , σ determines the magnitude of the average reliability of the ML estimates. We denote this average reliability using I , as defined in equation (5). I varies between 0.01 and 0.71 under our simulation conditions, with a mean of 0.25 and a median of 0.18 (see Figure B.1 in Appendix B.2). This configuration reflects the low-information data environments that are frequently encountered in multisite trials in education.

Finally, we consider three different population distributions G for τ_j : Gaussian, a mixture of two Gaussians, and asymmetric Laplace (AL), as illustrated in Figure 2. The Gaussian mixture represents a scenario where the actual G is multimodal, while the AL distribution exemplifies a situation where the true G is skewed and exhibits a long tail. We rescale the simulated τ_j so that the variance of G is σ . Additional details on the data-generation process can be found in Appendix B.3.

Using the five design factors (J , \bar{n}_j , CV, σ , and G), we generate 1,500 simulation conditions, each with 100 replications. We fit each replication with three data-analytic models: Gaussian, DP-diffuse, and DP-inform, and use Markov Chain Monte Carlo to obtain 4,000 posterior samples from the joint posterior distributions of the J site-specific effects for each model. Further details on the data-analytic models can be found in Appendix B.4. Finally, we apply the three posterior summary methods (PM, CB, and GR) to each model fit.

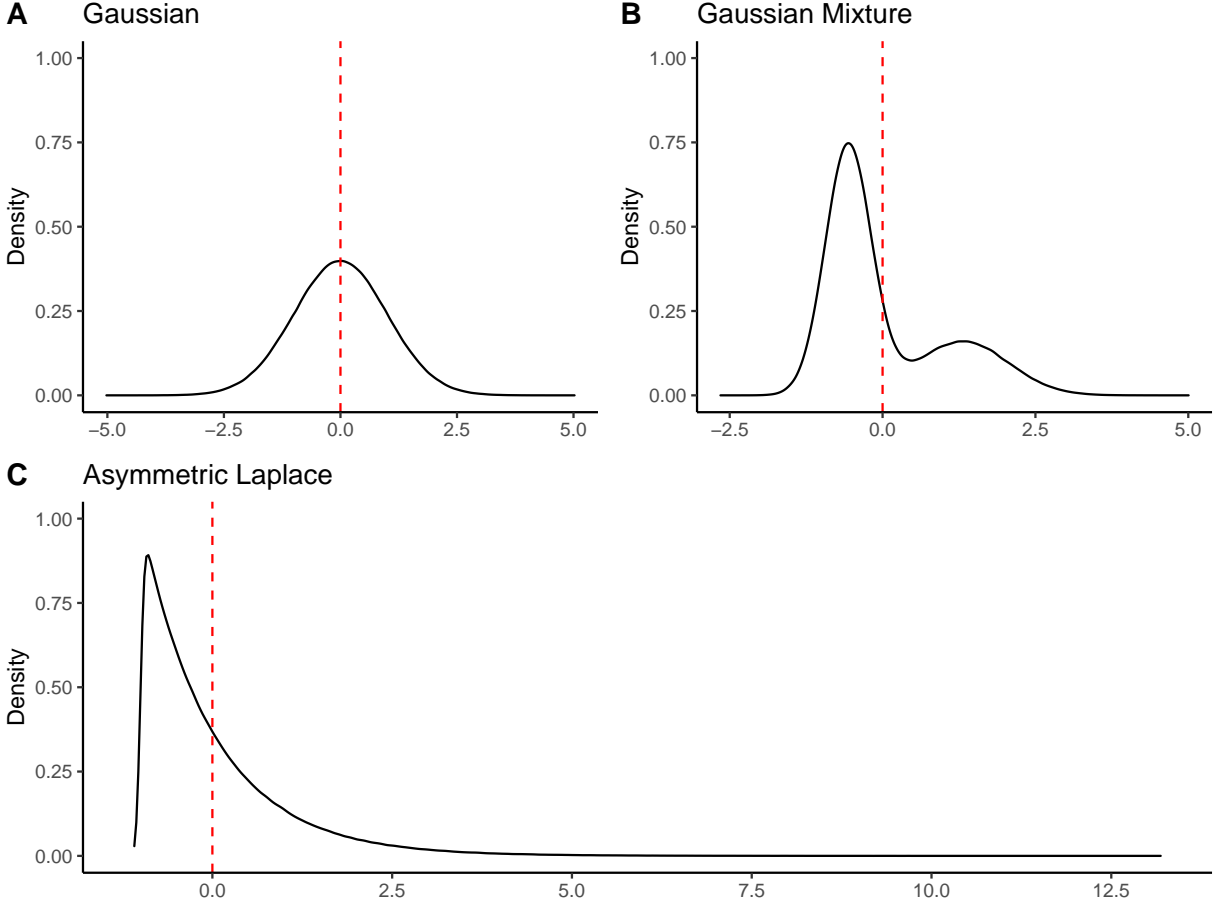


Figure 2: The true cross-site population distribution of τ_j 's (G): Gaussian, Gaussian mixture, and asymmetric Laplace distributions

To analyze the simulation results, we separate the three true population distributions G into samples of 450,000 observations each, generated as a factorial combination of the four remaining design factors (J , \bar{n}_j , CV, and σ), two data-analytic factors (data-analytic model and posterior summary method), and 100 replications. We finally construct 50,000 cluster (i.e., dataset) identifiers based on the four design factors and 100 replications to account for the statistical dependence induced by analyzing the same simulated dataset.

4.2 Simulation analysis

We employ meta-model regressions (Skrondal, 2000) to investigate the association between performance criteria and simulation factors. Meta-model regressions offer a comprehensive summary of results by regressing performance metrics on the experimental factors. In contrast to visual or descriptive analyses, meta-models deliver a model-based inferential analysis, guided by experimental design, that enables the accurate identification of significant patterns and precise estimation of their magnitudes (Boomsma, 2013; Paxton et al., 2001).

Our meta-model regressions follow the form: $\log(\text{performance}) = \beta_0 + X\beta + \epsilon$. We focus on the three performance criteria outlined in Section 3.1 as our target outcome variables: RMSE, ISEL, and MSEL. To ease the interpretation of the meta-model regression coefficients, we apply a logarithmic transformation to the outcome variables, which we discuss later. As for the explanatory variables X , we create a set of dummy variables representing the six design and data-analytic factors, along with their two-way interaction terms. The reference groups are $J = 25$, $\bar{n}_j = 10$, $\sigma = 0.05$, $\text{CV} = 0.00$, the Gaussian model, and the PM summary method. Lastly, since we include each dataset nine times in each meta-model regression (corresponding to every model/posterior summary method combination), we cluster our standard errors on datasets. This approach results in a model akin to a repeated-measures ANOVA, with data-analytic model and summary method serving as within-subject factors, and the remaining design variables acting as between-subject factors.

5 Results: Effects of data-generating factors

Our simulation produces nine (three performance criteria \times three true population distributions G) meta-model regressions, each summarizing a six-factor factorial experiment. Rather than exhaustively exploring these results, we divide our analyses into two simple, practical sections. We first explore how the four design factors (J , \bar{n}_j , CV , and σ) generally affect the performance of each model and posterior summary method. We then directly compare the model/method combinations, using hypothetical case studies to illustrate how they may perform relative to each other in real-world applications.

Figure 3 illustrates how the design factors affect the outcome metric for each model/method combination, under the Gaussian mixture data-generating distribution.³ The values within each cell represent the multiplicative change in average RMSE, ISEL, or MSELP that corresponds to changing a single data-generating factor from the base condition ($J = 25$, $\bar{n}_j = 10$, $\sigma = 0.05$, $CV = 0.00$) to the value indicated by the row.⁴ These values are provided for each model, posterior summary method, and outcome metric, as indicated by the column, column panel, and row panel, respectively. For example, the value 0.77 in the top-left cell indicates that for the Gaussian model using the PM estimator, increasing \bar{n}_j from 10 to 20 reduces the RMSE by approximately 23% on average, when all other design factors are held at their baseline levels. Values less than 1 indicate improvement compared to the base

³Results for the Gaussian and AL data-generating distributions are qualitatively similar. These results can be found in Figure C.1 and C.2, presented in Appendix C. No distinguishable patterns emerged in the results when comparing the Gaussian Mixture and AL data-generating distributions. In terms of performance metrics such as RMSE and MSELP, the Gaussian and Gaussian Mixture models yielded analogous patterns. The only discrepancy was observed in the ISEL metric, which was unique to the Gaussian model. The Gaussian model demonstrated superior efficacy in recovering the finite population distribution of τ_j 's, specifically when the true G conformed to a Gaussian distribution. However, even under these conditions, the performance of the DP-diffuse model was on par with the Gaussian model.

⁴In terms of the meta-model regression, Figure 3 visualizes the difference in predicted log-outcome between the given condition and the baseline condition, i.e., $\log(\widehat{\text{outcome}}) - \hat{\beta}_0 = (\hat{\beta}_0 + X\hat{\beta}) - \hat{\beta}_0 = X\hat{\beta}$, where X corresponds to the given design factor values and $\hat{\beta}_0$ corresponds to the average log-outcome in the baseline condition. Recall that for x and y close to each other, $\log(x) - \log(y) \approx \frac{x-y}{y}$, i.e., the difference in log-outcomes approximates the percent change.

condition, which can be viewed as the most challenging low-data environment for modeling site-specific effects.

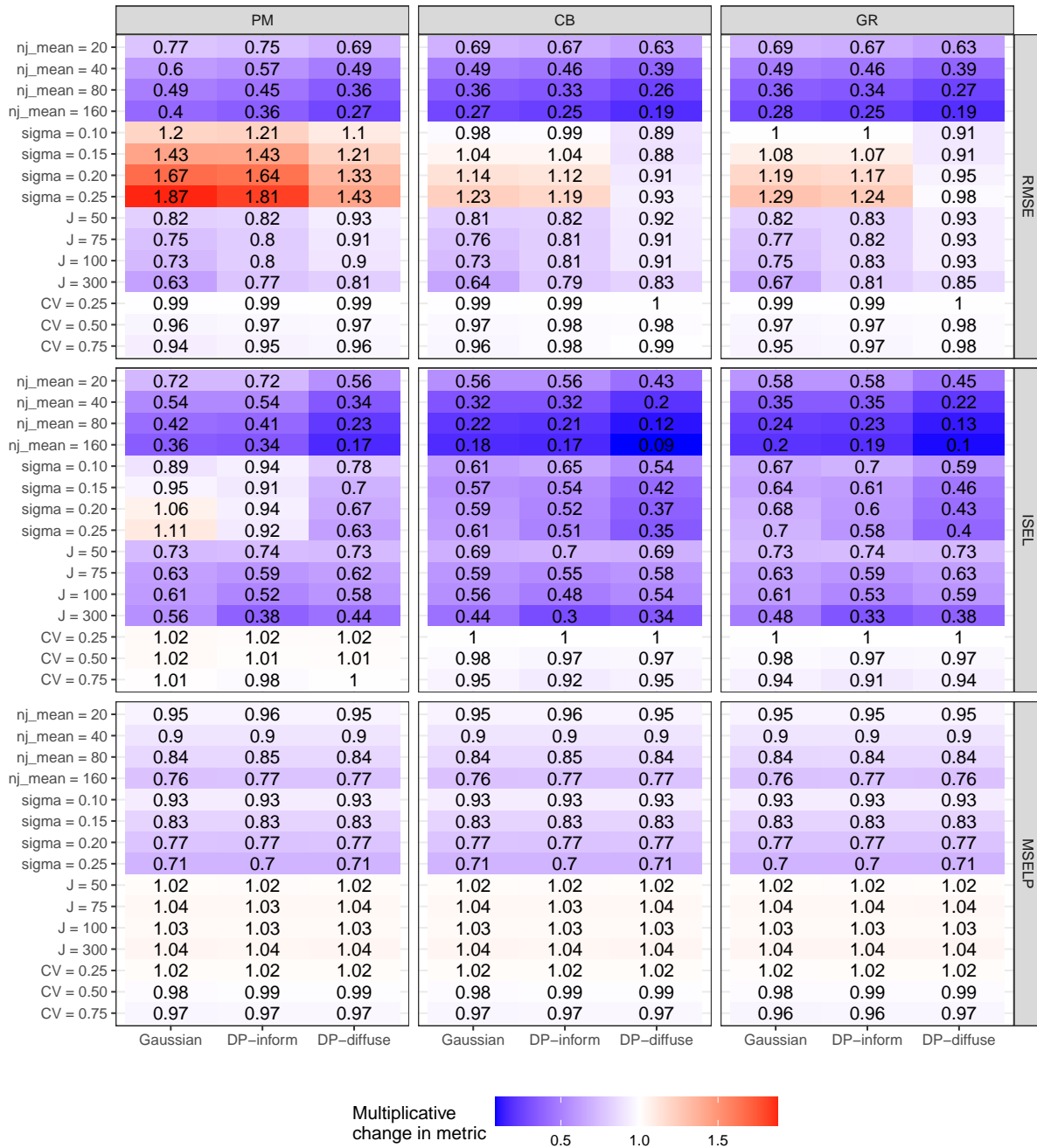


Figure 3: The multiplicative change in average RMSE, ISEL, and MSELP for a single data-generating factor change from the base condition ($J = 25$, $\bar{n}_j = 10$, $\sigma = 0.05$, and $CV = 0.00$), when the true G is Gaussian mixture

While the metrics respond differently to changes in the data-generating factors, we highlight some overall patterns in Figure 3. First, increasing \bar{n}_j significantly improves all three metrics. The three metrics all measure how well some feature of the finite population distribution of site-level effects $\{\tau_j\}_{j=1}^J$ is estimated; increasing the average site size increases the average precision of the site-level effect estimates $\{\hat{\tau}_j\}_{j=1}^J$, so it naturally improves these finite population metrics. Second, changing CV has little effect on any of the metrics, indicating that the variation in site sizes matters much less than the average site size. Our simulations posit that site size is independent from site-level treatment effect; thus, we may expect this result to change under a different simulation setup.

The RMSE metric demonstrates distinct responses to changes in J and σ . When J increases, the RMSE decreases. Adding sites increases the sample size used to estimate the cross-site variation. This improves the models' estimates of the cross-site variation, which in turn improves their site-specific effect estimates. Conversely, increasing σ generally results in a higher RMSE. The models all apply shrinkage to the raw site-specific estimates, which biases the estimates but typically reduces their RMSE by significantly decreasing their variance. As the variation σ of the true site-specific effects increases, however, the benefits of variance reduction no longer outweigh the costs of bias, and the models shrink less. For instance, Equation (4) illustrates how the estimates produced by the Gaussian/PM combination approach the initial raw site-specific estimates when σ increases for a fixed average site size. Consequently, increasing σ adversely impacts RMSE, particularly for models and methods that exhibit the most shrinkage in the base case. As observed in Figure 3, this effect is strongest for the Gaussian/PM combination and weaker for the DP-inform model and the CB and GR summary methods (see Figure C.3 in Appendix C for an example).

In terms of the ISEL metric, increasing J improves results. Similar to the RMSE, a larger J allows for better estimation of cross-site variation, thereby enhancing the estimates.

Adding more sites is equivalent to drawing additional noisy samples from the true EDF, which provides information about the true EDF's shape. The DP-inform model is particularly effective at incorporating this information, although the DP-diffuse and Gaussian models also show improvement.

In contrast to the RMSE, higher σ values result in better ISEL. Shrinkage causes systematic underestimation of large true effects and overestimation of small true effects. While this generally improves RMSE, which does not differentiate between overestimation and underestimation, excessive shrinkage can create significant discrepancies between the true and estimated EDFs, resulting in poor ISEL values. Consequently, ISEL rewards estimates that are not overly shrunk toward the overall mean. As σ increases, Figure 3 demonstrates how the CB/GR methods are better able to maintain correspondingly diffuse EDF estimates, while the PM method struggles in this regard.

Lastly, we observe that MSELP improves as either \bar{n}_j or σ increases and remains largely unaffected by J , CV, model, and summary method. MSELP assesses how well each model or method estimates the true rank order of site-specific effects. Generally, the primary factor influencing order estimation is the average reliability of the ML estimates I , which quantifies the relative magnitude of between-site and within-site variations. When most variation occurs between sites, it is easier to distinguish and accurately rank them. Increasing σ raises the proportion of total variation in the data that is between sites (rather than within sites), thereby enhancing MSELP. Similarly, a higher \bar{n}_j reduces the impact of within-site variation, which also improves MSELP. Employing different models and summary methods seldom alters the ordering of site-specific effect estimates when site sizes are constant (i.e., CV = 0), and thus, does not affect MSELP. The same overall patterns hold in the high site-size heterogeneity case as well (CV = 0.75).⁵

⁵In our simulation, we assume that site size and site-specific effect are uncorrelated, for simplicity. Introducing correlations here would likely impact the results for MSELP.

6 Results: Case studies of best model-method choices

We now directly compare the models and posterior summary methods to assess the most effective combinations under various design settings. Figure 4 illustrates the best model-method combinations, as indicated by the average outcome metric predicted by the meta-model regressions, for the Gaussian mixture data-generating distribution across different values of \bar{n}_j , σ , and J (with $CV = 0.50$ held constant, as results show minimal variation across different values of CV). In the figure, both the shape and color at each design setting represent the model-method combination yielding the lowest average error metric value, while the numbers indicate the value of I for each respective design setting.

Although Figure 4 may be subject to some simulation noise, it uncovers several intriguing patterns for the best posterior summary method. As anticipated, the posterior mean (PM) summary method consistently outperforms other methods in terms of RMSE. Since the PM method is designed to minimize RMSE, practitioners aiming to optimize RMSE should always employ the posterior mean summary method. Conversely, PM is seldom the best summary method for ISEL. The CB and GR summary methods typically exhibit less shrinkage than the PM method, leading to more accurate representations of the finite-population distribution of site-specific effects.

Figure 4 additionally highlights patterns for the best prior model for G . We observe that these patterns are predominantly influenced by the average reliability of $\hat{\tau}_j$, represented as I . As \bar{n}_j or σ increase, the value of I also increases, ranging from 0.01 to 0.71, indicating that the data becomes more informative. The number of sites J introduces an extra dimension of data informativeness; the patterns alter as J increases, since a higher number of sites supply more information, even if the value of I remains constant. Consequently, the model's performance depends on three variables that determine the overall informativeness of the data: \bar{n}_j , σ , and J .

Best model/method combinations (True G = Gaussian Mixture, CV = 0.50)

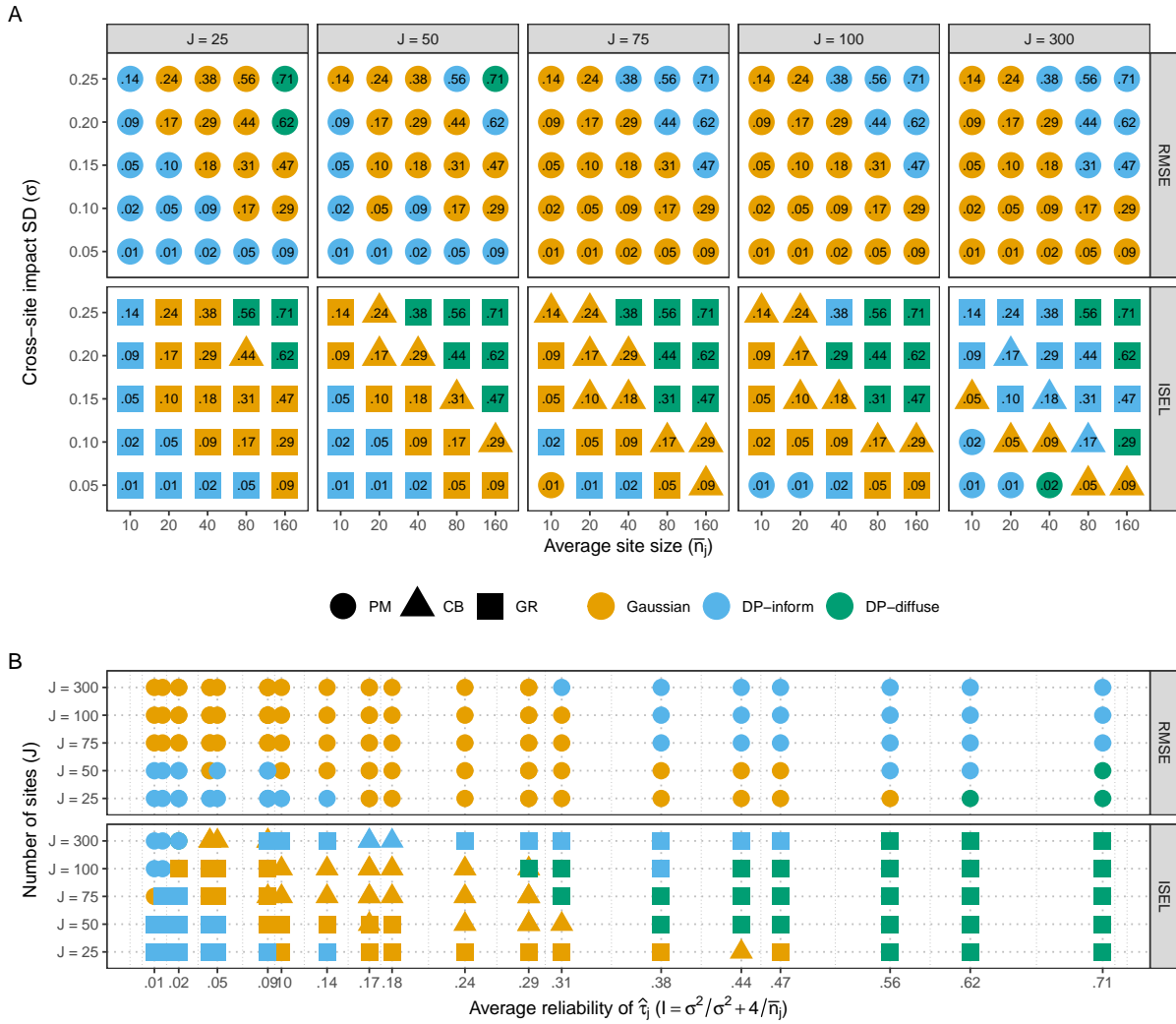


Figure 4: The best model-method combinations with the lowest average metric value (RMSE and ISEL) across the 100 simulation replications, for the Gaussian mixture data-generating distribution. Panel A presents the average reliability value of $\hat{\tau}_j(I)$ within each facet. Panel B offers a different organization of the same results where the x-axis corresponds to the level of I . MSELP results have been omitted, as the choice of model/method combinations was found to have no effect on these metrics.

The DP models typically outperform the Gaussian model in highly informative settings. We observe that the DP-inform model tends to yield the lowest RMSE when I is approximately greater than 0.38. Meanwhile, the DP-diffuse model performs best in terms of ISEL. Notably, this relationship is influenced by the number of sites, J . For example,

when $J = 300$, the DP models outperform the Gaussian model in terms of ISEL, even when I is as low as 0.10. In contrast, when $J = 25$, the DP-diffuse model requires an I value exceeding approximately 0.55 to outperform the Gaussian model regarding ISEL.

In less informative settings, however, Figure 4 demonstrates that the Gaussian model often has better performance. We note that while the DP-inform model performs the best when $J \leq 50$ and I is approximately less than 0.1, it only marginally outperforms the Gaussian model in these situations (refer to Figures C.4 and C.6 in Appendix C). Despite the true data-generating distribution not being Gaussian in these simulations, the Gaussian model combined with a suitable posterior summary method outperforms the DP models in settings with low-to-moderate informativeness, which is frequently the case in educational applications.

It is important to highlight that the performance of DP models is sensitive to the extent of between-site information present in the data. Figure 5 demonstrates the substantial improvement in the ISEL of the DP models (all employing the GR estimator) as both σ and J increase. Conversely, the Gaussian model's imposed shape constraint on G prevents it from effectively using the additional cross-site information, even when site sizes are substantially large ($\bar{n}_j = 160$). In scenarios characterized by a considerable amount of between-site information, the DP models' adaptive clustering facilitates the recovery of site-effect distributions with significantly higher accuracy compared to the Gaussian model. This is mirrored in the performance of DP models for tail area percentile estimation (specifically the 90th percentile) which follow patterns similar to those found for ISEL (refer to Figure C.7 in Appendix C). Especially under conditions of high between-site information, the DP-diffuse model were especially effective in tail percentile estimation.

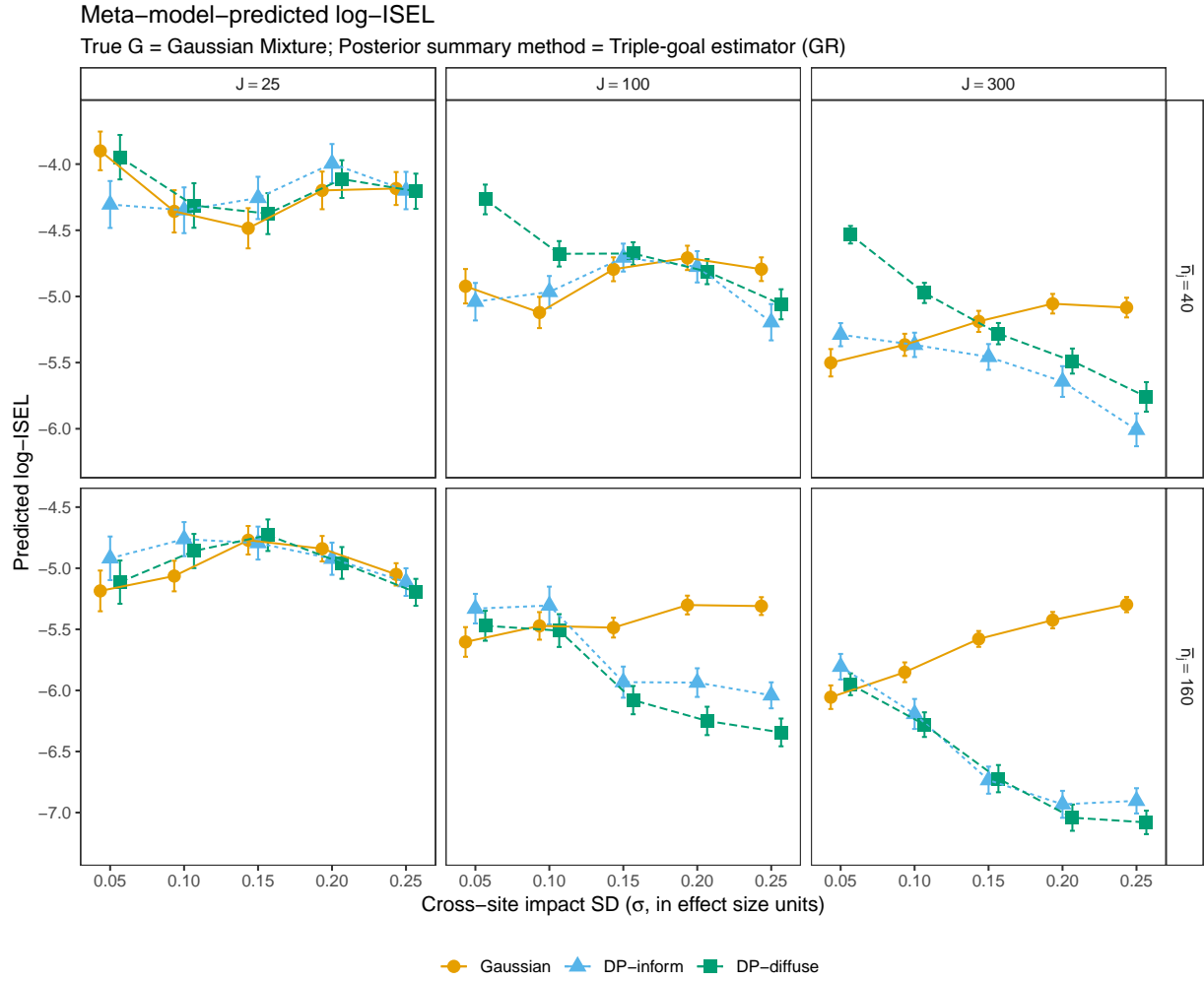


Figure 5: The meta-model predicted integrated squared error loss (ISEL) on a natural log scale, when the true G is a Gaussian mixture and the triple-goal estimator (GR) is used as the posterior summary method (Figure C.4 in Appendix C illustrates all possible combinations of J and \bar{n}_j). Plots include 95% prediction intervals around predicted values.

Figure 6 outlines the I ranges within which the simulations recommend selecting DP models for each of the 25 combinations of σ and \bar{n}_j levels, with the aim of accurately recovering the shape of site-specific effect distributions. The 95% prediction intervals plotted around the meta-model predicted values are due to Monte Carlo error.

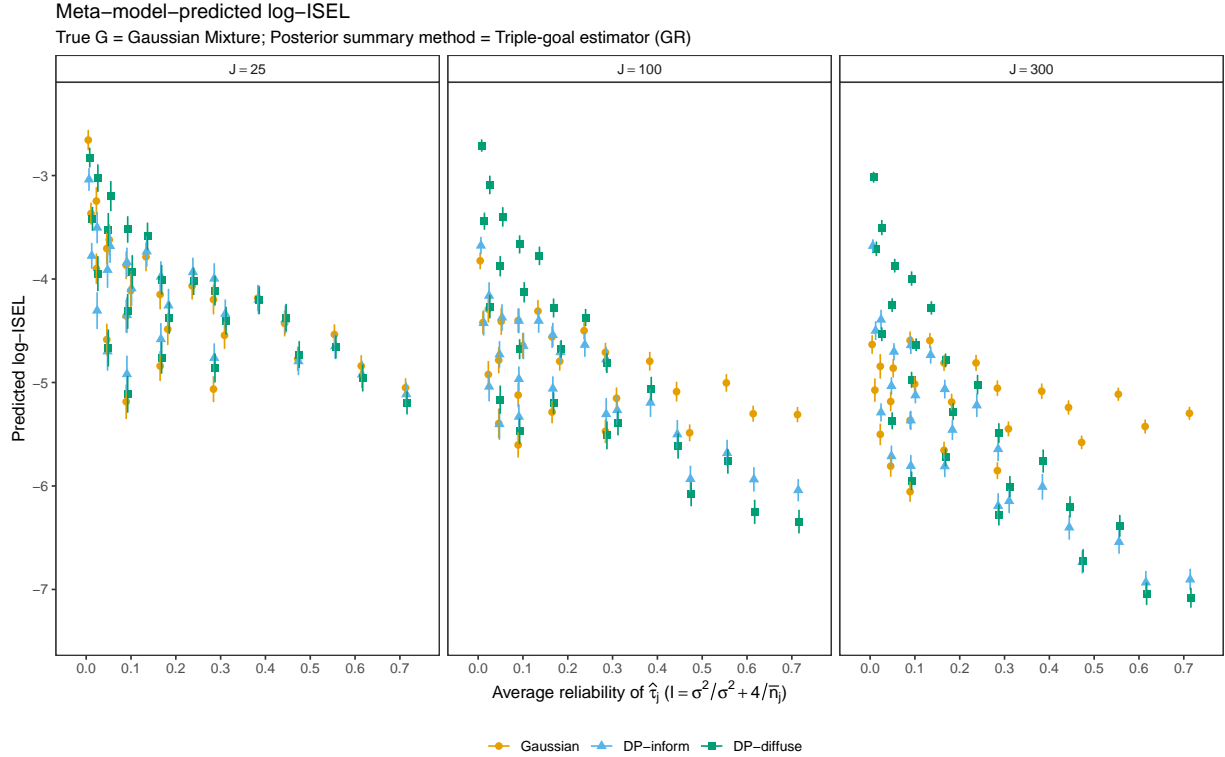


Figure 6: The meta-model predicted integrated squared error loss (ISEL) on a natural log scale, when the true G is a Gaussian mixture and the triple-goal estimator (GR) is used as the posterior summary method (Figure C.5 in Appendix C illustrates all J 's). Plots include 95% prediction intervals around predicted values.

In instances where the number of sites is 300 ($J = 300$), DP models significantly outperform the Gaussian model if the I level is above roughly 0.20. For $J = 100$, the DP models require an I level exceeding approximately 0.40 to significantly outperform the Gaussian model. With a low J of 25, the DP models' performance on ISEL is never significantly better than the Gaussian model, even at the maximum I level we explored ($I = 0.71$). Consequently, the corresponding I levels that must be exceeded for the DP models to be significantly effective when combined with the targeted posterior summary method are around $I = 0.20$ for $J = 300$, $I = 0.40$ for $J = 75$ or $J = 100$, and $I = 0.60$ for $J = 50$. When J is 25, the I level required to apply the DP models is expected to be well above 0.71. In summary, these findings emphasize the need to consider both the I and J

levels when choosing between DP and Gaussian models, particularly in research scenarios with resource constraints.

6.1 Case 1: Large between-site information & Large within-site information

We now examine a series of case studies to assess the relative performance of different model-method combinations in various real-world situations. Figure 7 displays the performance of each combination in a simulation scenario characterized by high informativeness, encompassing considerable between-site information ($J = 300$, $\sigma = 0.25$) and significant within-site information ($\bar{n}_j = 80$). Comparable scenarios can be observed in the Tennessee STAR and Small Schools of Choice studies (Word et al., 1990) (see Figures C.8 and C.9 in Appendix C). Nevertheless, it is crucial to note that Weiss et al. (2017) do not provide directly comparable cases, highlighting the challenge of acquiring highly informative data at both the within- and between-site levels in real-world multisite trials.

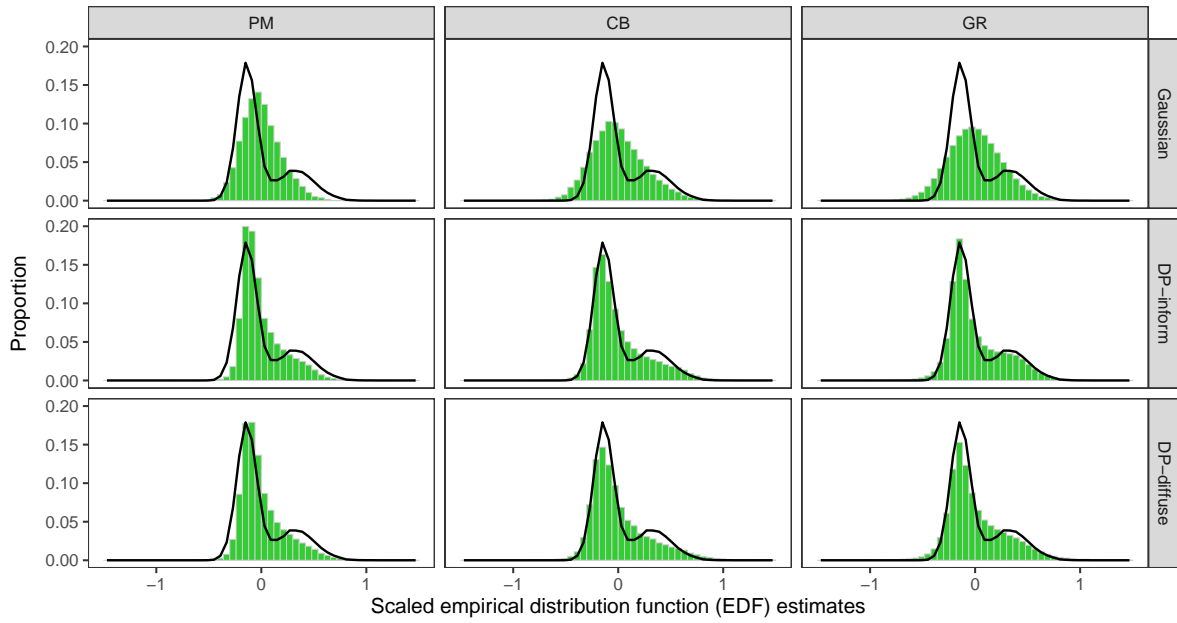
Panel A of Figure 7 plots histograms of the estimates made by the different model-method combinations against the super population density of true site-specific effects. Panel A aggregates estimates across all simulations, so it does not show how well these approaches estimate the true finite-population distribution of site-specific effects for any given simulation sample; nonetheless, it illustrates the general behaviors of each of these approaches. We see that in this highly informative setting, the DP models can consistently adapt to the sampled sites, while the Gaussian estimator tends to shrink estimates toward the overall average. Similarly, even in this highly informative setting, the PM estimator tends to shrink estimates much more than the CB or GR estimators.

To summarize these results, we visualize the log-outcomes predicted by the meta-model regressions in Panels B and C of Figure 7. In this highly informative setting, the DP models

outperform the Gaussian model in terms of both RMSE and ISEL. For example, using the DP-inform model with the GR estimator significantly improves ISEL compared to the Gaussian model with the same estimator. We see no significant differences in performance between the two DP models, suggesting that with sufficient information, the DP models are quite data-adaptive and insensitive to the choice of prior on α .

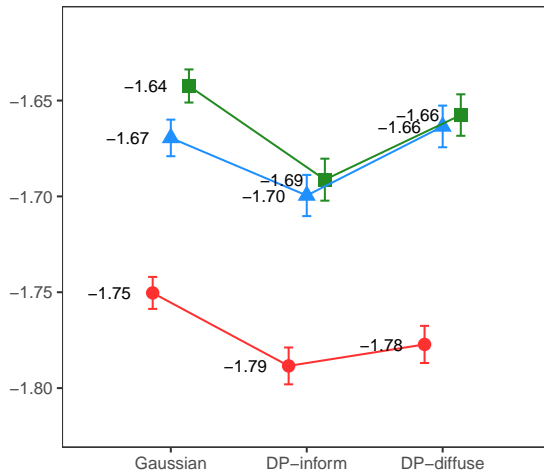
A

Highly informative scenario: $J = 300$, $l = 0.56$ ($\bar{n}_j = 80$, $\sigma = 0.25$), $CV = 0.5$



B

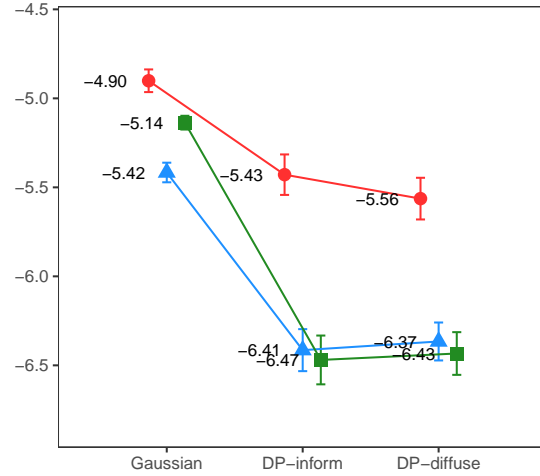
Meta-model-predicted log-RMSE



● PM ▲ CB ■ GR

C

Meta-model-predicted log-ISEL



● PM ▲ CB ■ GR

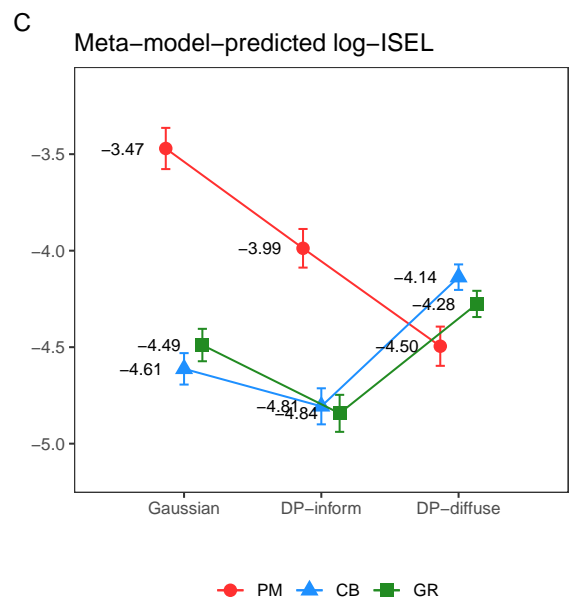
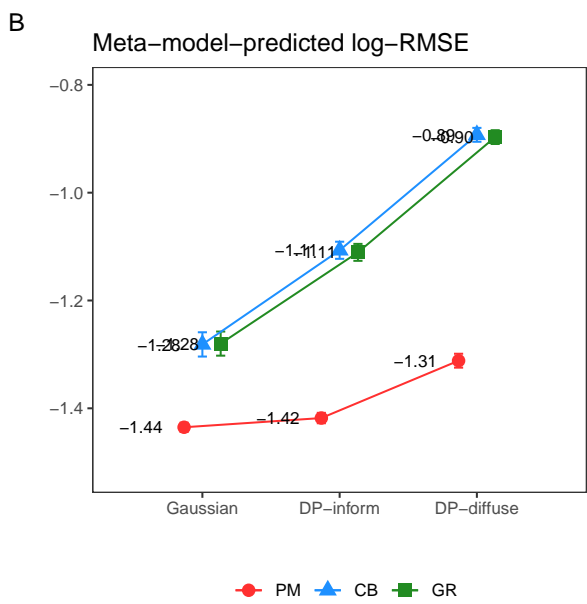
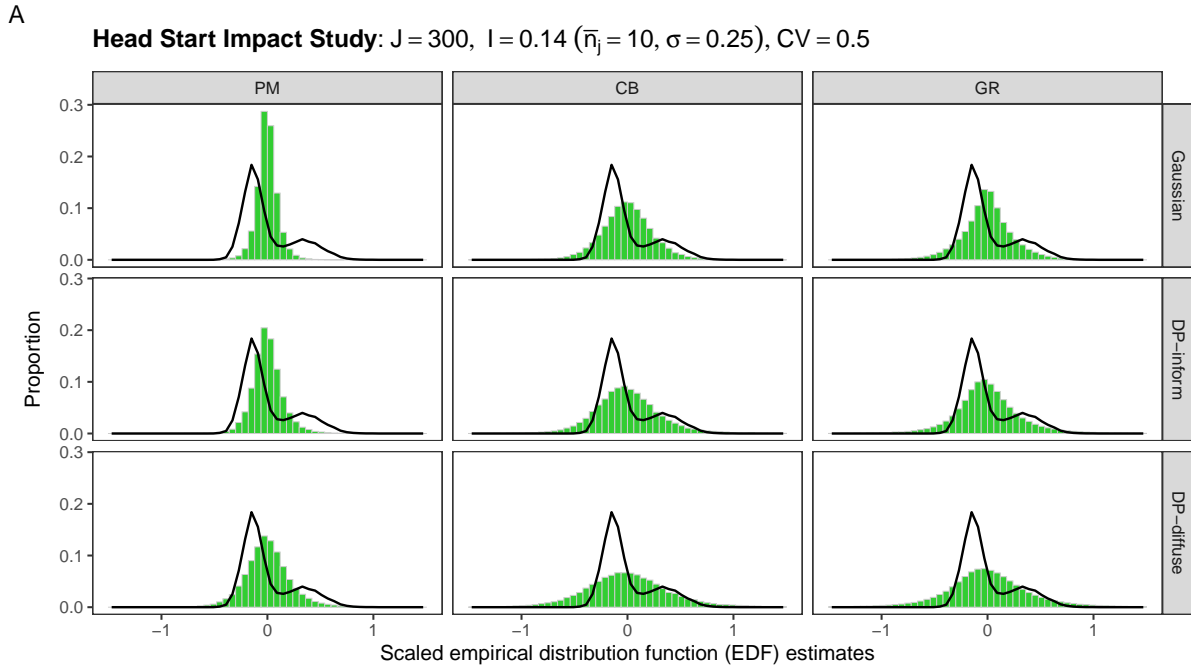
Figure 7: Scaled EDF estimates and meta-model-predicted log-RMSE and ISEL for each model-method combination. Simulation based on highly informative scenario. True G is Gaussian mixture, CV is fixed at 0.5. Plots include 95% prediction intervals around predicted values.

6.2 Case 2: Large between-site information & Small within-site information

Figure 8 shows results in a scenario similar to the Head Start Impact Study (Puma et al., 2010), which has significant between-site information ($J = 317$, $\sigma = 0.30$) but limited within-site information ($\bar{n}_j = 11.3$). In Panel A, we see how the lack of within-site information leads even the DP models to lean more heavily on the Gaussian base distribution, leading to roughly Gaussian histograms when aggregated across all simulations.

When there is significantly more between-site information than within-site information, shrinkage toward the overall mean effect can considerably influence model estimates. For instance, the DP-diffuse model is found to be unsuitable for both RMSE and ISEL due to undershrinkage, which can be attributed to the model’s assumption of a large number of clusters and the substantial between-site information. Consequently, this leads to excessive weight being placed on a broad spectrum of potential site-specific effects. Conversely, the Gaussian model exhibits excessive shrinkage as a result of its shape constraints. In this scenario, the DP-inform model demonstrates strong performance in terms of ISEL, as its flexible shape allows it to adapt appropriately to the considerable between-site information, while its limited number of assumed clusters prevents undershrinkage.

In general, the choice of posterior summary method appears to be more critical than the selection of the model. Employing the PM summary method leads to a 16-42% improvement in RMSE compared to the CB or GR methods, while only a marginal (1%) difference in RMSE is observed between the Gaussian and DP-inform models when PM is utilized. Regarding ISEL, the use of CB or GR methods yields performance that is 1.85 to 2.14 times better than the PM method. This improvement is substantially larger than the 20-35% better performance obtained by employing the DP-inform model over the Gaussian model, when paired with the CB/GR methods.



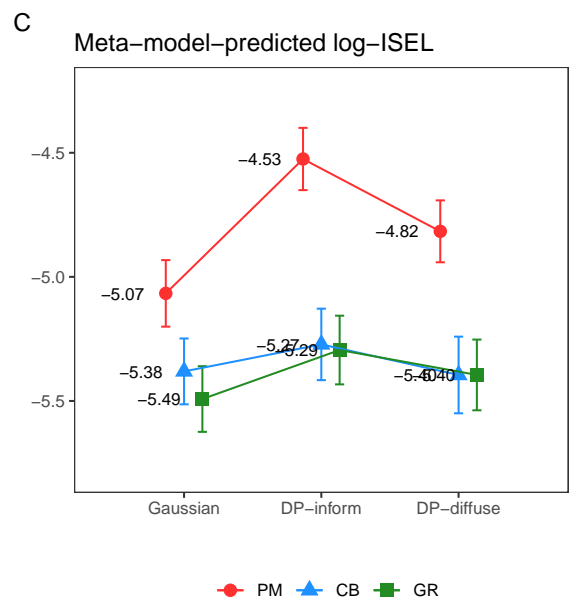
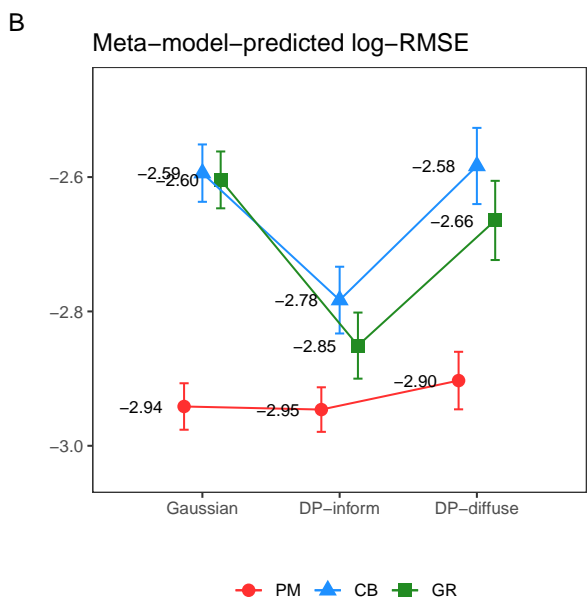
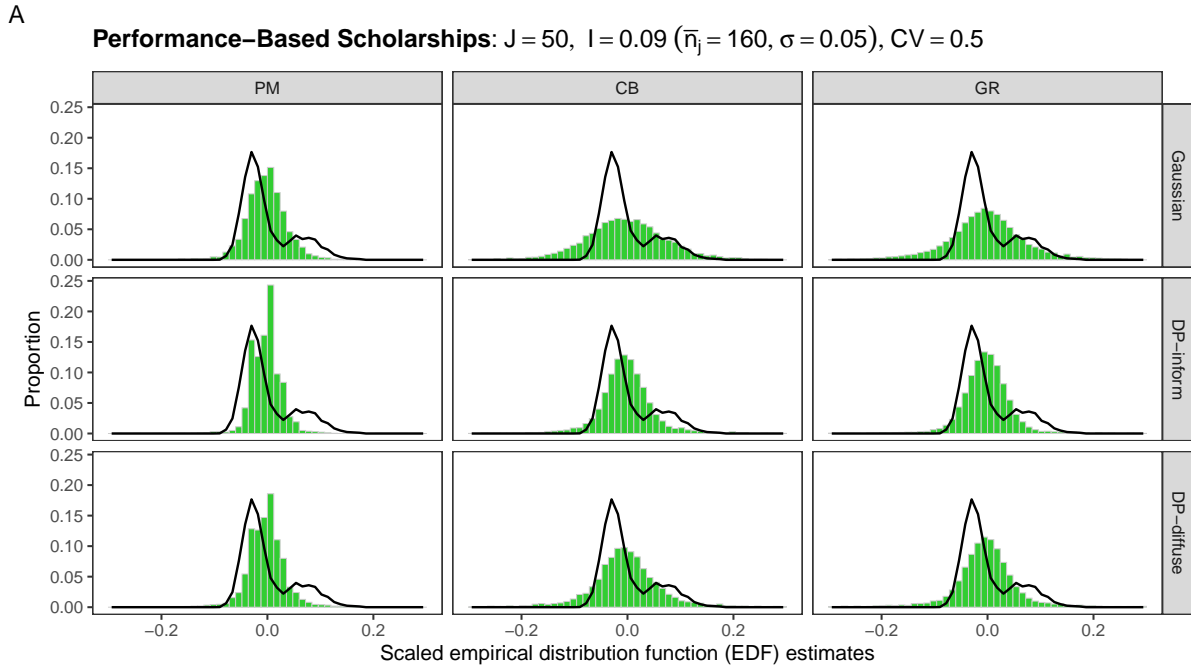
Outcome: WJ-III LW early reading, yr 1, Real Case: $J = 317, I = 0.16 (\bar{n}_j = 11.3, \sigma = 0.27)$

Figure 8: Scaled EDF estimates and meta-model-predicted RMSE and ISEL on log-scale for each model-method combination, when the data-generation is based on the scenario simulating the Head Start Impact Study ($J = 317, \bar{n}_j = 11.3$, and $\sigma = 0.30$ for the outcome, the Woodcock-Johnson III Letter-Word Identification subscale score for year 1). True G is Gaussian mixture, while CV is fixed at 0.5. Plots include 95% prediction intervals around predicted values.

6.3 Case 3: Small between-site information & Large within-site information

Figure 9 presents simulation results for a setting akin to the Performance-Based Scholarships study, characterized by limited between-site information ($J = 39$, $\sigma = 0.05$) but abundant within-site information ($\bar{n}_j = 177.9$). Corresponding studies in Weiss et al. (2017) encompass Career Academies (Figure C.10 in Appendix C), Learning Communities (Figure C.11 in Appendix C), and the Welfare-to-Work Program (Figure C.12 in Appendix C).

In this scenario, the choice of model does not substantially influence performance once a suitable posterior summary method is employed (i.e., PM for RMSE, CB/GR for ISEL). The data-adaptive nature of the DP models is evident; they exhibit less shrinkage than the Gaussian model in Case 2, where σ is large, but more shrinkage in the current scenario, where σ is small, even with the relatively significant within-site information. As demonstrated in Figure 5, the true cross-site impact variation, σ , tends to have a considerable impact on the DP models, particularly when J is moderate to large. In situations where σ is estimated to be very small (i.e., $\sigma \leq 0.10$), Gaussian models may help protect results from excessive shrinkage. Similar patterns are evident in scenarios with $J = 75$ or 100 , such as Enhanced Reading Opportunities (Somers et al., 2010) (Figure C.13 in Appendix C) and Job Corps Program (Schochet et al., 2008) (Figure C.14 in Appendix C).



Outcome: Cumulative total credits earned, yr 3, Real Case: $J = 39, I = 0.1$ ($\bar{n}_j = 177.9, \sigma = 0.05$)

Figure 9: Scaled EDF estimates and meta-model-predicted log-RMSE and ISEL for each model-method combination. Data-generating process based on the Performance-Based Scholarships study ($J = 39, \bar{n}_j = 177.9$, and $\sigma = 0.05$ for the outcome, cumulative total credits earned for year 3). True G is Gaussian mixture, CV is fixed at 0.5. Plots include 95% prediction intervals around predicted values.

7 Results: Real data example

In this section, we apply the strategies discussed in this paper to estimate the distribution of site-specific effects in the Conditional Subsidies for School Attendance program in Bogota, Colombia (Barrera-Osorio et al., 2019). The program conducted two conditional cash transfer (CCT) experiments in the San Cristobal and Suba districts, involving a total of 13,491 participants across 99 sites. In San Cristobal, eligible students in grades 6 to 11 were randomly assigned to a *basic* treatment, *savings* treatment, or control group, whereas, in Suba, eligible participants in grades 9 to 11 were randomly assigned to a *tertiary* treatment or control group. Our analysis focuses on the primary outcomes of secondary school enrollment, secondary school graduation, and tertiary enrollment in any institution or university. Further details can be found in Barrera-Osorio et al. (2019).

The implementation of the two CCT experiments across multiple schools offers a valuable opportunity to examine variation in site-specific treatment effects. To achieve this, we first extract the design characteristics of the multisite trials, presented in Table 1. In San Cristobal, a total of 6,506 participants were nested within 38 sites, with an average site size of 171.2. Site sizes varied considerably, ranging from 23 to 484, with a coefficient of variation (CV) of 0.67 (Figure D.1 in Appendix D). Similarly, in Suba, 1,496 student participants were nested within 27 sites ranging from 19 to 163 students, with an average site size of 55.4 and a CV of 0.63 (Figure D.2 in Appendix D). For San Cristobal, we combine the basic and savings treatments for analysis, resulting in an average treatment rate of 67% within each site. In Suba, 46% of the students within each site were treated on average.

Table 1: Multisite trial design characteristics of the Conditional Subsidies for School Attendance study and estimates of the mean and standard deviation of the distribution of site-specific treatment effects in effect size units.

Outcome:	Basic/Savings experiment		Tertiary experiment	
	On-time secondary enrollment	Secondary graduation	Tertiary enrollment, any time	Tertiary enrollment University
Average treatment effect ($\hat{\tau}_d$)	0.07	0.05	0.08	-0.06
Cross-site effect SD ($\hat{\sigma}_d$)	0.04	0.06	0.08	0.10
Geometric mean of \widehat{se}'_j 's	0.21	0.24	0.35	0.45
Average reliability of $\widehat{\tau}_j(I)$	0.04	0.06	0.05	0.05
Total sample size (N)	6,506		1,496	
Number of sites(J)	38		27	
Average site size (\bar{n}_j)	171.2		55.4	
Coefficient of variation of site sizes (CV)	0.67		0.63	
Range of site sizes	(23, 484)		(19, 163)	
Average proportion of units treated (\bar{p}_j)	0.67		0.46	

Note: Figure D.1 and D.2 in Appendix D provide detailed distributions of n_j and p_j , while Figure D.3 to D.6 in the same Appendix compare outcome means by experimental group across sites for each of the four outcomes presented in Table 1. We excluded sites with extreme probabilities, that is, we required both $n_j p_j$ and $n_j(1-p_j)$ to be at least 8, where n_j represents the site size and p_j denotes the proportion of participants treated in site j .

We then apply the basic Rubin model (Equations (1) and (2)) to estimate the cross-site impact variation (σ) and the sampling variation within sites. Calculating and reporting the average reliability of $\hat{\tau}_j(I)$ for each outcome is essential for assessing data informativeness within and between sites, which in turn helps to identify the optimal model/method combination. Since all four outcomes are binary variables, we summarize the observed site-specific effects using the log odds ratio (logOR), which results in τ and σ estimates on the logOR scale. To facilitate interpretation, we transformed these estimates to the standard mean difference scale, also known as Cohen’s d . Specifically, we used the following formulas for conversion: $\hat{\tau}_d = \widehat{\log\text{OR}} \cdot (\sqrt{3}/\pi)$ to estimate the average treatment effect, and $\hat{\sigma}_d = [\text{Var}(\widehat{\log\text{OR}}) \cdot (3/\pi^2)]^{-1/2}$ to estimate the cross-site effect standard deviation (Borenstein et al., 2009).

San Cristobal’s multisite CCT experiment exhibited small between-site information ($J = 38$, $\sigma = 0.04$ or 0.06) and large within-site information ($\bar{n}_j = 171.2$), as explored in the case study in Section 6.3. The estimated average reliability of $\hat{\tau}_j$ for the San Cristobal experiment were 0.04 and 0.06 for secondary on-time enrollment and graduation, respectively. As in Section 6.3, this led to significant shrinkage toward the prior mean effect τ , making it crucial to select an appropriate model-method combination to control shrinkage and achieve the desired inferential goals.

Figure 10 highlights the considerable differences in the distributions of site-specific effects estimated by the model/method combinations. The posterior mean summary method and the DP-inform model notably shrink estimates more strongly than the other methods and models. Using the case study from Section 6.3, we may be more inclined to trust the distribution estimates produced by the Gaussian or DP-diffuse model and the CB or GR summary methods, as they are less prone to excessive shrinkage in settings like these. Interestingly, the DP-diffuse model preserves the extreme estimates around -0.25 and 0.4 by assigning greater weight to a broad range of possible τ_j values, unlike the other two models.

We also observe that the GR summary method generates smoother site-effect histograms due to its use of quantile estimates.

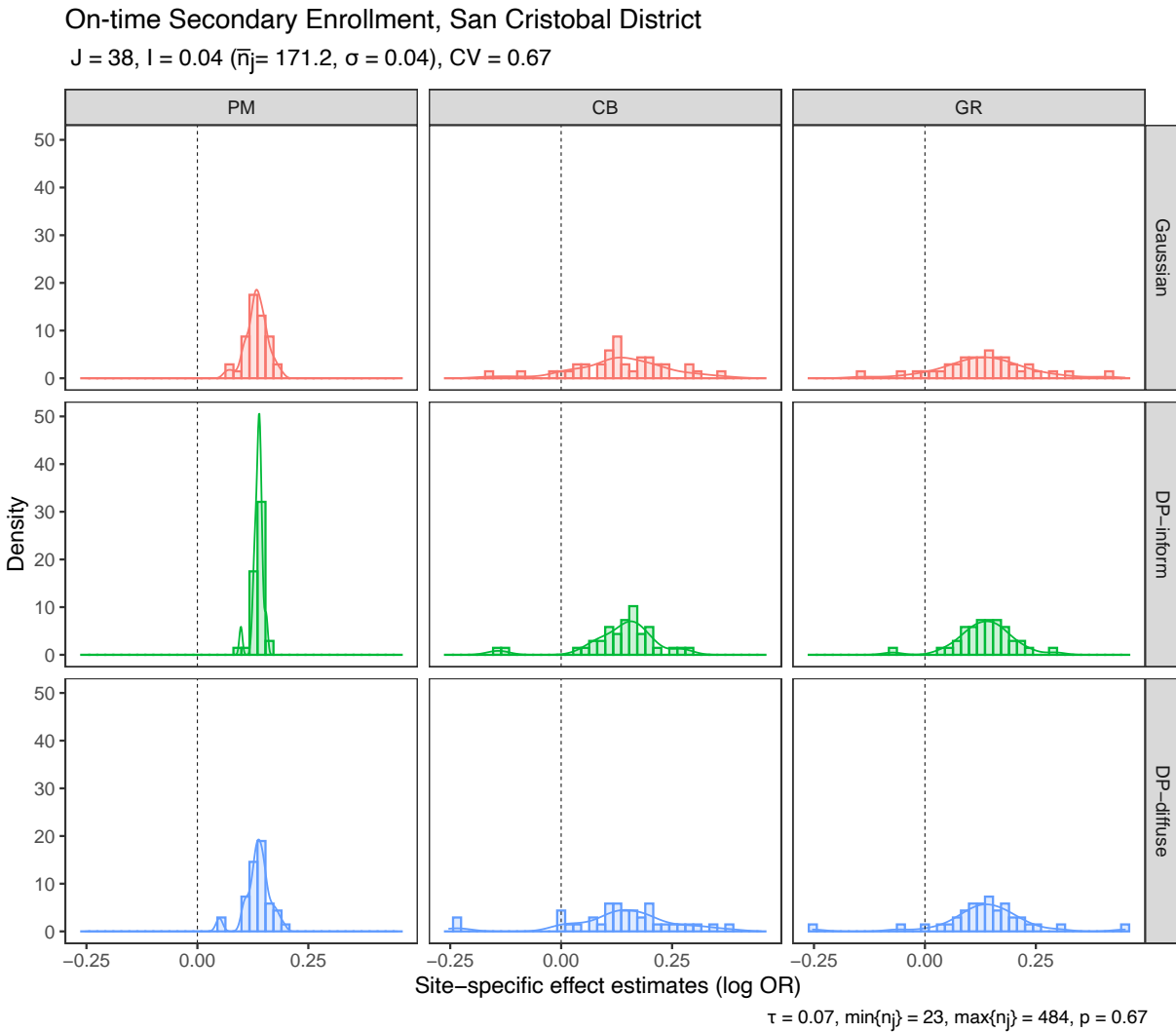


Figure 10: Distribution of site-specific treatment effect estimates on on-time secondary enrollment in San Cristobal district

We additionally conducted a simulated case study based on the San Cristobal experiment scenario, akin to those we have previously discussed. In our simulations, the Gaussian model with the PM and GR summary methods demonstrated the best performance for RMSE and ISEL, respectively (Figure D.10 in Appendix D). As in Section 6.3, the choice

of model did not have a statistically significant impact, while employing a posterior summary method tailored to each inferential goal improved RMSE and ISEL by approximately 10-30% and 46-49%, respectively. Based on these results, we ultimately use the Gaussian model with the PM method to target RMSE and the CB method to accurately represent the distribution of site-specific effects. If extreme effects were expected or of particular interest, we might choose to use the DP-diffuse model instead.

The estimated cross-site standard deviations for the Suba multisite CCT experiment range from 0.08 to 0.10, approximately twice as large as those for the San Cristobal experiment. However, the sites in the Suba trial were only about 30% as large as those in the San Cristobal trial, so the resulting I level remains around 0.05. The overall estimation results demonstrate similar patterns, as shown in Appendix D (Figures D.8 and D.9). For estimating individual site-specific effects, the PM method is optimal, while the GR method is most beneficial when the inferential goal is to recover the distribution of site-specific effects (Figure D.11). In this scenario, there were no statistically significant differences observed between the models, so the simplest Gaussian model could be considered the best choice.

8 Discussion

In the context of multisite randomized trials, there is a growing emphasis on analyzing heterogeneity in site-specific treatment effects. Since a single estimate of the global average effect may mask important site-level variation, it is vital to investigate individual site-specific effect parameters, their distribution across sites, and their rankings. This study primarily aimed to identify optimal approaches for enhancing inferences about site-specific effect estimates to address various inferential goals. We conducted a structured and systematic simulation study evaluating the performance of combinations of two strategies: flexible

prior modeling for G and posterior summary methods designed to minimize specific loss functions. We focused on the low-data environments commonly encountered in multisite trials. Below we discuss the key insights derived from this study.

The most influential factor for all inferential goals was the average reliability of raw site-specific effect estimates, which we have denoted I in this study. In the data analysis stage, researchers should initially estimate the reliability of ML estimates I , as it dictates data informativeness and affects the ideal model-method combination. Increasing \bar{n}_j , which enhances the average precision of the $\hat{\tau}_j$ estimates, significantly improved the results for all three loss functions: RMSE, ISEL, and MSELP. This aligns with insights from the statistical power literature, suggesting that when exploring treatment effect variation, power is predominantly influenced by the number of individuals per site (Raudenbush and Liu, 2000; Spybrook, 2014). Thus, when confronted with budgetary or logistical constraints during the design phase of multisite trials, it is important to prioritize increasing the average number of subjects per site (irrespective of the variation in site sizes) when the focus is on estimating site-specific effects. This holds especially true if the goal is to rank the τ_j values, given that MSELP was only affected by \bar{n}_j and σ .

In scenarios characterized by high data informativeness or a large average reliability of $\hat{\tau}_j$ (I), semiparametric Dirichlet Process (DP) models typically outperform Gaussian models. Numerous studies advocate for the use of flexible DP estimation for G to protect against model misspecification while minimizing the loss of computational efficiency (e.g., Antonelli et al., 2016; Paddock et al., 2006; Paganin et al., 2022). Our results corroborate these conclusions under specific simulation conditions. However, we also found that certain requirements must be satisfied to employ flexible DP priors with a reasonable degree of confidence in practical applications.

First, the performance of DP models is particularly sensitive to the amount of between-site information in the data. For a fixed average site size, the ability of DP models to

recover the distribution of τ_j 's is greatly enhanced by a large σ and a large number of sites, J . Specifically, the level of cross-site impact variation, σ , dramatically alters the DP model's relative performance on ISEL compared to the Gaussian model. The case studies also demonstrated that when the value of I is low (around $I = 0.10$), the estimates of τ_j obtained using the DP models exhibited shrinkage behavior that was sensitive to the value of σ , shrinking less when σ was large and more when σ was small. These results indicate the necessity to assess whether sufficient cross-site information (σ and J) is available to effectively apply semiparametric estimation in practice. Flexible models such as DP models and recent NPML-based deconvolution methods ([Armstrong et al., 2022](#); [Gu and Koenker, 2023](#)) are designed to adapt to cluster-level data, and their mathematical guarantees are asymptotic in nature. Consequently, their suitability for analyzing multisite trial data, where the number of sites is generally small to moderate, must be carefully assessed. In real-world multisite trials, obtaining highly informative data both within and between sites is extremely challenging, requiring researchers to allocate additional resources and attention to the design process.

Second, even in highly informative settings with abundant between-site information, DP priors must be used jointly with targeted posterior summary methods to achieve specific inferential goals. Our simulations demonstrate that, even in highly informative settings, the posterior mean method combined with DP priors consistently outperforms both CB and GR in terms of RMSE, while it is rarely the best estimator for ISEL. We emphasize the joint use of flexible distributions for G and targeted posterior summary methods because estimators that produce optimal estimates of the collection of individual site-specific effects may produce poor estimates of the shape of their distribution, and vice versa.

In scenarios characterized by low-to-moderate data informativeness, typically observed in multisite trials with an average reliability level of less than approximately 0.20, the choice of prior model for G is less important than selecting an appropriate posterior summary

method. In simulations under these conditions, the Gaussian model combined with a suitable posterior summary method performed on par with the DP models, even when the true data-generating distribution was non-Gaussian. Generally, uninformative data leads to considerable shrinkage, irrespective of the model. Therefore, targeting the posterior summary to the metric of interest is more important than choosing a specific model.

In practice, researchers may prefer Gaussian models in uninformative settings. While the performance of DP models is data-adaptive and insensitive to the choice of prior on α when sufficient information is available, the choice of prior can substantially affect the degree of shrinkage in uninformative settings. As a result, the Gaussian model offers a somewhat less assumption-heavy approach for estimation, which may be preferable in such cases.

This research presents several notable limitations. First, we chose to exclude site-level covariates in the data-generating and data-analytic scenarios. Covariates would generally improve the precision of site-specific estimates, effectively leading to increased values of \bar{n}_j . More generally, if covariates moderate treatment effects and are unevenly distributed between sites (Lu et al., 2023), it becomes important to shrink toward a predicted value based on site-level covariates, rather than toward the overall mean. Consequently, it is a valuable avenue of inquiry to examine how the two strategies for improving inferences for a distribution of τ_j perform or fail in scenarios where shrinkage occurs misleadingly toward the overall mean, despite the presence of meaningful site-level moderators.

Another limitation of this study is the assumption that site size is independent of site-specific treatment effects, i.e., zero correlation between τ_j and \widehat{se}_j^2 in our data-generation and analytic methods. In general, smaller school sites may be less (or more) efficient than larger school sites in implementing efficacious interventions and thus tend to have smaller (or larger) τ_j values (Angrist et al., 2022). One advantage of the Bayesian model-based approach is the ability to estimate models with and without restrictions on the bivariate

distribution of τ_j and \widehat{se}_j^2 , and assess the sensitivity of site-specific effect estimates to this assumption. Alternatively, we can treat \widehat{se}_j^2 as a covariate in the conditional distribution of G , or apply [Brown \(2008\)](#)'s variance-stabilizing transform to τ_j to achieve approximately constant sampling variance. It would also be interesting to investigate whether different estimation strategies, when relaxing these assumptions, yield comparable results.

While the RMSE, ISEL, and MSELP metrics are popular and straightforward, they also have limitations. Both RMSE and ISEL are scale-dependent, meaning that multiplying all τ_j and $\widehat{\tau}_j$ values by a constant c results in a corresponding multiplication of RMSE and ISEL by c . This characteristic complicates the comparison of these metrics across datasets with varying levels of dispersion, such as different σ values. Alternative metrics for assessing the differences between the true and estimated EDFs of site-level effects could also be explored. By squaring the difference between EDFs, the ISEL metric disproportionately penalizes large discrepancies in EDFs, which may not be suitable for some applications.⁶

In conclusion, no single estimation strategy universally excels across varied data scenarios and inferential goals. Flexible semiparametric models are not a panacea, given the complex interplay between study design characteristics and modeling choices. Researchers should carefully select methods tailored to their specific inferential goals, taking into account the amount of within-site and between-site information. Ideally, multisite trials should be prospectively designed to address inferential goals related to site-specific treatment effects.

⁶Although not included in this paper, we also evaluated the integrated absolute error loss (IAEL = $\int |(A(t) - G_J(t))| dt$) and the Kolmogorov-Smirnov statistic (KS = $\max_t |A(t) - G_J(t)|$). However, these assessments did not yield significant differences in the overall results.

References

- Angrist, J., Hull, P., and Walters, C. R. (2022). Methods for measuring school effectiveness. Technical Report Working Paper No. 30803, National Bureau of Economic Research.
- Angrist, J. D., Hull, P. D., Pathak, P. A., and Walters, C. R. (2017). Leveraging lotteries for school value-added: Testing and estimation. *The Quarterly Journal of Economics*, 132(2):871–919.
- Antonelli, J., Trippa, L., and Haneuse, S. (2016). Mitigating bias in generalized linear mixed models: The case for bayesian nonparametrics. *Statistical science: a review journal of the Institute of Mathematical Statistics*, 31(1):80.
- Antoniak, C. E. (1974). Mixtures of dirichlet processes with applications to bayesian non-parametric problems. *The Annals of Statistics*, 2(6):1152–1174.
- Armstrong, T. B., Kolesár, M., and Plagborg-Møller, M. (2022). Robust empirical bayes confidence intervals. *Econometrica*, 90(6):2567–2602.
- Barrera-Osorio, F., Linden, L. L., and Saavedra, J. E. (2019). Medium-and long-term educational consequences of alternative conditional cash transfer designs: Experimental evidence from colombia. *American Economic Journal: Applied Economics*, 11(3):54–91.
- Bloom, H. S., Raudenbush, S. W., Weiss, M. J., and Porter, K. (2017). Using multisite experiments to study cross-site variation in treatment effects: A hybrid approach with fixed intercepts and a random treatment coefficient. *Journal of Research on Educational Effectiveness*, 10(4):817–842.
- Bloom, H. S. and Weiland, C. (2015). Quantifying variation in head start effects on young children’s cognitive and socio-emotional skills using data from the national head start impact study. Technical report, MDRC, New York, NY.
- Boomsma, A. (2013). Reporting monte carlo studies in structural equation modeling. *Structural Equation Modeling: A Multidisciplinary Journal*, 20(3):518–540.
- Borenstein, M., Hedges, L. V., Higgins, J. P., and Rothstein, H. R. (2009). Converting among effect sizes. In *Introduction to Meta-Analysis*, chapter 7, pages 45–49. John Wiley & Sons, Ltd. DOI: <https://doi.org/10.1002/9780470743386.ch7>.
- Brown, L. D. (2008). In-season prediction of batting averages: A field test of empirical bayes and bayes methodologies. *Annals of Applied Statistics*, 2(1):113–152.
- Chetty, R., Friedman, J. N., and Rockoff, J. E. (2014a). Measuring the impacts of teachers i: Evaluating bias in teacher value-added estimates. *American economic review*, 104(9):2593–2632.

- Chetty, R., Friedman, J. N., and Rockoff, J. E. (2014b). Measuring the impacts of teachers ii: Teacher value-added and student outcomes in adulthood. *American economic review*, 104(9):2633–2679.
- Congdon, P. D. (2020). *Bayesian Hierarchical Models: With Applications Using R*. CRC Press, 2 edition.
- Conlon, E. and Louis, T. (1999). Addressing multiple goals in evaluating region-specific risk using bayesian methods. *Disease mapping and risk assessment for public health*, pages 31–47.
- DerSimonian, R. and Laird, N. (1986). Meta-analysis in clinical trials. *Controlled clinical trials*, 7(3):177–188.
- Dorazio, R. M. (2009). On selecting a prior for the precision parameter of dirichlet process mixture models. *Journal of Statistical Planning and Inference*, 139(9):3384–3390.
- Dunson, D. B., Pillai, N., and Park, J.-H. (2007). Bayesian density regression. *Journal of the Royal Statistical Society Series B: Statistical Methodology*, 69(2):163–183.
- Efron, B. (2014). Two modeling strategies for empirical bayes estimation. *Statistical science: a review journal of the Institute of Mathematical Statistics*, 29(2):285.
- Efron, B. (2016). Empirical bayes deconvolution estimates. *Biometrika*, 103(1):1–20.
- Escobar, M. D. and West, M. (1995). Bayesian density estimation and inference using mixtures. *Journal of the American Statistical Association*, 90(430):577–588.
- Gelman, A. (2006). Prior distributions for variance parameters in hierarchical models. *Bayesian Analysis*, 1(3):515–533.
- Gelman, A., Carlin, J. B., Stern, H. S., Dunson, D. B., Vehtari, A., and Rubin, D. B. (2013). *Bayesian Data Analysis*. Chapman and Hall/CRC, 3rd edition.
- Ghidey, W., Lesaffre, E., and Eilers, P. (2004). Smooth random effects distribution in a linear mixed model. *Biometrics*, 60(4):945–953.
- Ghosh, M. (1992). Constrained bayes estimation with applications. *Journal of the American Statistical Association*, 87(418):533–540.
- Gilraine, M., Gu, J., and McMillan, R. (2020). A new method for estimating teacher value-added. Technical report, National Bureau of Economic Research.
- Goldstein, H. and Spiegelhalter, D. J. (1996). League tables and their limitations: statistical issues in comparisons of institutional performance. *Journal of the Royal Statistical Society: Series A (Statistics in Society)*, 159(3):385–409.

- Gu, J. and Koenker, R. (2023). Invidious comparisons: Ranking and selection as compound decisions. *Econometrica*, 91(1):1–41.
- Harris, D. N. and Sass, T. R. (2014). Skills, productivity and the evaluation of teacher performance. *Economics of Education Review*, 40:183–204.
- Ishwaran, H. and Zarepour, M. (2000). Markov chain monte carlo in approximate dirichlet and beta two-parameter process hierarchical models. *Biometrika*, 87(2):371–390.
- Jiang, W. and Zhang, C.-H. (2009). General maximum likelihood empirical bayes estimation of normal means. *The Annals of Statistics*, 37(4):1647–1684.
- Kline, P., Rose, E. K., and Walters, C. R. (2022). Systemic discrimination among large us employers. *The Quarterly Journal of Economics*, 137(4):1963–2036.
- Koenker, R. and Mizera, I. (2014). Convex optimization, shape constraints, compound decisions, and empirical bayes rules. *Journal of the American Statistical Association*, 109(506):674–685.
- Kontopantelis, E. and Reeves, D. (2012). Performance of statistical methods for meta-analysis when true study effects are non-normally distributed: A comparison between dersimonian–laird and restricted maximum likelihood. *Statistical Methods in Medical Research*, 21(6):657–659.
- Laird, N. (1978). Nonparametric maximum likelihood estimation of a mixing distribution. *Journal of the American Statistical Association*, 73(364):805–811.
- Leslie, D. S., Kohn, R., and Nott, D. J. (2007). A general approach to heteroscedastic linear regression. *Statistics and Computing*, 17:131–146.
- Liu, J. and Dey, D. K. (2008). Skew random effects in multilevel binomial models: an alternative to nonparametric approach. *Statistical modelling*, 8(3):221–241.
- Lockwood, J., Castellano, K. E., and Shear, B. R. (2018). Flexible bayesian models for inferences from coarsened, group-level achievement data. *Journal of Educational and Behavioral Statistics*, 43(6):663–692.
- Lockwood, J., Louis, T. A., and McCaffrey, D. F. (2002). Uncertainty in rank estimation: Implications for value-added modeling accountability systems. *Journal of educational and behavioral statistics*, 27(3):255–270.
- Louis, T. A. (1984). Estimating a population of parameter values using bayes and empirical bayes methods. *Journal of the American Statistical Association*, 79(386):393–398.
- Lu, B., Ben-Michael, E., Feller, A., and Miratrix, L. (2023). Is it who you are or where you are? accounting for compositional differences in cross-site treatment effect variation. *Journal of Educational and Behavioral Statistics*, 48(4):420–453.

- Marshall, E. and Spiegelhalter, D. (2007). Identifying outliers in bayesian hierarchical models: a simulation-based approach. *Bayesian Analysis*, 2(2):409–444.
- Marshall, E. C. and Spiegelhalter, D. J. (1998). Comparing institutional performance using markov chain monte carlo methods. *Statistical analysis of medical data: new developments*, pages 229–249.
- McCulloch, C. E. and Neuhaus, J. M. (2011). Misspecifying the shape of a random effects distribution: Why getting it wrong may not matter. *Statistical Science*, pages 388–402.
- Meager, R. (2019). Understanding the average impact of microcredit expansions: A bayesian hierarchical analysis of seven randomized experiments. *American Economic Journal: Applied Economics*, 11(1):57–91.
- Miratrix, L. W., Weiss, M. J., and Henderson, B. (2021). An applied researcher’s guide to estimating effects from multisite individually randomized trials: Estimands, estimators, and estimates. *Journal of Research on Educational Effectiveness*, 14(1):270–308.
- Mislevy, R. J., Beaton, A. E., Kaplan, B., and Sheehan, K. M. (1992). Estimating population characteristics from sparse matrix samples of item responses. *Journal of Educational Measurement*, 29(2):133–161.
- Mogstad, M., Romano, J. P., Shaikh, A., and Wilhelm, D. (2020). Inference for ranks with applications to mobility across neighborhoods and academic achievement across countries. Technical report, National Bureau of Economic Research.
- Mountjoy, J. and Hickman, B. R. (2021). The returns to college (s): Relative value-added and match effects in higher education. Technical report, National Bureau of Economic Research.
- Murugiah, S. and Sweeting, T. (2012). Selecting the precision parameter prior in dirichlet process mixture models. *Journal of Statistical Planning and Inference*, 142(7):1947–1959.
- Normand, S.-L. T., Ash, A. S., Fienberg, S. E., Stukel, T. A., Utts, J., and Louis, T. A. (2016). League tables for hospital comparisons. *Annual Review of Statistics and Its Application*, 3:21–50.
- Ohlssen, D. I., Sharples, L. D., and Spiegelhalter, D. J. (2007). A hierarchical modelling framework for identifying unusual performance in health care providers. *Journal of the Royal Statistical Society: Series A (Statistics in Society)*, 170(4):865–890.
- Paddock, S. M., Ridgeway, G., Lin, R., and Louis, T. A. (2006). Flexible distributions for triple-goal estimates in two-stage hierarchical models. *Computational statistics & data analysis*, 50(11):3243–3262.
- Padilla, C. M. (2020). Beyond just the average effect: Variation in head start treatment effects on parenting behavior. *AERA Open*, 6(4):2332858420969691.

- Paganin, S., Paciorek, C. J., Wehrhahn, C., Rodríguez, A., Rabe-Hesketh, S., and de Valpine, P. (2022). Computational strategies and estimation performance with bayesian semiparametric item response theory models. *Journal of Educational and Behavioral Statistics*, page 10769986221136105.
- Paxton, P., Curran, P. J., Bollen, K. A., Kirby, J., and Chen, F. (2001). Monte carlo experiments: Design and implementation. *Structural Equation Modeling*, 8(2):287–312.
- Pinheiro, J. C., Liu, C., and Wu, Y. N. (2001). Efficient algorithms for robust estimation in linear mixed-effects models using the multivariate t distribution. *Journal of Computational and Graphical Statistics*, 10(2):249–276.
- Puma, M., Bell, S., Cook, R., Heid, C., Shapiro, G., Broene, P., Jenkins, F., et al. (2010). Head start impact study. final report. Technical report, Administration for Children & Families.
- Rabe-Hesketh, S., Pickles, A., and Skrondal, A. (2003). Correcting for covariate measurement error in logistic regression using nonparametric maximum likelihood estimation. *Statistical Modelling*, 3(3):215–232.
- Rabe-Hesketh, S. and Skrondal, A. (2022). *Multilevel and Longitudinal Modeling Using Stata, Volume I: Continuous Responses*. Stata Press, College Station, TX, 4 edition.
- Raudenbush, S. W. and Bloom, H. S. (2015). Learning about and from a distribution of program impacts using multisite trials. *American Journal of Evaluation*, 36(4):475–499.
- Raudenbush, S. W. and Bryk, A. S. (1985). Empirical bayes meta-analysis. *Journal of educational statistics*, 10(2):75–98.
- Raudenbush, S. W. and Liu, X. (2000). Statistical power and optimal design for multisite randomized trials. *Psychological methods*, 5(2):199.
- Robbins, H. (1951). Asymptotically subminimax solutions of compound statistical decision problems. In *Proceedings of the second Berkeley symposium on mathematical statistics and probability*, volume 2, pages 131–149. University of California Press.
- Rosenbaum, P. R. and Rubin, D. B. (1983). The central role of the propensity score in observational studies for causal effects. *Biometrika*, 70(1):41–55.
- Rubin, D. B. (1981). Estimation in parallel randomized experiments. *Journal of Educational Statistics*, 6(4):377–401.
- Rubio-Aparicio, M., Marin-Martinez, F., Sanchez-Meca, J., and Lopez-Lopez, J. A. (2018). A methodological review of meta-analyses of the effectiveness of clinical psychology treatments. *Behavior Research Methods*, 50:2057–2073.

- Sabol, T. J., McCoy, D., Gonzalez, K., Miratrix, L., Hedges, L., Spybrook, J. K., and Weiland, C. (2022). Exploring treatment impact heterogeneity across sites: Challenges and opportunities for early childhood researchers. *Early Childhood Research Quarterly*, 58:14–26.
- Schochet, O. N. and Padilla, C. M. (2022). Children learning and parents earning: Exploring the average and heterogeneous effects of head start on parental earnings. *Journal of Research on Educational Effectiveness*, 15(3):413–444.
- Schochet, P. Z., Burghardt, J., and McConnell, S. (2008). Does job corps work? impact findings from the national job corps study. *American economic review*, 98(5):1864–1886.
- Shen, W. and Louis, T. A. (1998). Triple-goal estimates in two-stage hierarchical models. *Journal of the Royal Statistical Society: Series B (Statistical Methodology)*, 60(2):455–471.
- Shen, W. and Louis, T. A. (1999). Empirical bayes estimation via the smoothing by roughening approach. *Journal of Computational and Graphical Statistics*, 8(4):800–823.
- Skrondal, A. (2000). Design and analysis of monte carlo experiments: Attacking the conventional wisdom. *Multivariate Behavioral Research*, 35(2):137–167.
- Somers, M.-A., Corrin, W., Sepanik, S., Salinger, T., Levin, J., and Zmach, C. (2010). The enhanced reading opportunities study final report: The impact of supplemental literacy courses for struggling ninth-grade readers. NCEE Report 2010-4021, U.S. Department of Education, Institute of Education Sciences, National Center for Education Evaluation and Regional Assistance.
- Spybrook, J. (2014). Detecting intervention effects across context: An examination of the precision of cluster randomized trials. *The Journal of Experimental Education*, 82(3):334–357.
- Spybrook, J. and Raudenbush, S. W. (2009). An examination of the precision and technical accuracy of the first wave of group-randomized trials funded by the institute of education sciences. *Educational Evaluation and Policy Analysis*, 31(3):298–318.
- Stefanski, L. A. and Carroll, R. J. (1990). Deconvolving kernel density estimators. *Statistics*, 21(2):169–184.
- Stuart, E. A., Cole, S. R., Bradshaw, C. P., and Leaf, P. J. (2011). The use of propensity scores to assess the generalizability of results from randomized trials. *Journal of the Royal Statistical Society: Series A (Statistics in Society)*, 174(2):369–386.
- Tipton, E. and Olsen, R. B. (2018). A review of statistical methods for generalizing from evaluations of educational interventions. *Educational Researcher*, 47(8):516–524.

- Tipton, E., Spybrook, J., Fitzgerald, K. G., Wang, Q., and Davidson, C. (2021). Toward a system of evidence for all: Current practices and future opportunities in 37 randomized trials. *Educational Researcher*, 50(3):145–156.
- Verbeke, G. and Lesaffre, E. (1996). A linear mixed-effects model with heterogeneity in the random-effects population. *Journal of the American Statistical Association*, 91(433):217–221.
- Weiss, M. J., Bloom, H. S., Verbitsky-Savitz, N., Gupta, H., Vigil, A. E., and Cullinan, D. N. (2017). How much do the effects of education and training programs vary across sites? evidence from past multisite randomized trials. *Journal of Research on Educational Effectiveness*, 10(4):843–876.
- Word, E. et al. (1990). *Student/Teacher Achievement Ratio (STAR) Tennessee's K-3 Class Size Study. Final Summary Report 1985-1990*. Tennessee State Department of Education.

Appendix A Estimator and model details

A.1 Constrained Bayes (CB) estimator

The choice of rescaling for the CB estimator is derived as follows. [Shen and Louis \(1998\)](#) showed that the optimal EDF estimator that minimizes the ISEL in equation (9) is

$$\bar{G}_J = E[G_J(t) | \hat{\boldsymbol{\tau}}] = \frac{1}{J} \cdot \sum \Pr(\tau_j \leq t | \hat{\tau}_j) \quad (\text{A.1})$$

where $\hat{\boldsymbol{\tau}} = (\hat{\tau}_1, \dots, \hat{\tau}_J)$. Let the posterior mean of τ_j , $E(\tau_j | \hat{\tau}_j)$, be η_j and the posterior variance of τ_j , $\text{Var}(\tau_j | \hat{\tau}_j)$, be λ_j . Then, the marginal mean of \bar{G}_J and the finite population version of the marginal variance of \bar{G}_J can be written as follows ([Shen and Louis, 1998](#)):

$$E[\bar{G}_J] = \int t d\bar{G}_J(t) = \frac{\sum \eta_j}{J} = \bar{\eta}, \quad (\text{A.2})$$

$$\widehat{\text{Var}}[\bar{G}_J] = \int t^2 d\bar{G}_J(t) - \bar{\eta}^2 = \frac{\sum \lambda_j}{J} + \frac{\sum (\eta_j - \bar{\eta})^2}{J - 1}. \quad (\text{A.3})$$

The finite population variance of posterior means η_j appears in the second term of equation (A.3). PMs tend to be under-dispersed because their variance lacks the first term in the estimated marginal variance of \bar{G}_J , $\sum \lambda_j / J$. The goal of the CB estimator is to adjust the posterior means to have a variance equal to the estimated marginal variance specified in equation (A.3). As a result, the CB estimate a_j^{CB} is defined as follows ([Ghosh, 1992](#)):

$$a_j^{CB} = \bar{\eta} + (\eta_j - \bar{\eta}) \cdot \sqrt{1 + \frac{J^{-1} \sum \lambda_j}{(J - 1)^{-1} \sum (\eta_j - \bar{\eta})^2}}. \quad (\text{A.4})$$

A.2 Triple-goal (GR) estimator

The triple-goal estimator aims to obtain a single set of estimates that simultaneously targets all three inferential goals. In practice, however, the triple-goal estimator is designed to minimize the losses for two of the goals: estimating the EDF of τ_j values, G_J , and estimating the rank of τ_j , R_j . The abbreviation “GR” reflects the two direct inferential targets and is often used to denote the triple-goal estimator in the literature (e.g., [Paddock et al., 2006](#)).

[Shen and Louis \(1998\)](#) show that $\bar{G}_J(t)$ minimizes the expected ISEL, which is the loss function that targets the EDF of τ_j values. The GR estimator therefore uses the sample estimate of $\bar{G}_J(t)$ to minimize ISEL. To parallel the EDF estimates made using PMs or the CB estimator, the sample estimate of $\bar{G}_J(t)$ is then discretized to contain only J mass points.

Similarly, some basic calculus shows us that the posterior expected ranks $\bar{R}_j = \sum_{k=1}^J \Pr(\tau_j \leq \tau_k | \hat{\boldsymbol{\tau}})$ minimize MSELR. The GR estimator therefore ranks sites using the sample estimated ranks to minimize MSELR. Again, to parallel the EDF estimates made using PMs or the CB estimator, the sample estimated ranks are discretized to J discrete rank values.

As a result, the GR estimator intuitively minimizes both ISEL and MSELR, since it makes use of optimal estimators for both metrics. The GR estimator pays no explicit attention to reducing the MSEL of the individual site-specific parameters τ_j . However, [Shen and Louis \(1998\)](#) argued that the GR estimator tends to produce small MSEL for the individual τ_j 's because assigning the \hat{U} values by a permutation vector \mathbf{z} to minimize $\sum (\hat{U}_{z_j} - \eta_j)^2$ results in the same assignments as assigning them to minimize $\sum (a_j - \eta_j)^2$. Regardless, the focus of the GR estimator is on estimating the EDF and ranks of τ_j 's. Thus, it remains an open question whether it performs well in estimating the individual site-specific parameters under various conditions.

A.3 Dirichlet process priors

G_0 provides an initial best guess of the shape of the prior distribution G , which is commonly taken to be a Gaussian distribution in practice. The precision parameter α then controls the degree of shrinkage of G to G_0 . In other words, α determines the extent to which distributions in the sample space partitioned into measurable subsets G_1, \dots, G_s are divergent from G_0 . To understand the role of G_0 and α more intuitively, it is helpful to refer to a form of the induced prior distribution on the site-specific parameter τ_j , so-called the *Polya urn scheme* (Dunson et al., 2007):

$$\tau_j | G_0, \alpha, \tau_1, \dots, \tau_{j-1} \sim \left(\frac{\alpha}{\alpha + j - 1} \right) \cdot G_0 + \left(\frac{1}{\alpha + j - 1} \right) \cdot \sum_{k=1}^{j-1} \delta(\tau_k), \quad (\text{A.5})$$

where $\delta(\tau_k)$ denotes a point mass at τ_k . This conditional prior distribution for τ_j is a weighted mixture of the base distribution G_0 and probability masses at the previous site's parameter values, that is, the EDF of $(\tau_1, \dots, \tau_{j-1})$. In this scheme, the first site's treatment effect τ_1 is drawn from G_0 . Then the second site's treatment effect τ_2 is drawn from G_0 with probability of $\alpha/(\alpha + 1)$ or a new empirical distribution $\delta(\tau_1)$ with probability of $1/(\alpha + 1)$. This sampling rule continues, and for the j th site, τ_j is drawn from G_0 with probability proportional to $j - 1$, the number of previous sites which already have realized site-specific parameters, or is sampled from the new empirical distribution of $\sum_{k=1}^{j-1} \delta(\tau_k)$ with probability proportional to α (Gelman et al., 2013).

α can be viewed as a prior sample size in some sense (Gelman et al., 2013), as opposed to the sample size of empirical data J . Thus, a huge α value implies an extreme weight on the (prior) base distribution G_0 . In that case, the joint distribution of τ_j 's tends to be the product of J independent draws from G_0 (Antonelli et al., 2016) and the second-stage model in equation (14) converges to the Rubin (1981) model with a Gaussian prior. On the other hand, a zero α value imposes a null weight on G_0 , which leads to the distribution

of τ_j being a point mass of $\delta(\tau_1)$. Then, the second-stage model in equation (14) collapses to a model with all sites sharing the common value of τ_1 .

Hence, we can infer that α determines the number of distinct values of τ_j , often referred to as the unique number of *clusters* K generated by the DP. The K is not necessarily an exact representation of the number of *mixture components* C (latent subpopulation with substantive meaning) as specified in finite mixture models, but K can be considered as an upper bound of the C (Ishwaran and Zarepour, 2000). The expected number of K is a function of α and J , given by the sum of the weights of G_0 in equation (A.5) over all J sites:

$$E(K|G_0, \alpha, J) = \sum_{j=1}^J \frac{\alpha}{\alpha + j - 1}. \quad (\text{A.6})$$

The hyper prior for α plays an essential role in determining the expected number of clusters and therefore in controlling the posterior distribution over clusters. In practice, it is a standard approach to use a Gamma(a, b) distribution with fixed hyperparameters, the shape parameter a and the rate parameter b , to capture the uncertainty in α (Escobar and West, 1995). A key issue is whether the choice of a and b may have a substantial impact on the posterior distribution of α , and in turn on the clustering behavior. There exist a group of studies arguing that the choice of hyperparameters is a less of concern because the data tend to be quite informative, resulting in a concentrated posterior even with a high variance prior for α (Leslie et al., 2007; Gelman et al., 2013). On the other hand, another group of studies report that estimation or inference can be sensitive to the specific choice of the hyperparameters and in general to the strategies for selecting α (Dorazio, 2009; Paddock et al., 2006; Murugiah and Sweeting, 2012). Our interest is to evaluate the sensitivity under two different options, diffuse and informative DP priors, particularly in the context of recovering the EDF of τ_j 's.

The first option is to specify a diffuse Gamma distribution when a priori knowledge on α or K is absent. [Antonelli et al. \(2016\)](#) chose values of a and b such that α is centered between 1 and J with a large variance to assign a priori mass to a wide range of α values. If $J = 50$, for example, we can assign 25 as the mean of the α distribution and 250 as a variance which is ten times the magnitude of the mean. Given these a priori values for the mean and variance of α , we can obtain the corresponding values of $a = 2.5$ and $b = 0.1$ based on the moments of a Gamma distribution: $E(\alpha|a, b) = a/b$ and $\text{Var}(\alpha|a, b) = a/b^2$.

This study suggests the second option, using χ^2 distribution to construct an informative prior for α . This strategy is based on the probability mass function for the prior distribution of K induced by a $\text{Gamma}(a, b)$ prior for α and the number of sites J ([Dorazio, 2009](#); [Antonelli et al., 2016](#)):

$$\Pr(K|J, a, b) = \frac{b^a \cdot S_1(J, K)}{\Gamma(a)} \cdot \int_0^\infty \frac{\alpha^{K+a-1} \cdot \exp(-b\alpha) \cdot \Gamma(\alpha)}{\Gamma(\alpha + J)} d\alpha, \quad (\text{A.7})$$

where $S_1(J, K)$ is the unsigned Stirling number of the first kind and $K = 1, \dots, J$. Suppose $\Pr(K)$ that encodes our prior information for the distribution of the expected number of clusters K . We can obtain a solution for a and b by minimizing the discrepancy between the encoded prior $\Pr(K)$ and the α -induced prior $\Pr(K|J, a, b)$, defined by the following Kullback-Leibler (KL) divergence measure:

$$D_{\text{KL}}(a, b) = \sum_{K=1}^J \Pr(K) \cdot \log \left\{ \frac{\Pr(K)}{\Pr(K|J, a, b)} \right\}. \quad (\text{A.8})$$

[Dorazio \(2009\)](#) proposed specifying a and b to be the values for which $\Pr(K|J, a, b)$ most closely matches the discrete uniform distribution to reflect the absence of explicit prior information. This method attempts to mimic a noninformative prior for K .

Our proposal is to take $\Pr(K) \sim \chi^2(\text{df} = u)$ to more intuitively encode our prior knowledge on the expected number of clusters K and its uncertainty. The χ^2 distribution

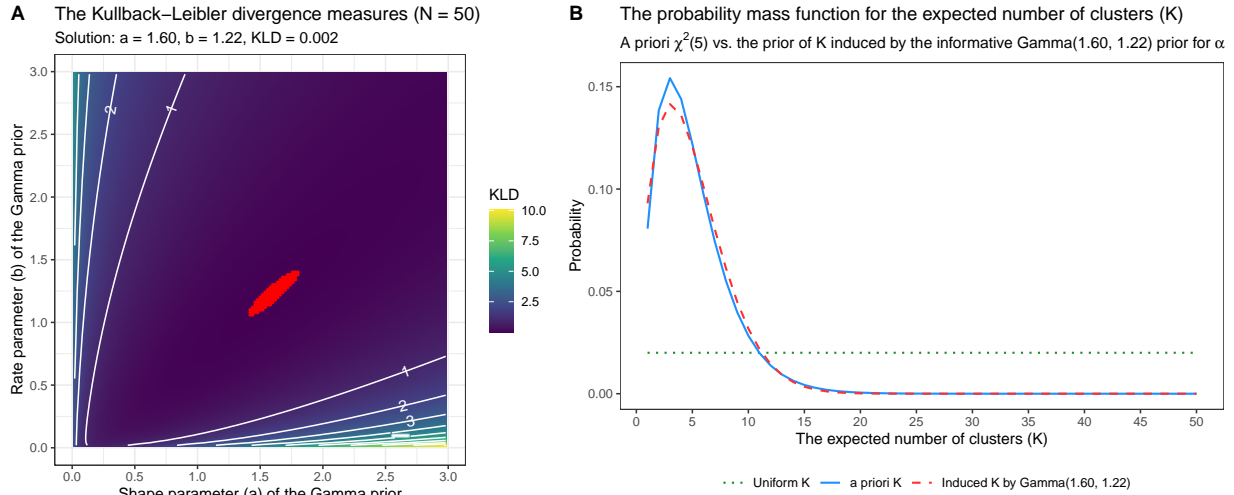


Figure A.1: The derivation of the informative prior for the precision parameter α by approximating a $\text{Gamma}(a, b)$ to $\chi^2(5)$. *Note:* The area highlighted by red dots corresponds to the region where the KL divergence measures are minimized.

has only one parameter: a positive integer u that specifies the number of degrees of freedom. Our framework is mainly motivated by the feature of the χ^2 distribution that its mean and variance are u and $2u$, respectively. If it is expected that there are approximately five clusters ($K = 5$) and $J = 50$, then one can simply assume that $\text{Pr}(K)$ follows $\chi^2(5)$ distribution and specify a $\text{Gamma}(a, b)$ that closely matches $\chi^2(5)$ using equation (A.7) and (A.8). Panel A of Figure A.1 shows the result of the numerical analysis based on a grid search algorithm designed to identify the global minimum of the KL divergence measure defined in equation (A.8). The Gamma distribution with $(a, b) = (1.60, 1.22)$ obtained as the solution that minimizes the KL closely matches the $\chi^2(5)$ distribution as shown in Panel B of Figure A.1. This strategy is useful for constructing an informative prior for K , particularly when one wants to impose near-zero probabilities beyond a certain threshold ($K = 25$ in the example shown in Figure A.1) and to be clear about the prior mean and variance of K .

Appendix B Simulation details

B.1 Connecting sampling errors to site sizes

For a simple design-based estimator for site-specific effects $\hat{\tau}_j$, the sampling variation of each $\hat{\tau}_j$ around its true effect τ_j within sites will be approximately

$$\widehat{se}_j^2 = \frac{1}{n_j} \cdot \left(\frac{1}{p_j} + \frac{1}{1-p_j} \right) \cdot \text{Var}(Y) \cdot (1 - R^2) \quad (\text{B.1})$$

where n_j is sample size at site j and p_j is the proportion of units treated in site j , which [Rosenbaum and Rubin \(1983\)](#) refer to as the *propensity score*. $\text{Var}(Y)$ represents the assumed constant variation in outcome for a given treatment arm in a given site. R^2 is the explanatory power of level-1 covariates. This expression is Neyman’s classic formula under the assumption of homoskedasticity ([Miratrix et al., 2021](#)).

In effect size units, $\text{Var}(Y) = 1$. If we further assume constant proportion treated, for convenience, we have

$$\widehat{se}_j^2 = \frac{1}{n_j} \cdot \left(\frac{1}{p} + \frac{1}{1-p} \right) \cdot (1 - R^2) = \frac{1}{n_j} \kappa \quad (\text{B.2})$$

for some constant κ . If $p = 0.5$ and $R^2 = 0.6$ with a reasonable pre-test score, $\kappa = 2.4$. Without level-1 covariates, κ equals 4. Now we can obtain a vector of simulated \widehat{se}_j^2 's, denoted as \hat{E} , by directly controlling two constants, p and R^2 , and one variable, n_j . Our data-generating function for \hat{E} follows this relationship assuming $p = 0.5$ and $R^2 = 0$. Consequently, the magnitude of the sampling errors were set to be $\widehat{se}_j^2 = 4/n_j$.

B.2 The shrinkage factor I under the simulation conditions of this study

The average reliability I determines how informative the first-stage ML estimates $\hat{\tau}_j$'s are on average. I is calculated as $\sigma^2/(\sigma^2 + \text{GM}(\widehat{se}_j^2))$ where $\text{GM}(\widehat{se}_j^2)$ is the geometric mean of \widehat{se}_j^2 , $\exp(\sum_{j=1}^J \ln(\widehat{se}_j^2))$. Consequently, a large average reliability value indicates less noisy and more informative observed ML estimates $\hat{\tau}_j$'s relative to the degree of cross-site impact heterogeneity.

Figure B.1 illustrates the magnitudes of I assumed by the simulation conditions we chose for σ and \bar{n}_j . The assumed I level is equal to 0.714 if the average size of sites is 160 and the cross-site impact standard deviation is 0.25. In this situation, the cross-site impact variance is approximately 2.5 times the average within-site sampling variance ($\sigma^2/\text{GM}(\widehat{se}_j^2) = 2.5$). In contrast, if $I = 0.184$, the average \widehat{se}_j^2 is roughly four times as large as σ^2 ($\sigma^2/\text{GM}(\widehat{se}_j^2) = 0.225$), resulting in noisy $\hat{\tau}_j$'s. Since $I = 0.184$ is the median of the possible I levels shown in Figure B-1, half of our simulation conditions assume quite noisy and low informative data environments, which are often encountered in practical applications with small site sizes.

B.3 Data-generating models for G

Note that the Gaussian distribution in Figure 2 has a mean of zero and a variance of one ($\tau_j \sim N(0, 1)$). For comparability with the Gaussian model, the Gaussian mixture and AL models were also normalized to have zero means and unit variances. Then, we rescaled the G by multiplying the sampled distributions by σ .

Suppose that the Gaussian mixture data-generating model has two mixture components, $N(\tau_1, \sigma_1^2)$ and $N(\tau_2, \sigma_2^2)$, with a mixture weight for the first component, w . To force this mixture distribution to have mean 0 and variance 1, we define a normalizing factor

The average reliability of ML estimates (Shrinkage factor I)
 By simulation conditions \bar{n}_j and σ

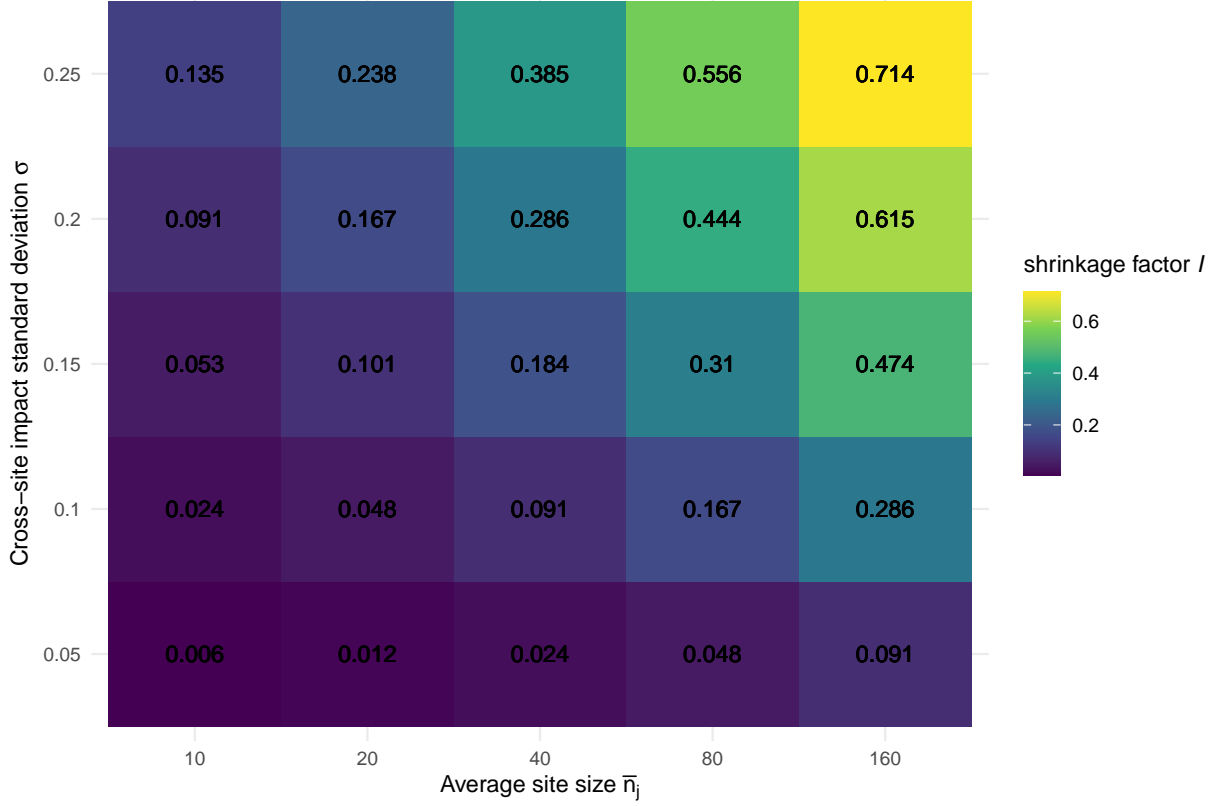


Figure B.1: The magnitude of the average reliability of ML estimates, the shrinkage factor I , implied by the simulation conditions of the cross-site impact standard deviation (σ) and the average site size \bar{n}_j . *Note:* The proportion treated within each site (p) is assumed to be 0.5. No within-site level-1 covariates are included ($R^2 = 0$).

denoted as C :

$$C = [wu^2 + (1 - w) + w(1 - w)\delta^2]^{1/2}, \quad (\text{B.3})$$

where $\delta = \tau_2 - \tau_1$ and $u = \sigma_2^2/\sigma_1^2$. Then, with probability w , τ_j is simulated from the first normalized component $N(-\frac{w\delta}{C}, \frac{1}{C})$, otherwise from the second normalized component $N(-\frac{(1-w)\delta}{C}, \frac{u}{C})$ with probability of $1 - w$.

To simulate G from the AL distribution with zero mean and unit variance, the location

and scale parameters, μ and ψ , are adjusted as follows as function of the skewness parameter ρ :

$$\tau_j | \mu, \psi, \rho \sim \text{AL}(\mu, \psi, \rho) \quad j = 1, \dots, J$$

where

$$\mu = -\frac{\psi(1 - \rho^2)}{\sqrt{2}\rho}, \quad \psi = \left[\frac{2\rho^2}{1 + \rho^4} \right]^{1/2}. \quad (\text{B.4})$$

The skewness parameter ρ is set to 0.1 so that the resulting G can have a right-skewed distribution with a long tail. This AL data-generating model is useful to evaluate whether the two strategies for the improved τ_j inferences help to recover large but rare site-level effects.

B.4 Data-analytic models

We fit three models to each of the simulated datasets: (a) G is standard Gaussian model, (b) G is a Dirichlet process mixture (DPM) model with a diffuse α prior (DP-diffuse), and (c) G is a DPM model with an informative α prior (DP-inform). These three models share the same first stage model specifications: $\hat{\tau}_j | \tau_j, \hat{s}e_j^2 \sim N(\tau_j, \hat{s}e_j^2)$. The models differ based on the second stage specifications for modeling G , $\tau_j | \boldsymbol{\theta} \sim G$ where $\boldsymbol{\theta}$ represents a vector of hyperparameters for G .

The Gaussian model assumes that $G \sim N(\tau, \sigma^2)$ where hyperpriors are set to be vague: $\tau \sim N(0, 100)$ and $\sigma^2 \sim \text{Unif}(0, 100)$. We avoid using the inverse-gamma prior for σ^2 because it does not have any proper limiting posterior distribution particularly for the simulation settings we have, where the number of sites J is small or the site-level variation σ^2 is small by design (Gelman, 2006). The two DPM models assume that $G \sim \text{DP}(\alpha, G_0)$ where G_0 is a Gaussian base distribution and α is a precision parameter, and differ in their

priors for the precision parameter. Both DPM models, DP-diffuse and DP-inform, share the same base distribution $G_0 \sim N(\tau_j | \tau, \sigma^2)$ with non-informative hyperpriors as in the Gaussian model: $\tau \sim (0, 100)$ and $\sigma^{-2} \sim \text{Unif}(0, 100)$.

The two DPM models differ in their specification of the $\text{Gamma}(a, b)$ priors for α . In the DP-diffuse models, a and b are chosen such that the mean and variance of α are $E(\alpha | a, b) = J/2$ and $\text{Var}(\alpha | a, b) = J/5$, respectively. For the five choices of $J = 25, 50, 75, 100,$ and 300 , the pairs of (a, b) for the DP-diffuse model are $(1.25, 0.1), (2.5, 0.1), (3.75, 0.1), (5.0, 0.1),$ and $(15, 0.1)$, respectively. Conversely, for the DP-inform models, a and b are chosen as the solution that minimizes the KL distance of the distribution of the number of clusters to the χ^2 distribution with $\text{df} = J/10$. This means that the DP-inform models assume the expected number of clusters K is $J/10$. The obtained solutions were $(1.24, 0.64), (1.60, 1.22), (2.72, 1.36), (3.88, 1.44),$ and $(9.32, 0.88)$ for the five choices of $J = 25, 50, 75, 100,$ and 300 , respectively.

Appendix C Detailed simulation results

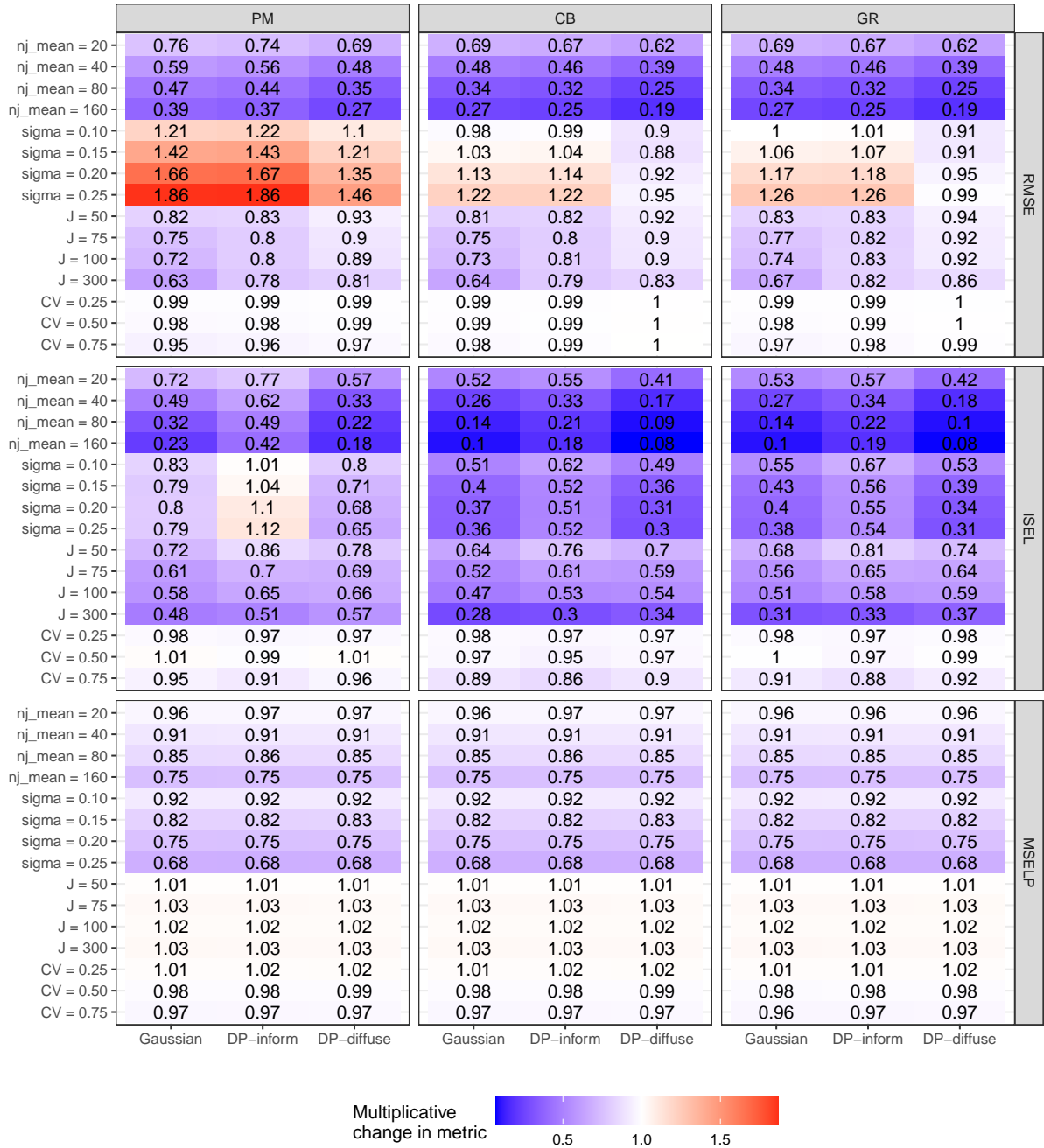


Figure C.1: The multiplicative change in average RMSE, ISEL, and MSELP for a single data-generating factor change from the base condition ($J = 25$, $\bar{n}_j = 10$, $\sigma = 0.05$, and $CV = 0.00$), when the true G is Gaussian

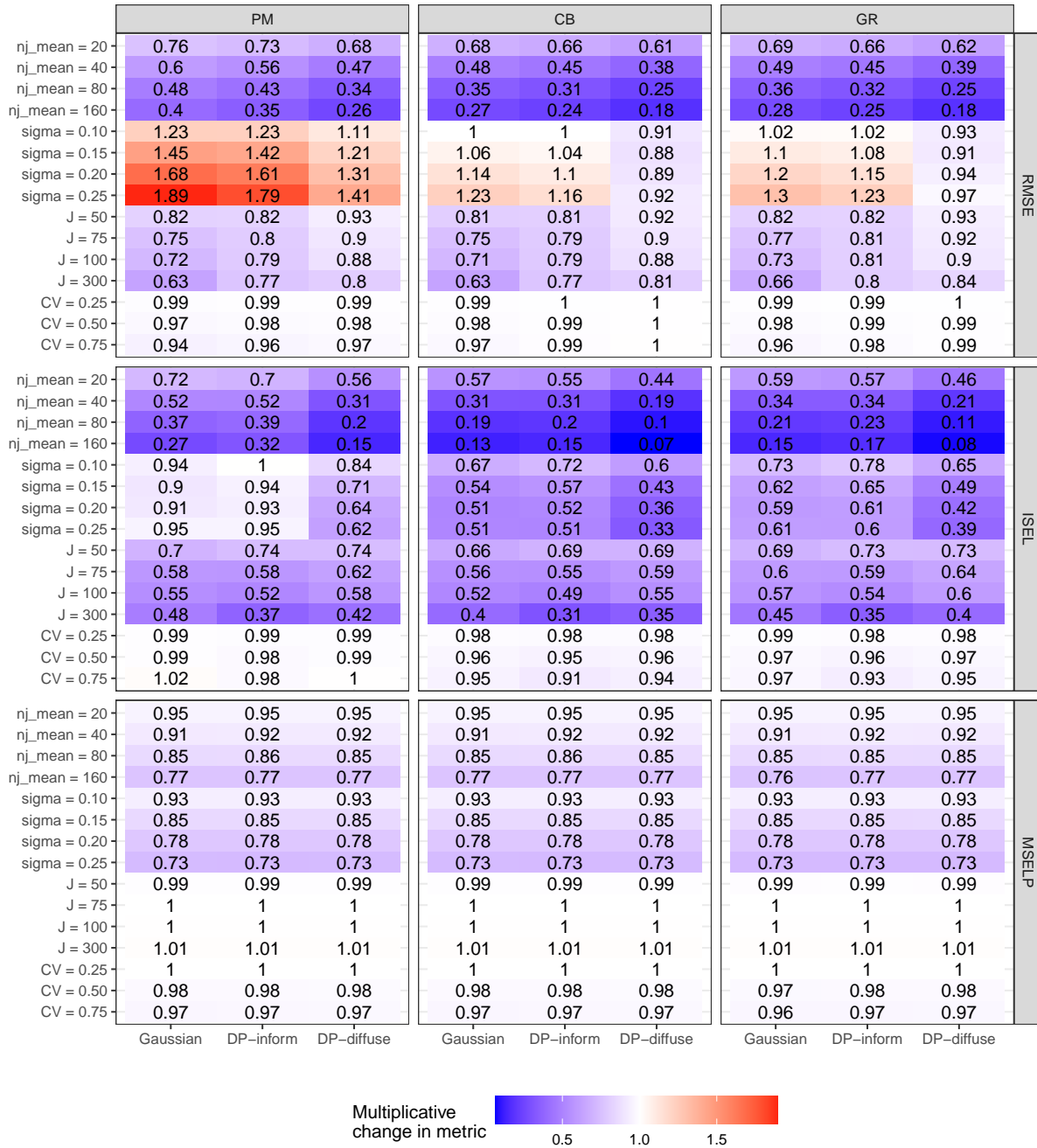


Figure C.2: The multiplicative change in average RMSE, ISEL, and MSELP for a single data-generating factor change from the base condition ($J = 25$, $\bar{n}_j = 10$, $\sigma = 0.05$, and $CV = 0.00$), when the true G is Asymmetric Laplace (AL) distribution with $\rho = 0.1$

Scaled empirical distribution function (EDF) vs. True effect distribution

True $G = \text{Mixed}$, $J = 25$, $n_{j_mean} = 10$, $CV = 0.00$

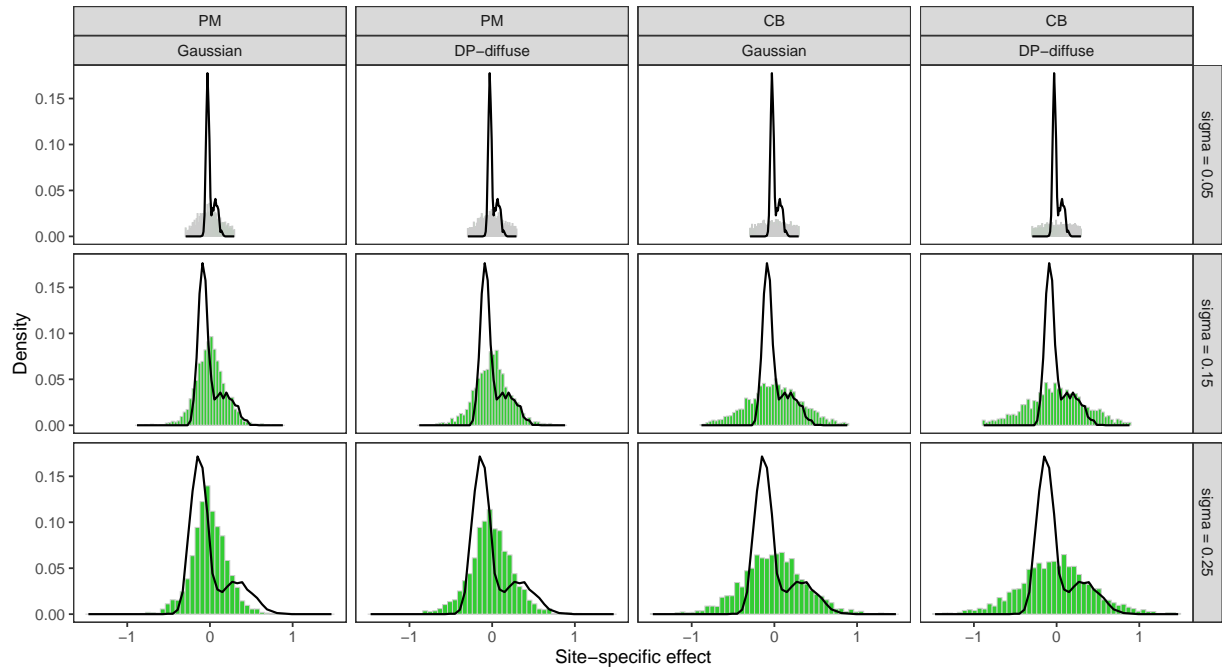


Figure C.3: Changes in the empirical distribution function (EDF) of the estimated site-specific effects ($\hat{\tau}_j$'s), as the cross-site impact standard deviation σ increases from the base condition ($J = 25$, $\bar{n}_j = 10$, and $CV = 0.00$), when true G is Gaussian mixture.

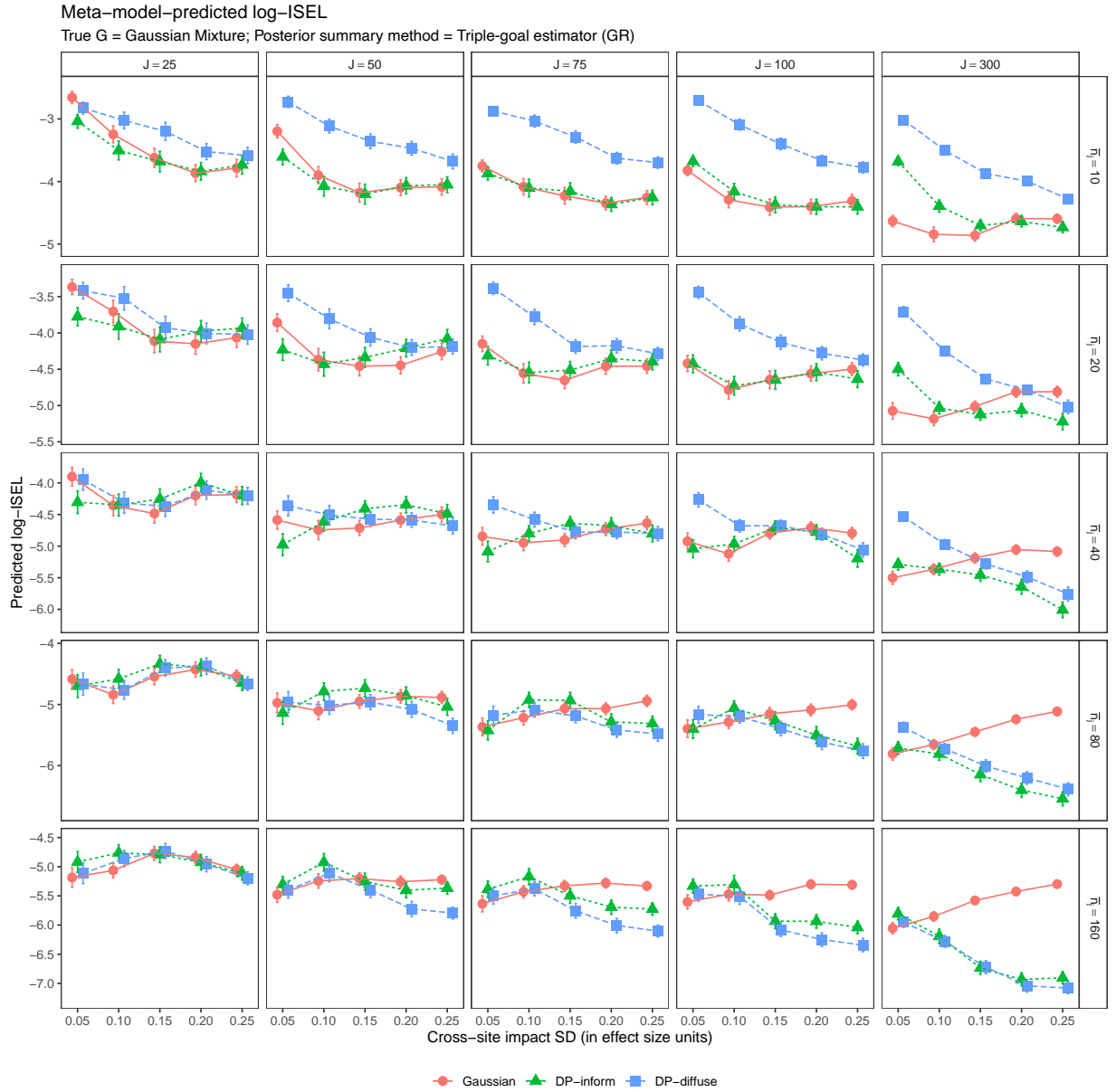


Figure C.4: The meta-model predicted integrated squared error loss (ISEL) on a natural log scale, when the true G is a Gaussian mixture and the triple-goal estimator (GR) is used as the posterior summary method. Plots include 95% prediction intervals around predicted values.

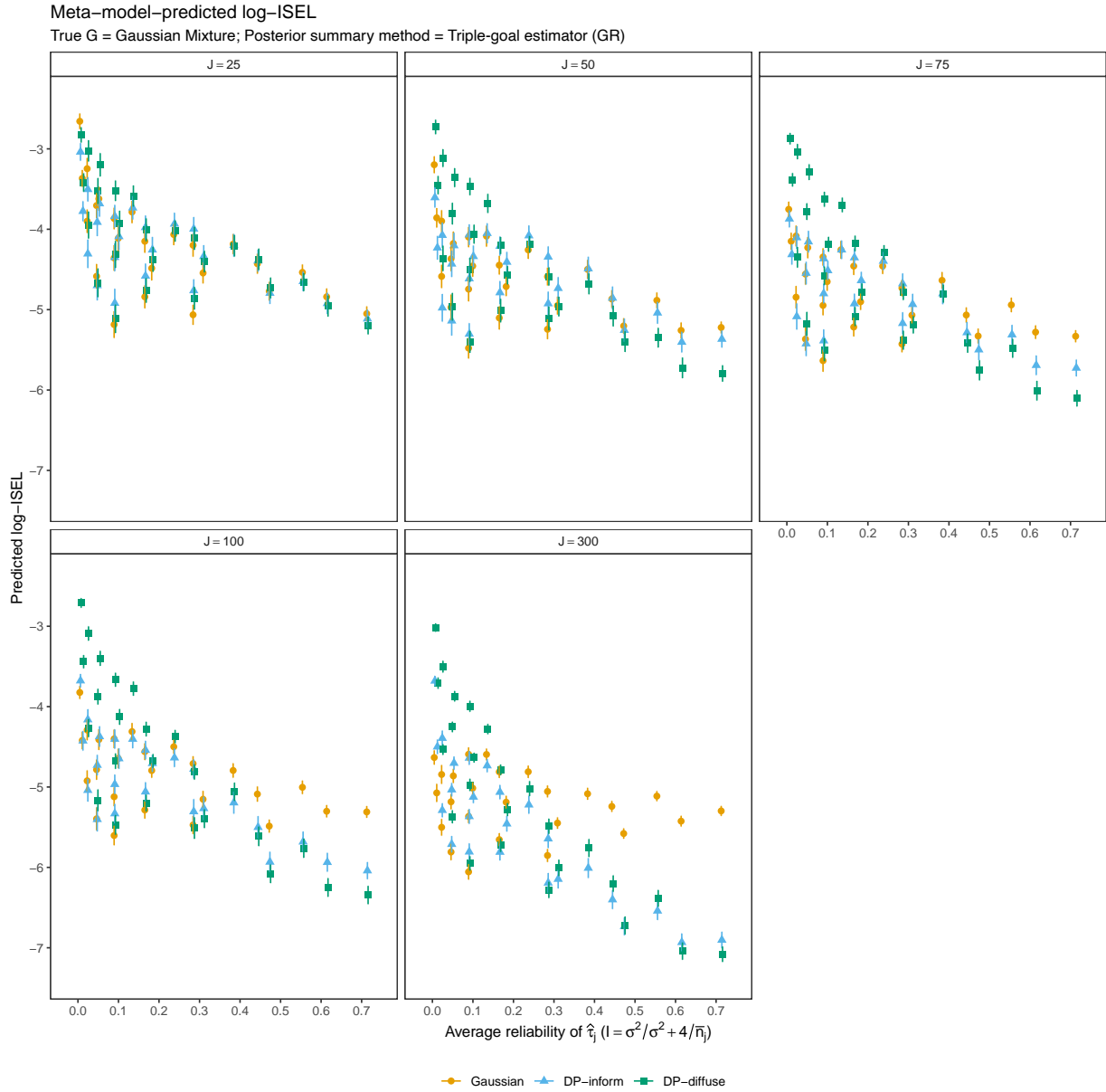


Figure C.5: The meta-model predicted integrated squared error loss (ISEL) on a natural log scale, when the true G is a Gaussian mixture and the triple-goal estimator (GR) is used as the posterior summary method. Plots include 95% prediction intervals around predicted values.

Meta-model-predicted log-RMSE

True G = Gaussian Mixture; Posterior summary method = Posterior mean (PM)

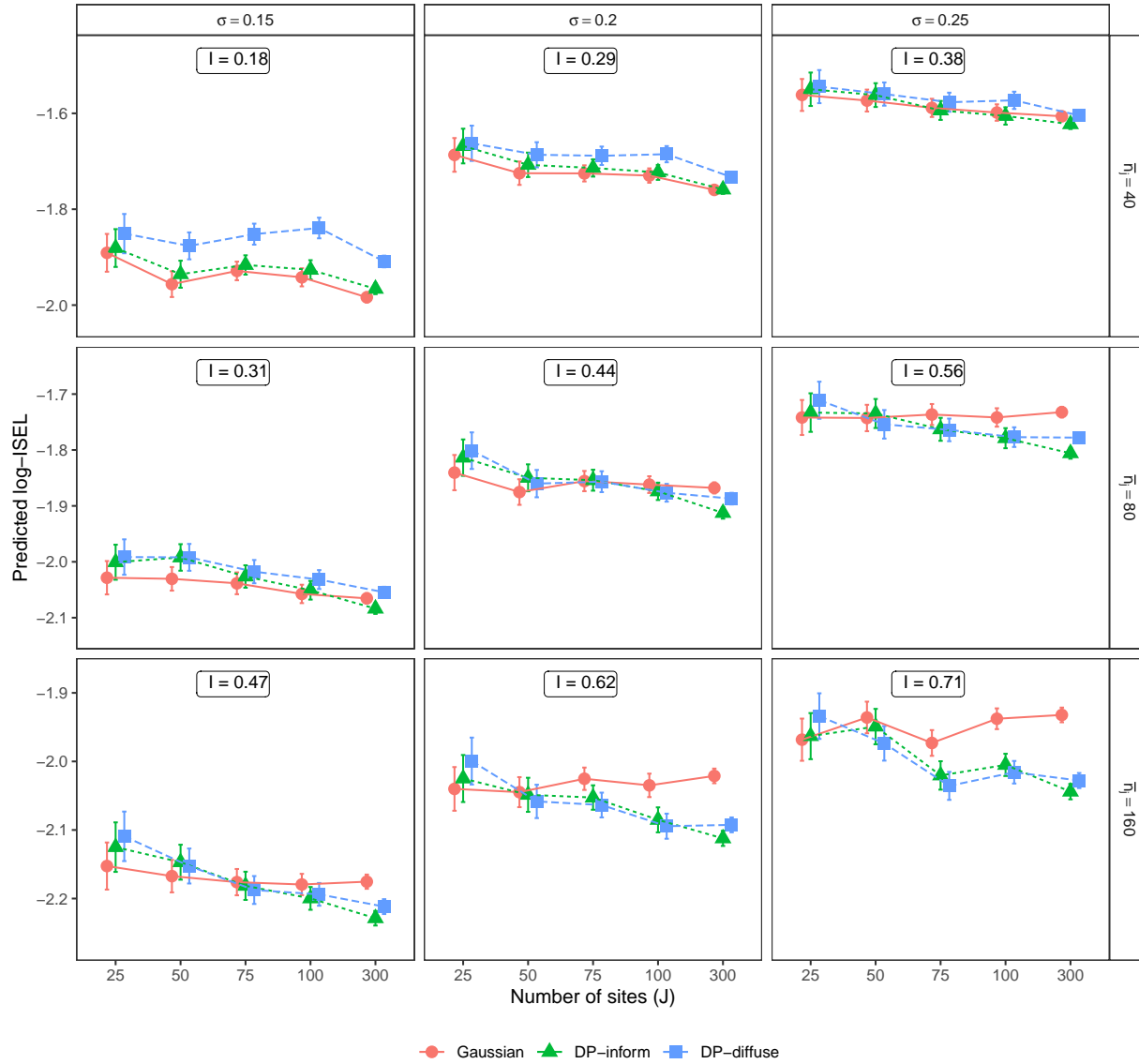


Figure C.6: The meta-model predicted root mean squared error loss (RMSE) on a natural log scale, when the true G is a Gaussian mixture and the posterior mean (PM) is used as the posterior summary method. Plots include 95% prediction intervals around predicted values.

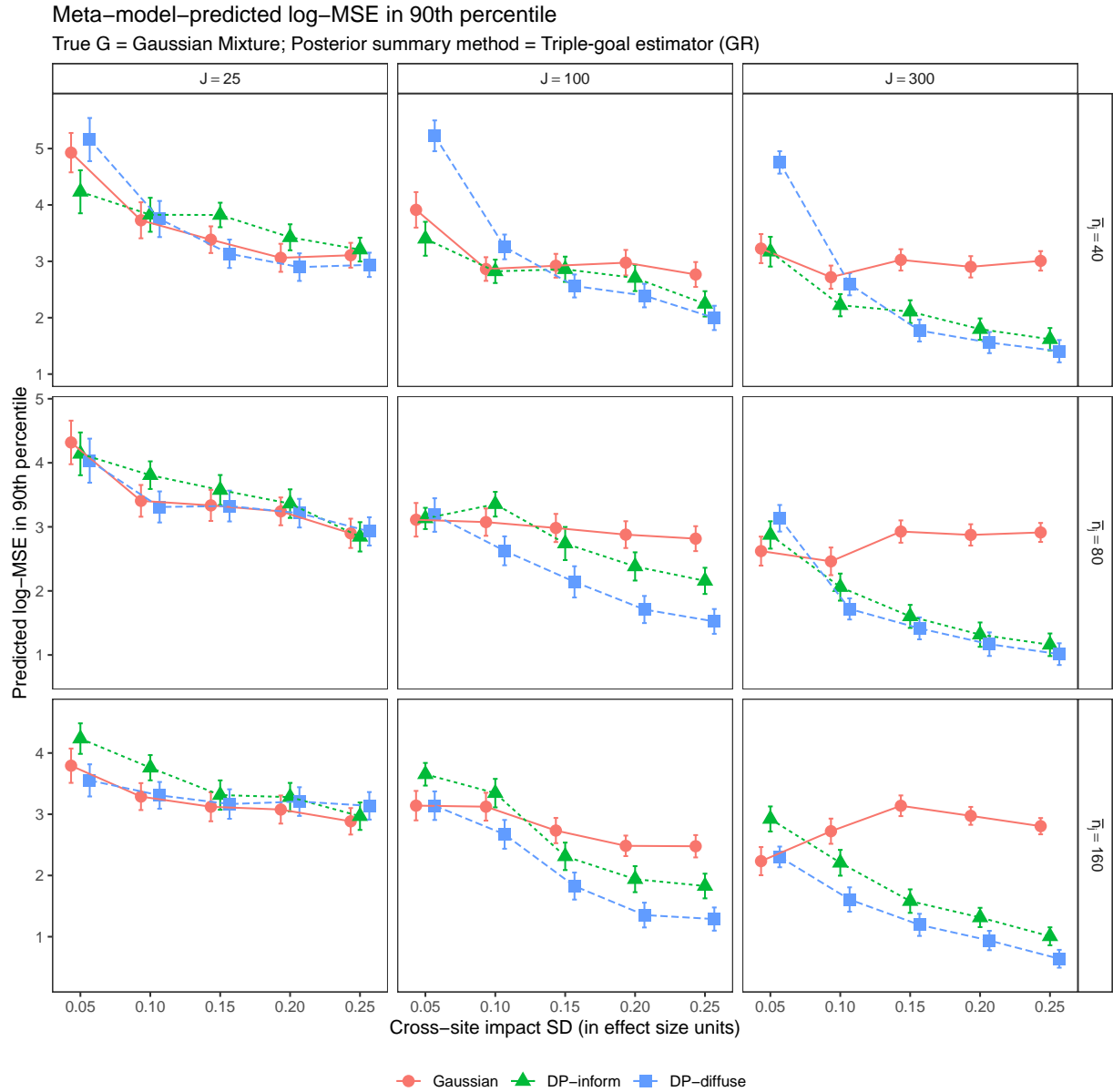
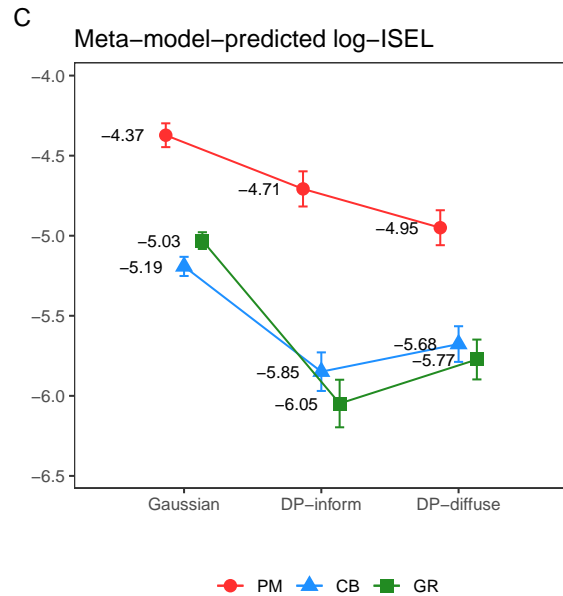
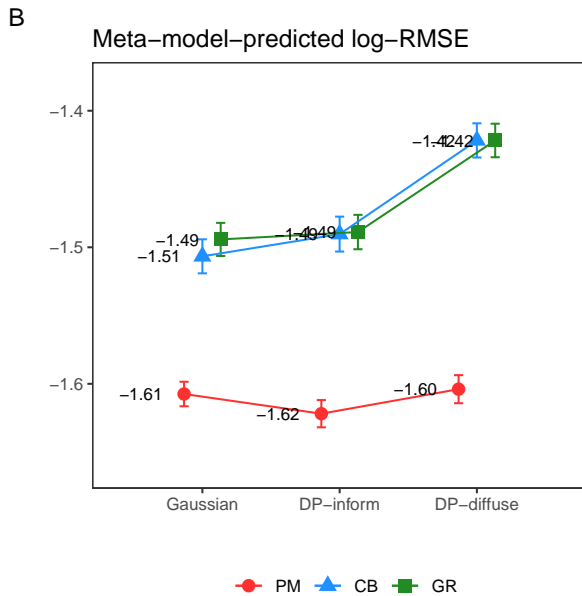
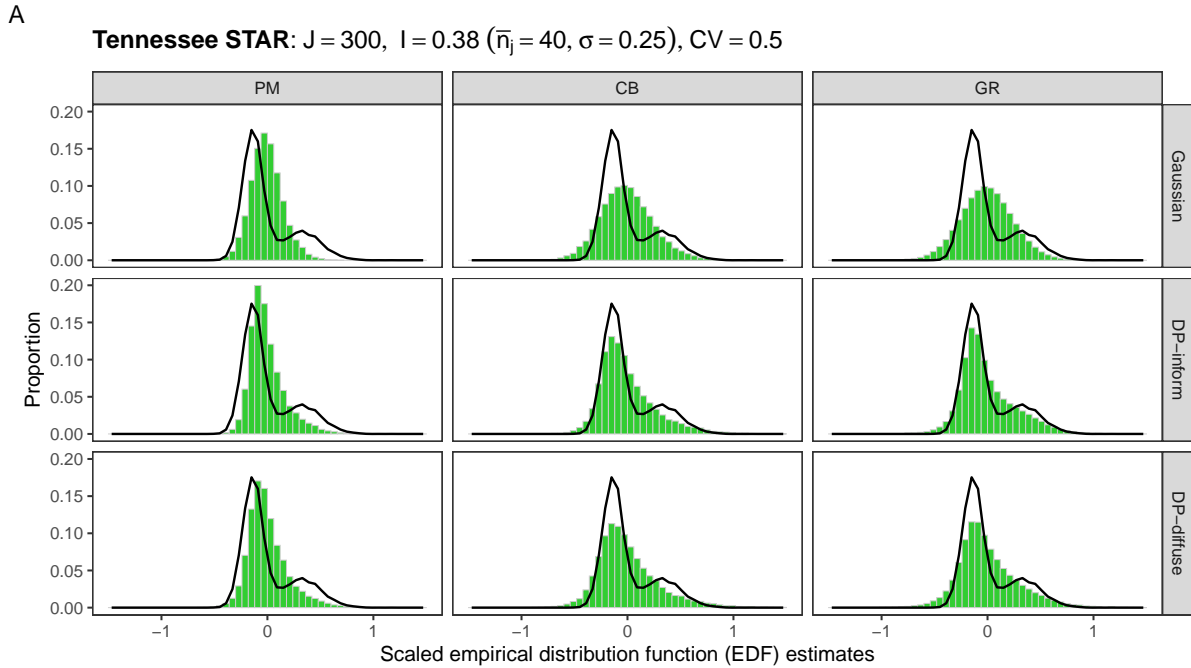
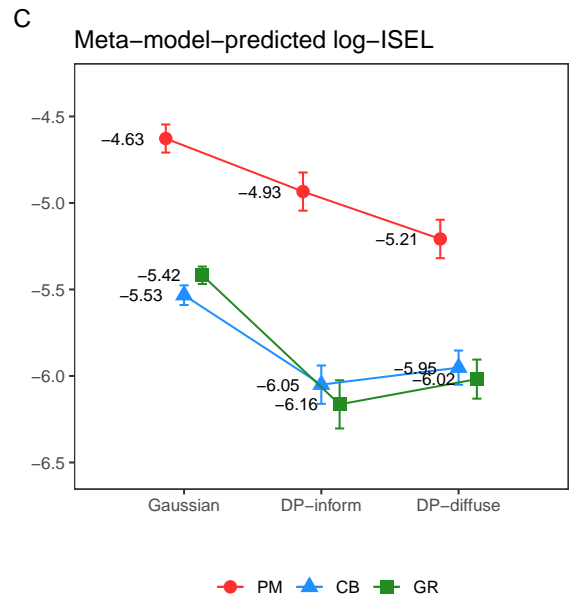
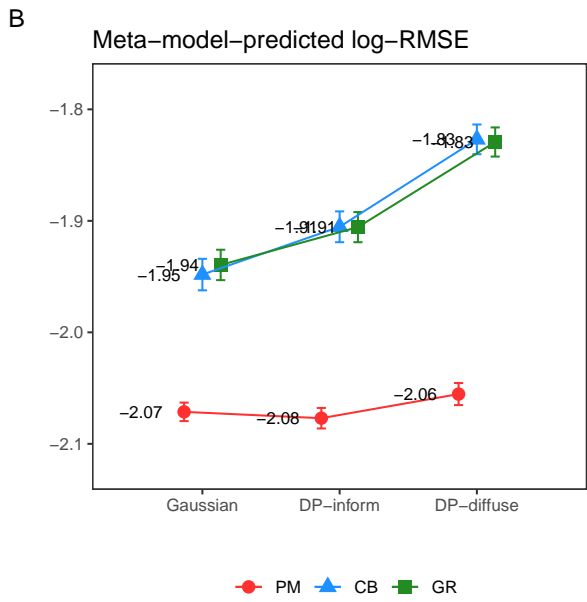
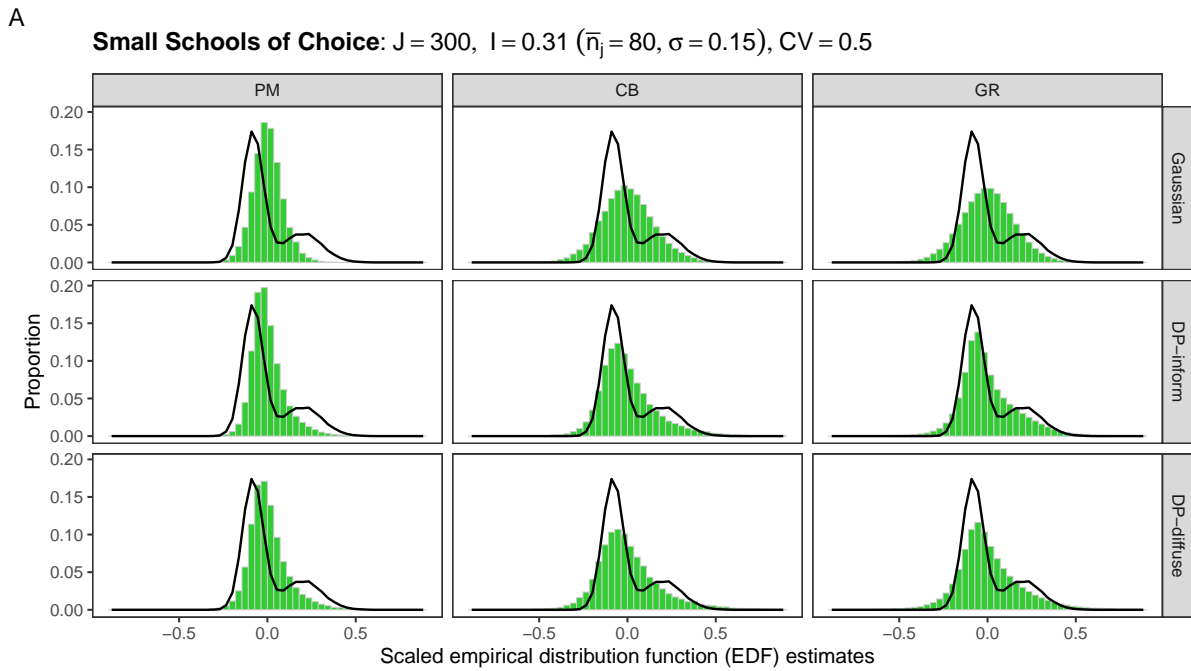


Figure C.7: The meta-model predicted mean squared error (MSE) in 90th percentile on a natural log scale, when the true G is a Gaussian mixture and the triple-goal estimator (GR) is used as the posterior summary method. Plots include 95% prediction intervals around predicted values.



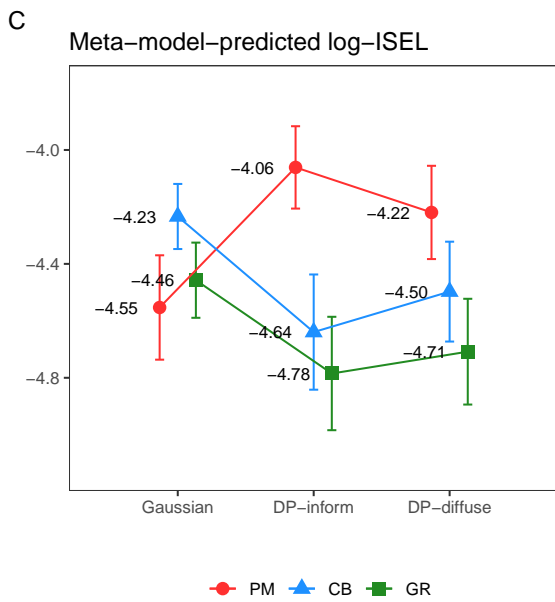
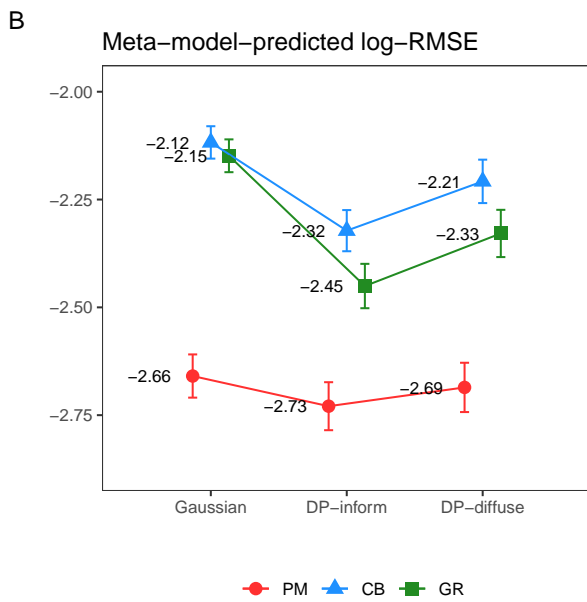
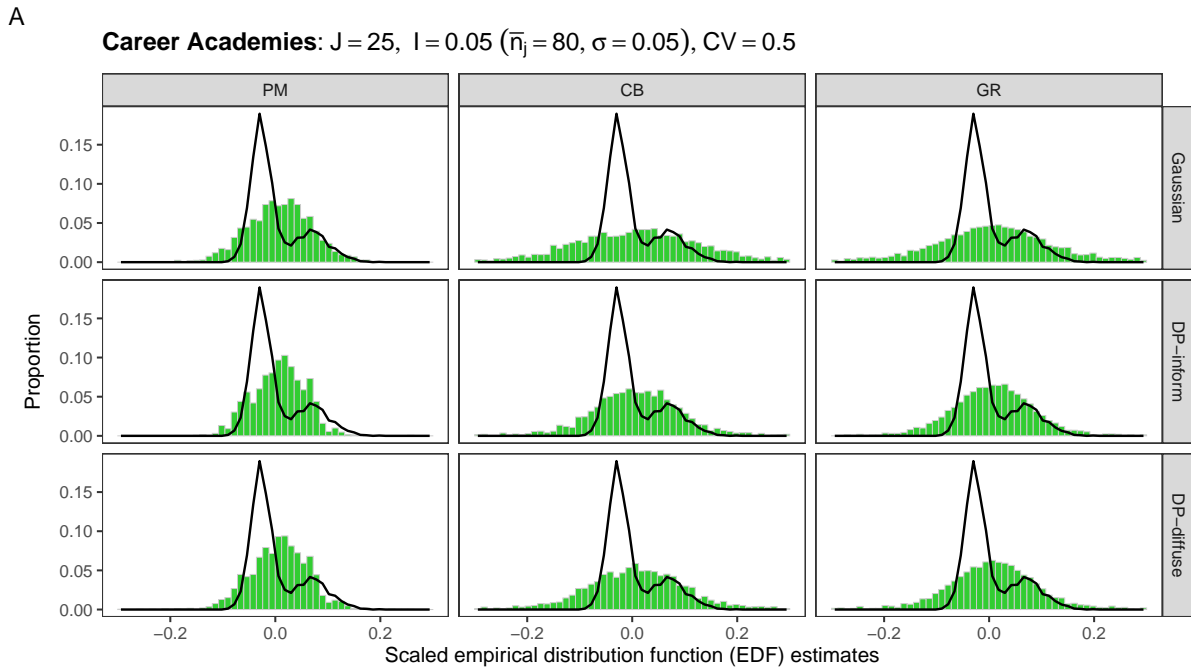
Outcome: SAT-7 total reading, yr 1, Real Case: $J = 280$, $I = 0.26$ ($\bar{n}_j = 35.3$, $\sigma = 0.23$)

Figure C.8: Scaled EDF estimates and meta-model-predicted RMSE and ISEL on log-scale for each model-method combination, when the data-generation is based on the scenario simulating the Tennessee STAR data ($J = 280$, $\bar{n}_j = 35.9$, and $\sigma = 0.26$ for the outcome, SAT-7 Total Math at the end of a student’s first year in the study). True G is Gaussian mixture, while CV is fixed at 0.5. Plots include 95% prediction intervals around predicted values.



Outcome: Earned a high school diploma, yr 4, Real Case: $J = 227$, $l = 0.21$ ($\bar{n}_j = 62.3$, $\sigma = 0.13$)

Figure C.9: Scaled EDF estimates and meta-model-predicted RMSE and ISEL on log-scale for each model-method combination, when the data-generation is based on the scenario simulating the Small Schools of Choice data ($J = 356$, $\bar{n}_j = 72.8$, and $\sigma = 0.16$ for the outcome, Ninth-grade “on-track” indicator). True G is Gaussian mixture, while CV is fixed at 0.5. Plots include 95% prediction intervals around predicted values.

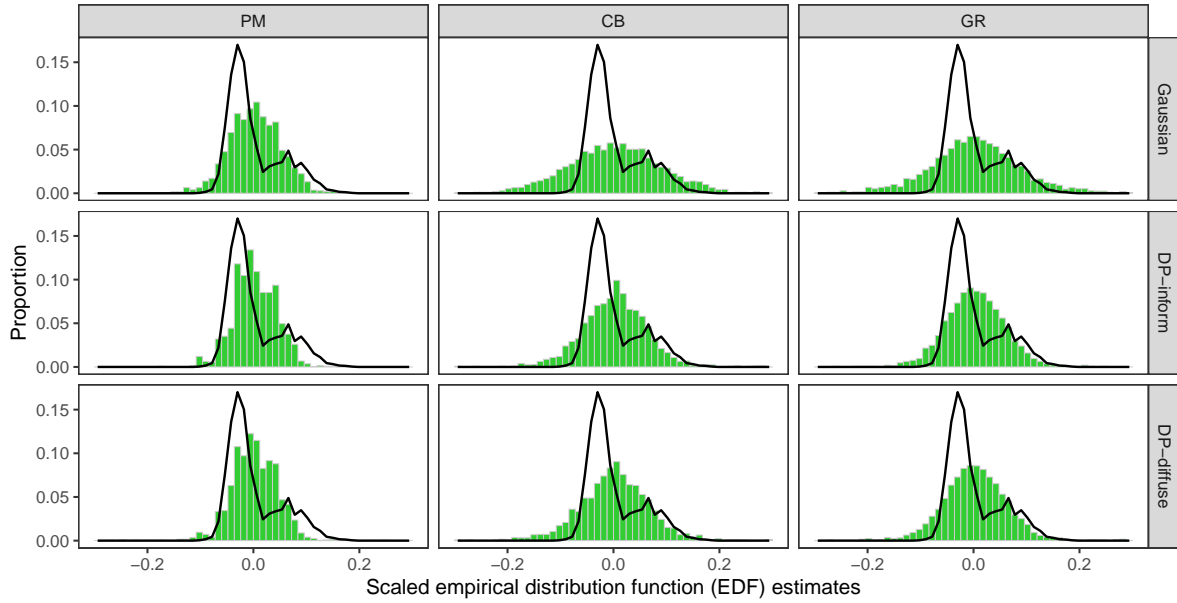


Outcome: Avg. annual earnings, yrs 1...4, Real Case: $J = 20$, $I = 0$ ($\bar{n}_j = 72.9$, $\sigma = 0$)

Figure C.10: Scaled EDF estimates and meta-model-predicted RMSE and ISEL on log-scale for each model-method combination, when the data-generation is based on the scenario simulating the Career Academies study ($J = 20$, $\bar{n}_j = 74.1$, and $\sigma = 0.07$ for the outcome, enrolled in postsecondary measured 14 months after expected high school graduation). True G is Gaussian mixture, while CV is fixed at 0.5. Plots include 95% prediction intervals around predicted values.

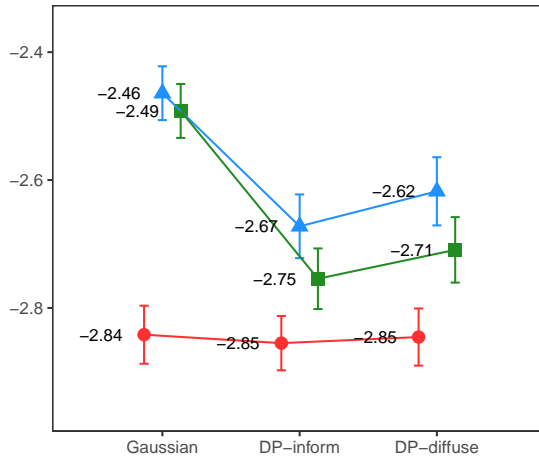
A

Learning Communities: $J = 25$, $I = 0.09$ ($\bar{n}_j = 160$, $\sigma = 0.05$), $CV = 0.5$



B

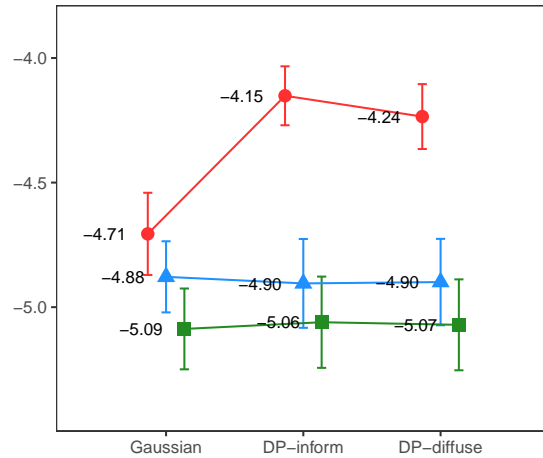
Meta-model-predicted log-RMSE



● PM ▲ CB ■ GR

C

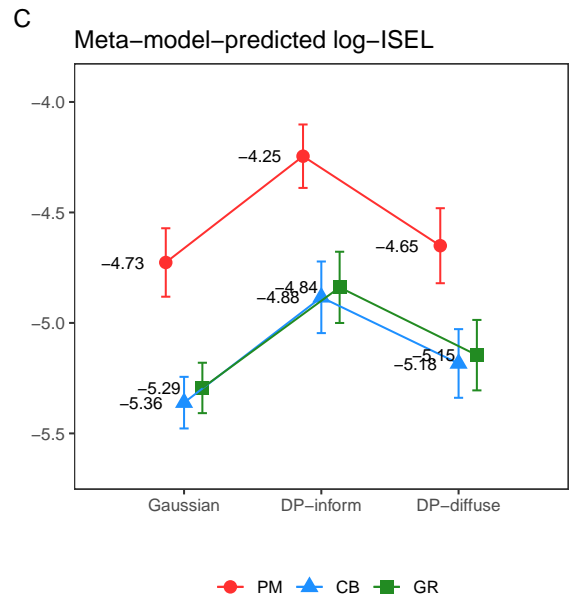
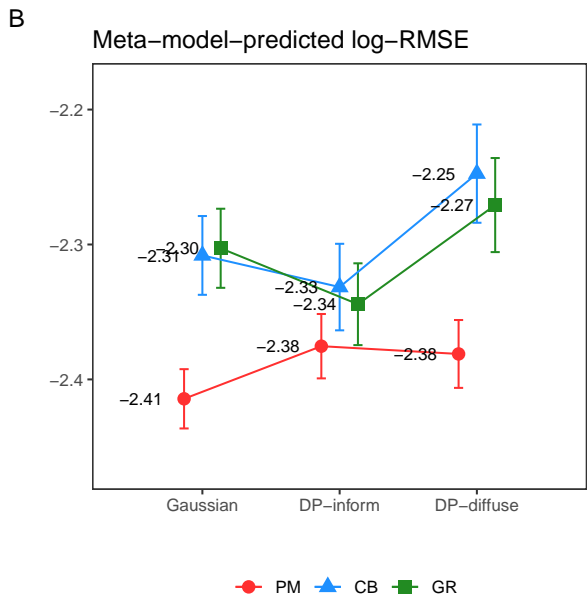
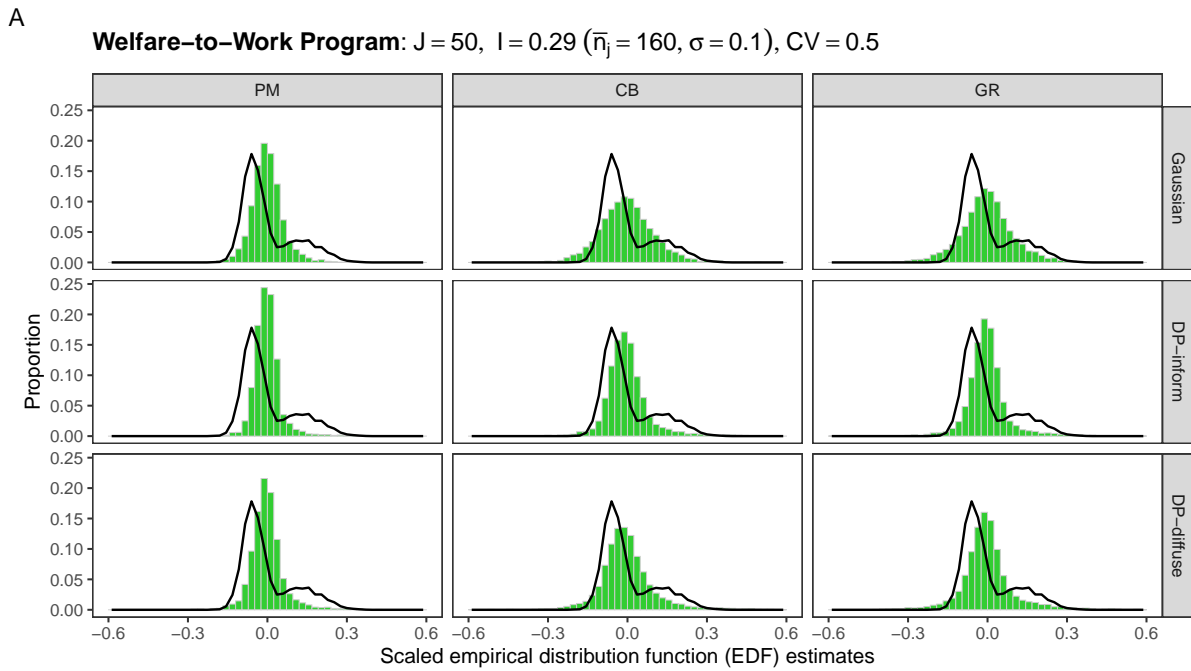
Meta-model-predicted log-ISEL



● PM ▲ CB ■ GR

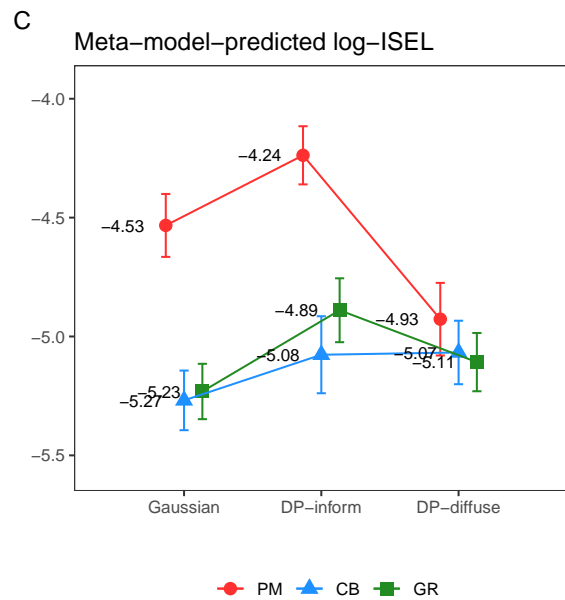
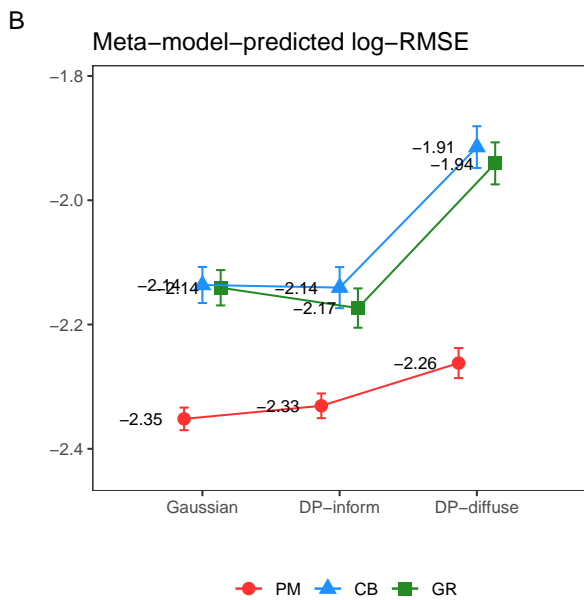
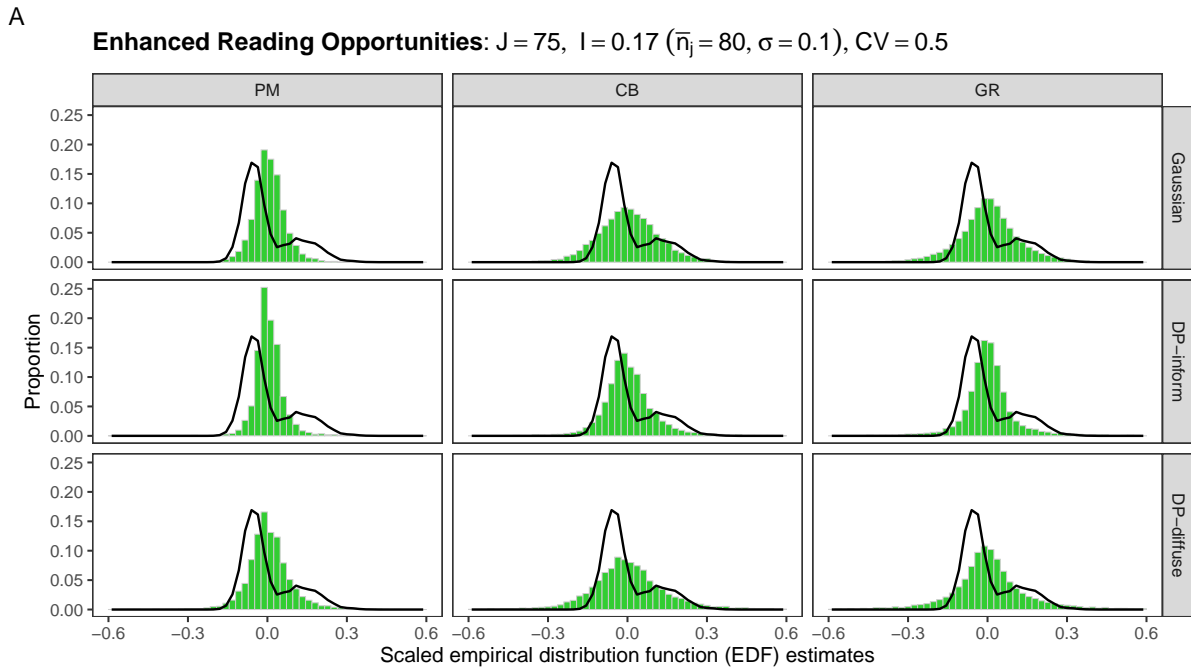
Outcome: Cumulative total credits earned, sem 3, Real Case: $J = 36$, $I = 0$ ($\bar{n}_j = 193.7$, $\sigma = 0$)

Figure C.11: Scaled EDF estimates and meta-model-predicted RMSE and ISEL on log-scale for each model-method combination, when the data-generation is based on the scenario simulating the Learning Communities study ($J = 36$, $\bar{n}_j = 193.7$, and $\sigma = 0.04$ for the outcome, credit accumulation at the end-of-the-program semester). True G is Gaussian mixture, while CV is fixed at 0.5. Plots include 95% prediction intervals around predicted values.



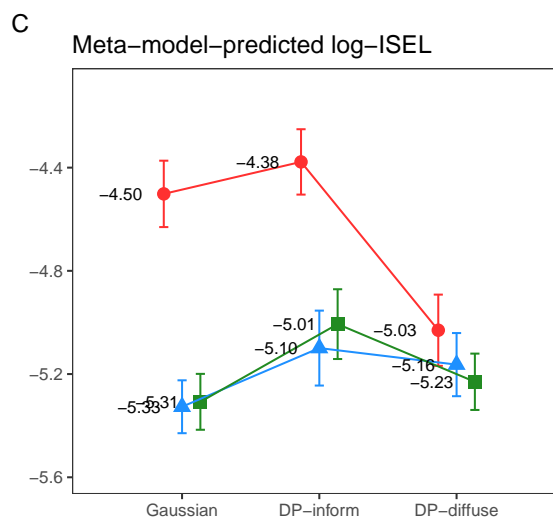
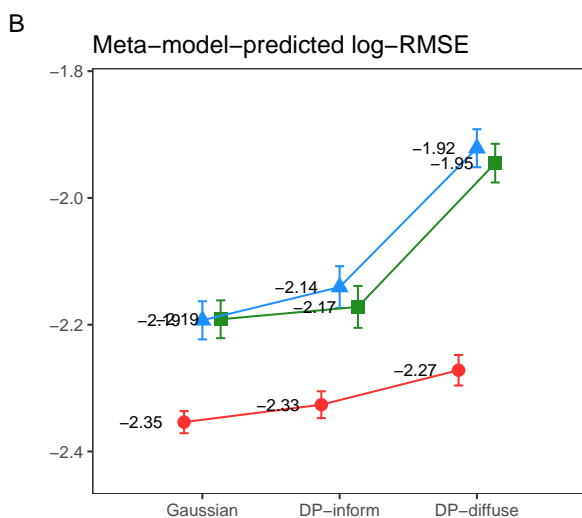
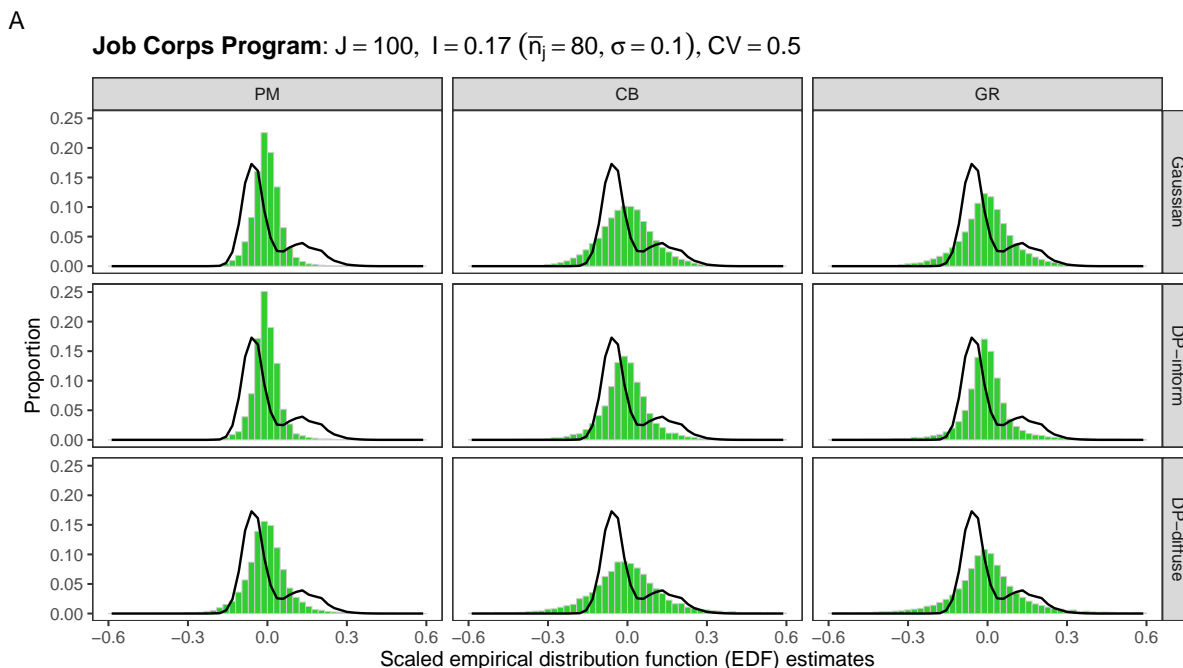
Outcome: Avg. annual earnings, quarters 1–8, Real Case: $J = 59, I = 0.69$ ($\bar{n}_j = 1176.3, \sigma = 0.09$)

Figure C.12: Scaled EDF estimates and meta-model-predicted RMSE and ISEL on log-scale for each model-method combination, when the data-generation is based on the scenario simulating the Welfare-to-Work Program study ($J = 59, \bar{n}_j = 1176.3$, and $\sigma = 0.09$ for the outcome, average annual earnings over two years). True G is Gaussian mixture, while CV is fixed at 0.5. Plots include 95% prediction intervals around predicted values.



Outcome: GRADE reading comprehension, yr 1, Real Case: $J = 70$, $l = 0.19$ ($\bar{n}_j = 65.4$, $\sigma = 0.12$)

Figure C.13: Scaled EDF estimates and meta-model-predicted RMSE and ISEL on log-scale for each model-method combination, when the data-generation is based on the scenario simulating the Enhanced Reading Opportunities study ($J = 70$, $\bar{n}_j = 65.4$, and $\sigma = 0.12$ for the outcome, Reading comprehension and reading vocabulary GRADE assessment). True G is Gaussian mixture, while CV is fixed at 0.5. Plots include 95% prediction intervals around predicted values.



● PM ▲ CB ■ GR

● PM ▲ CB ■ GR

Outcome: Total annual earnings, yr 2, Real Case: $J = 100$, $I = 0.16$ ($\bar{n}_j = 102.2$, $\sigma = 0.09$)

Figure C.14: Scaled EDF estimates and meta-model-predicted RMSE and ISEL on log-scale for each model-method combination, when the data-generation is based on the scenario simulating the Job Corps Program study ($J = 100$, $\bar{n}_j = 102.2$, and $\sigma = 0.09$ for the outcome, Annual earnings outcomes at the second year after random assignment). True G is Gaussian mixture, while CV is fixed at 0.5. Plots include 95% prediction intervals around predicted values.

Appendix D Detailed analysis results of real-world data

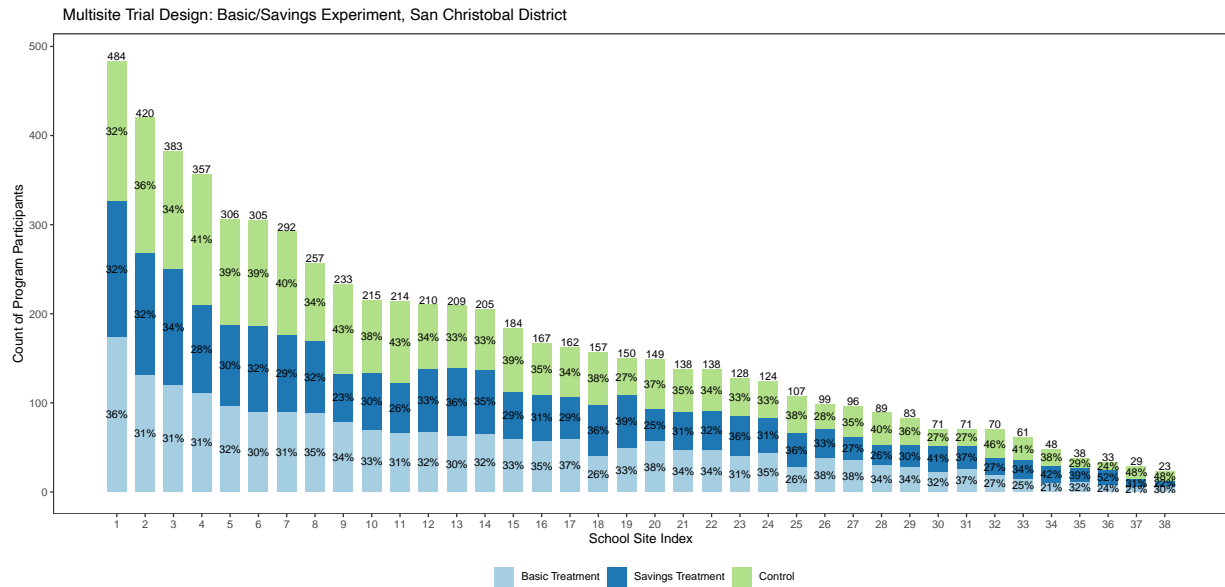


Figure D.1: Multisite trial design of Basic/Savings conditional cash transfer program in San Christobal district

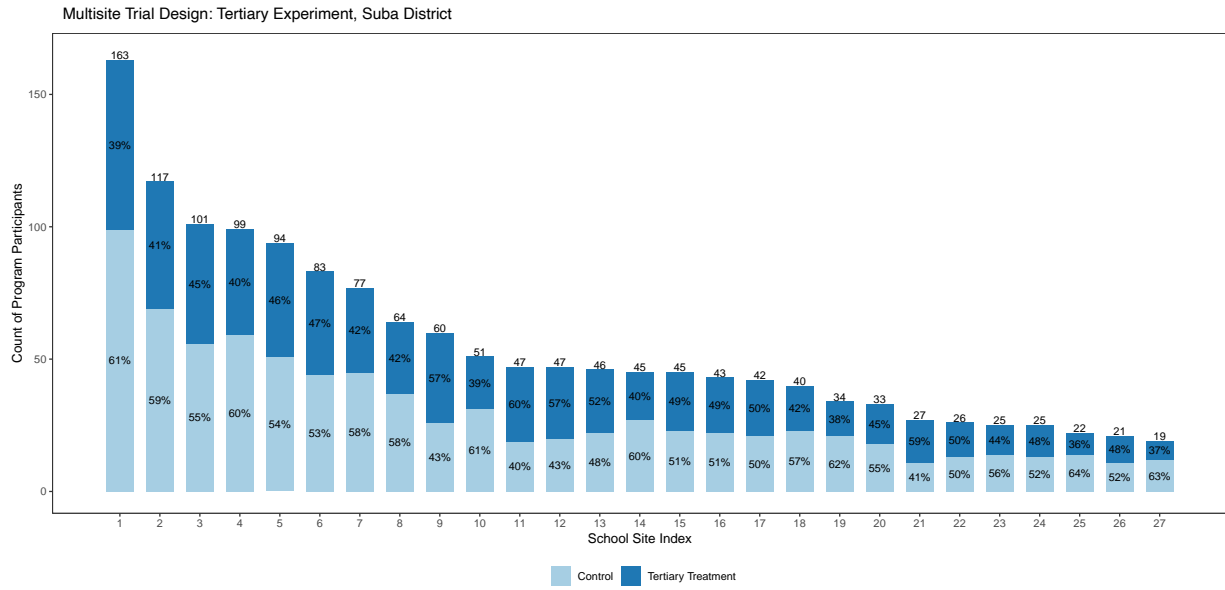


Figure D.2: Multisite trial design of Tertiary conditional cash transfer program in Suba district

Outcome Means by Experimental Groups
 Outcome: On-time Secondary Enrollment, San Christobal District

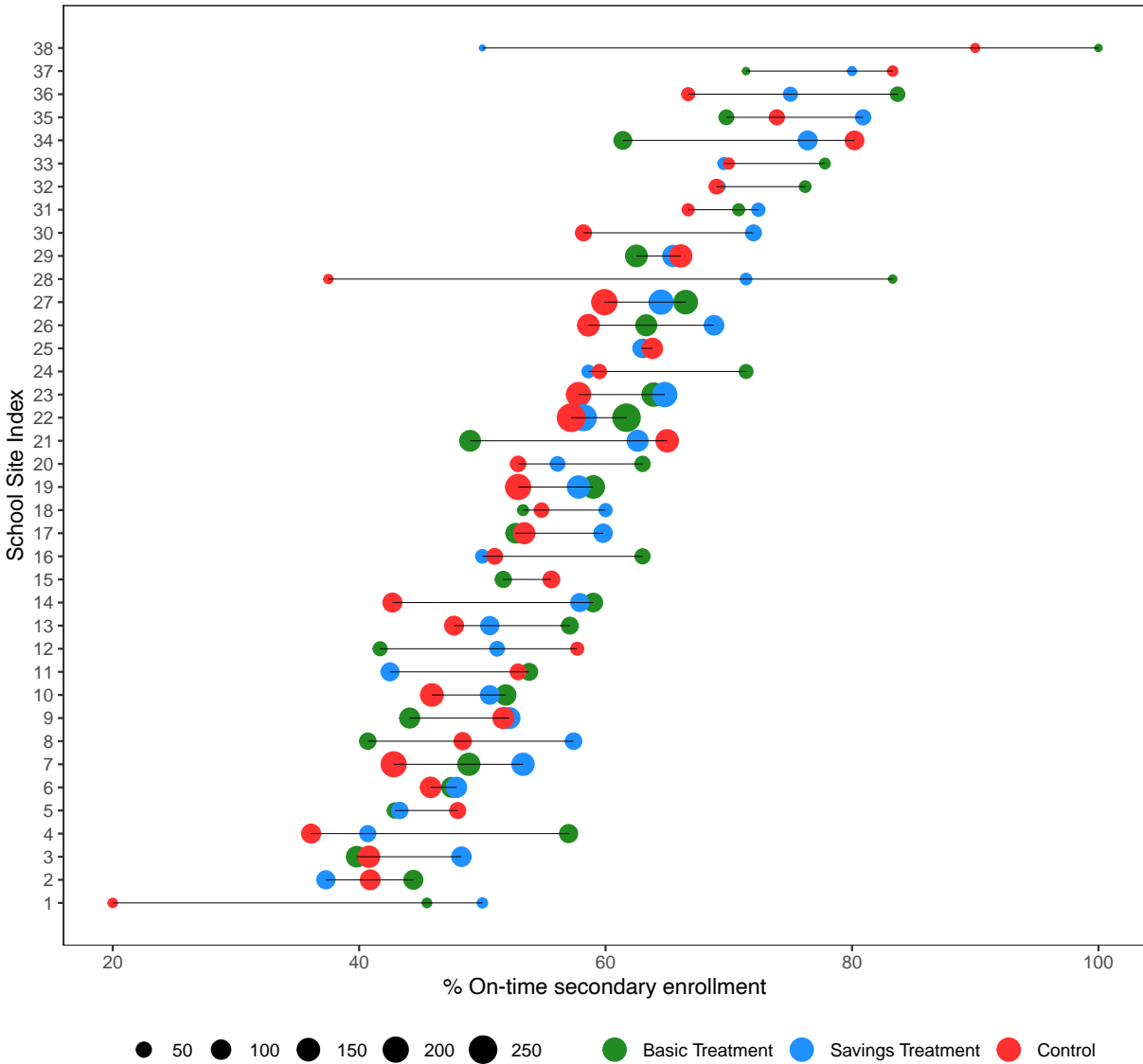


Figure D.3: On-time secondary enrollment outcome mean (percentage) by experimental group and site in San Christobal district

Outcome Means by Experimental Groups
 Outcome: Secondary Graduation, San Cristobal District

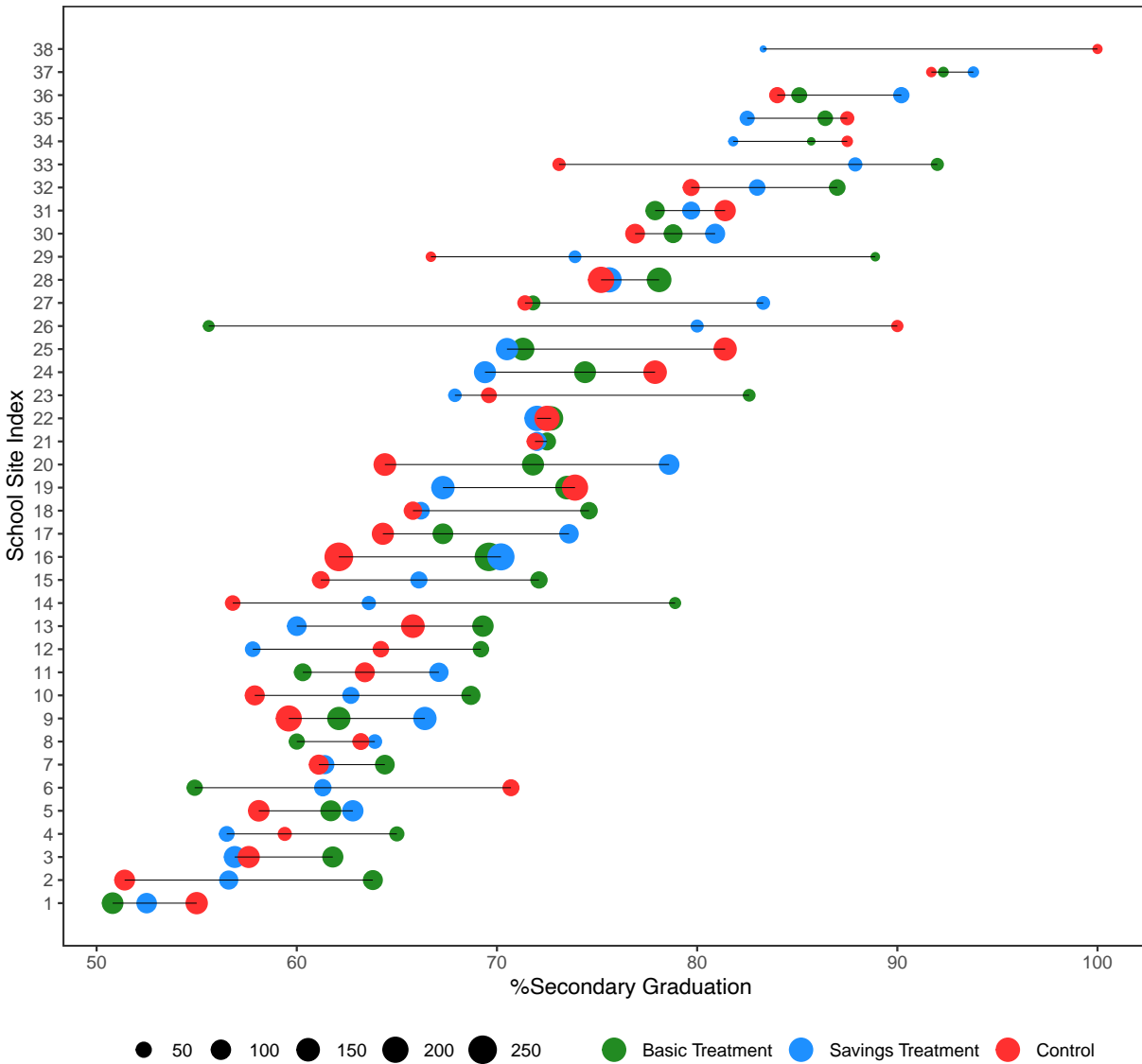


Figure D.4: Secondary graduation outcome mean (percentage) by experimental group and site in San Cristobal district

Outcome Means by Experimental Groups
 Outcome: Tertiary Enrollment - Any Time, Suba District

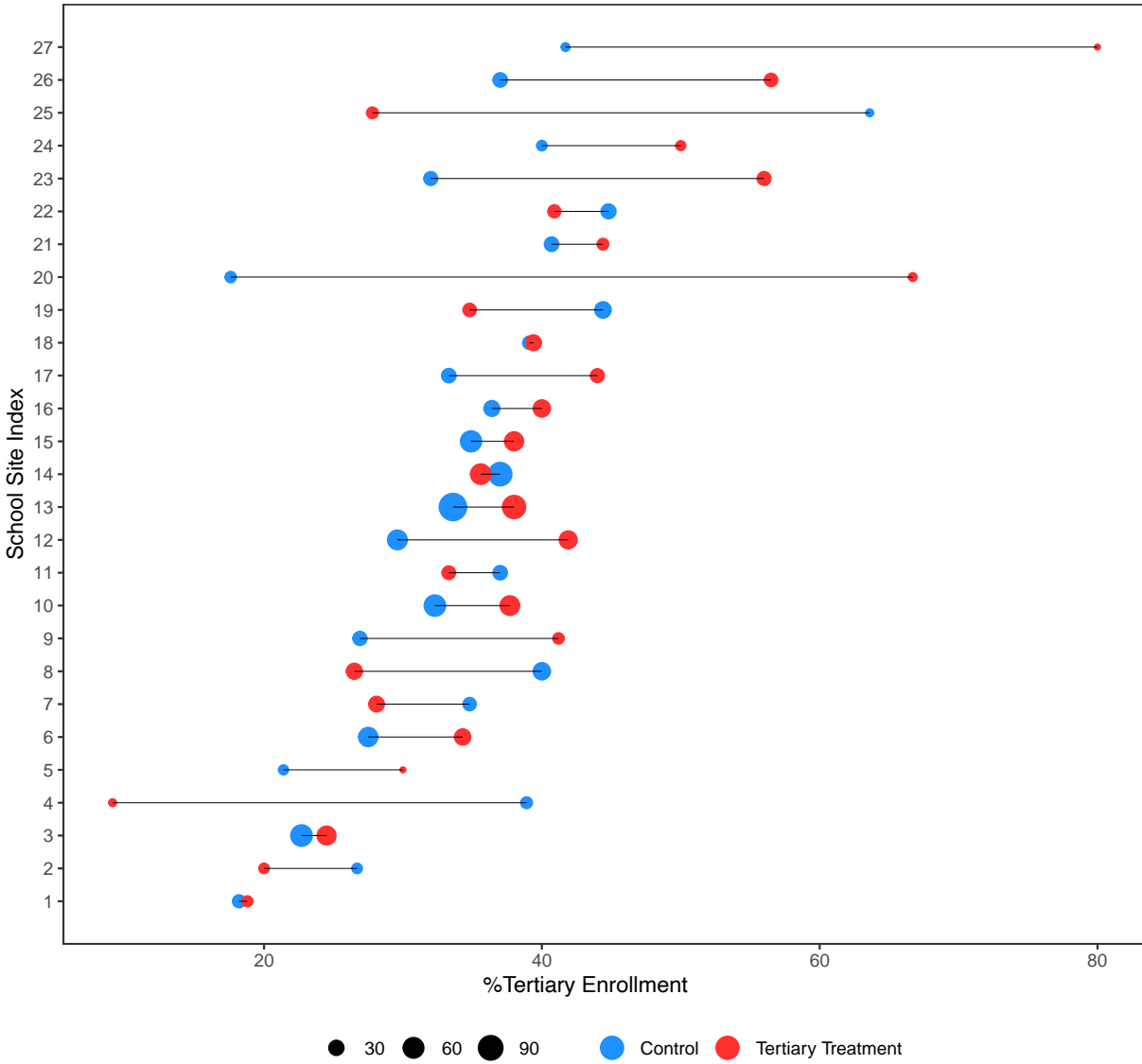


Figure D.5: Tertiary enrollment outcome mean (percentage) by experimental group and site in Suba district

Outcome Means by Experimental Groups
 Outcome: Tertiary Enrollment in Universities, Suba District

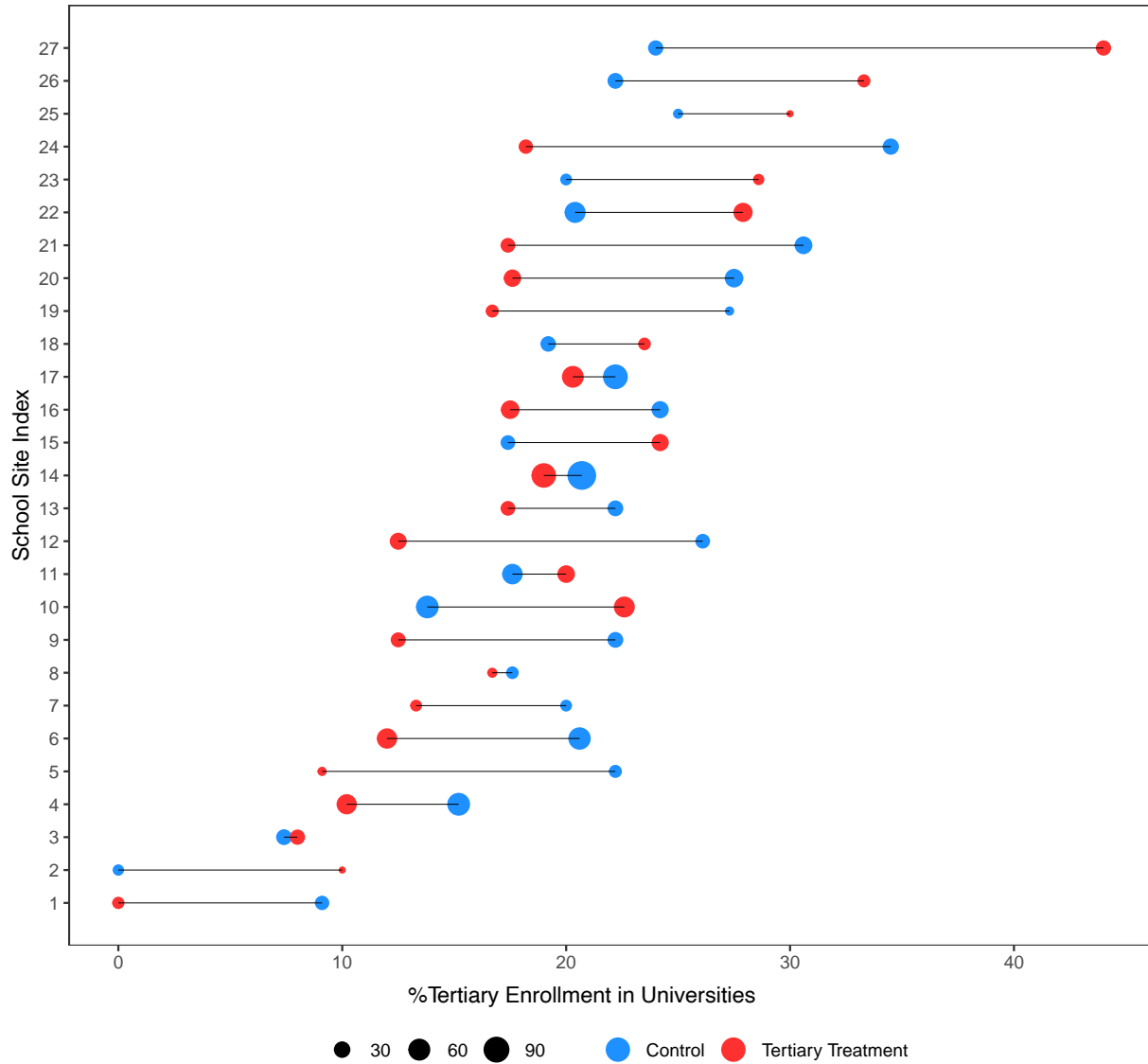


Figure D.6: Tertiary enrollment in universities outcome mean (percentage) by experimental group and site in Suba district

Secondary Graduation, San Christobal District

$J = 38, I = 0.06$ ($\bar{n}_j = 171.2, \sigma = 0.06, CV = 0.67$)

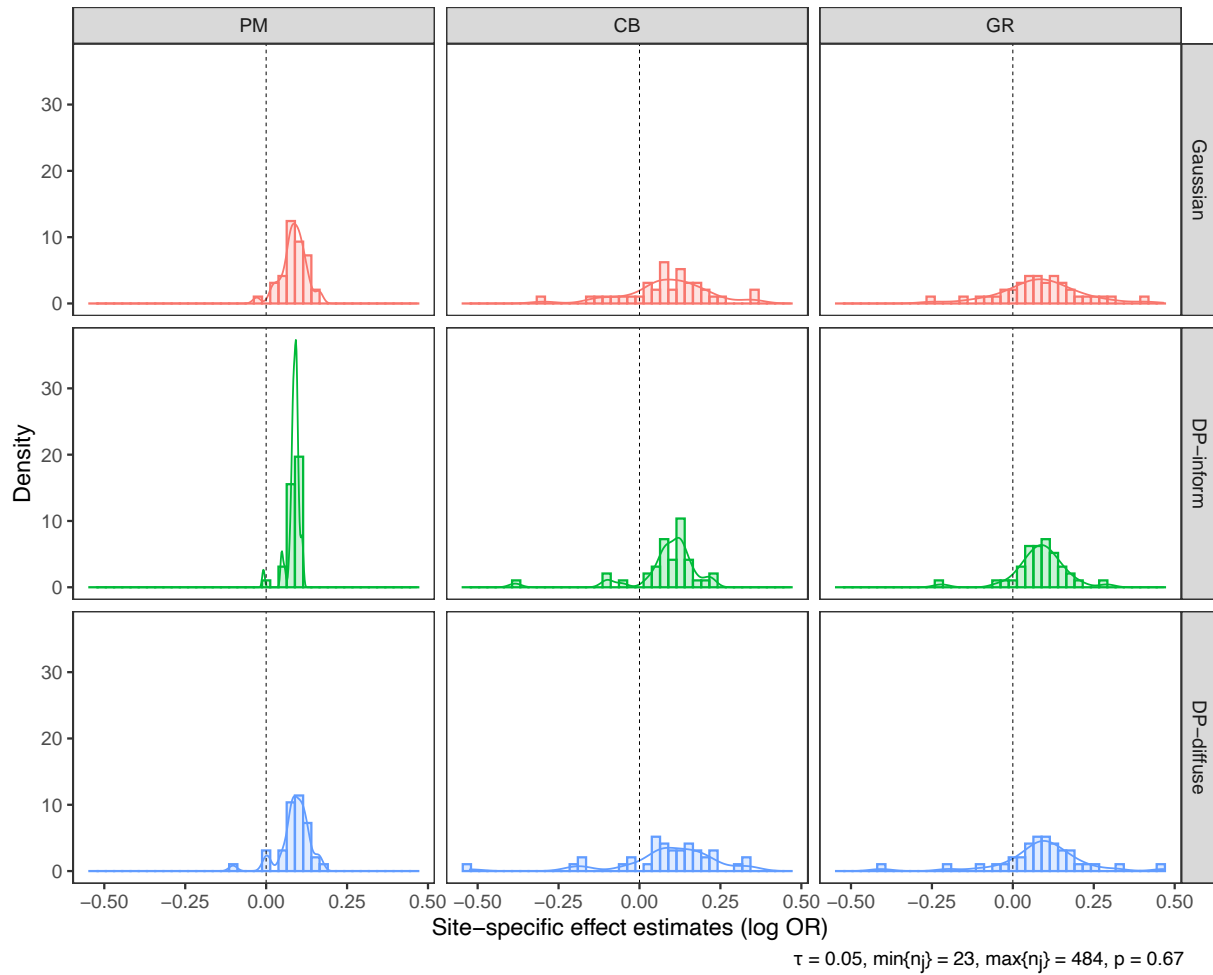


Figure D.7: Distribution of site-specific treatment effect estimates on secondary graduation in San Christobal district

Tertiary Enrollment (Any Time), Suba District

$J = 27, I = 0.05$ ($\bar{n}_j = 55.4, \sigma = 0.08$), $CV = 0.63$

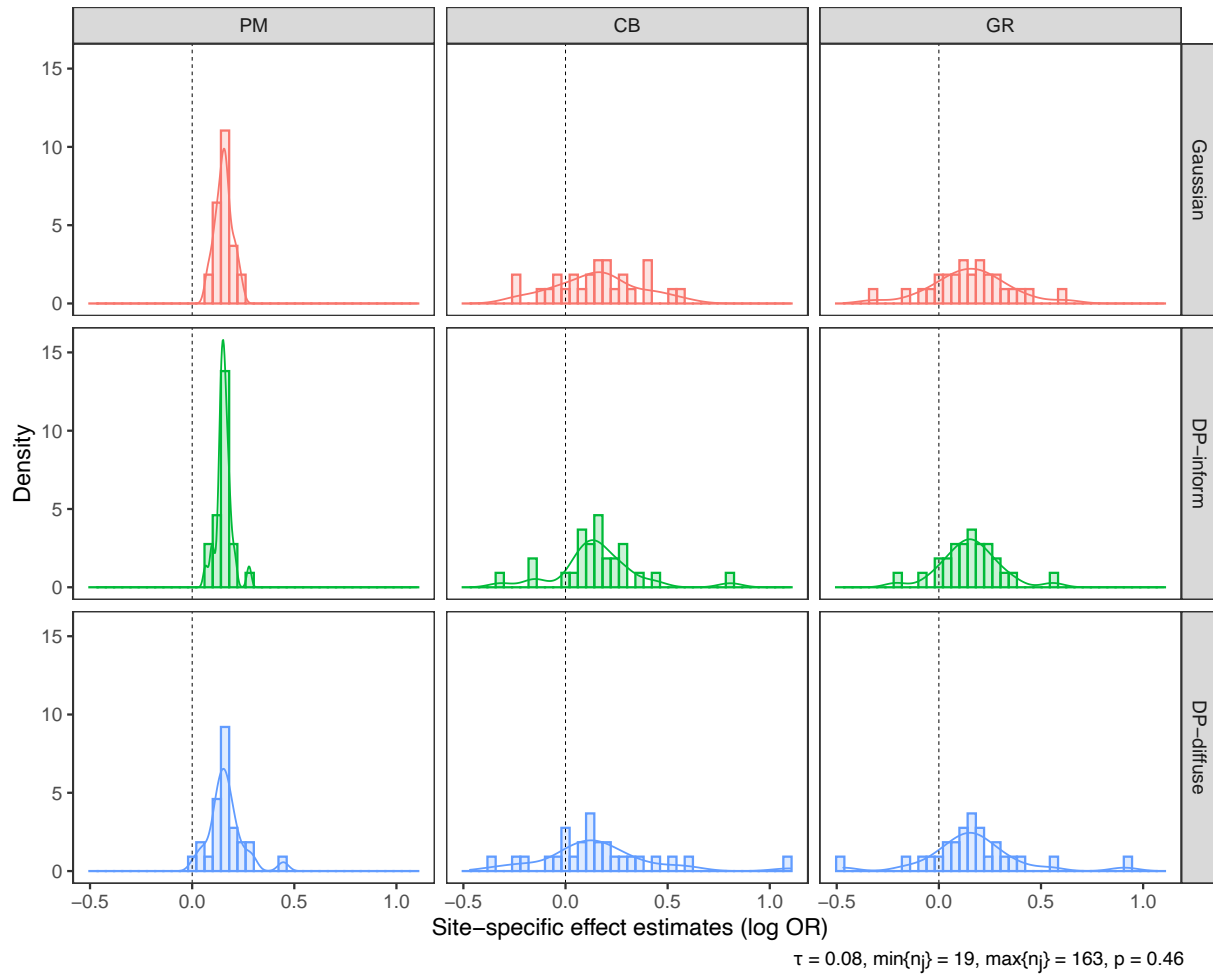


Figure D.8: Distribution of site-specific treatment effect estimates on tertiary enrollment in Suba district

Tertiary Enrollment in Universities, Suba District

$J = 27, I = 0.05$ ($\bar{n}_j = 55.4, \sigma = 0.10$), $CV = 0.63$

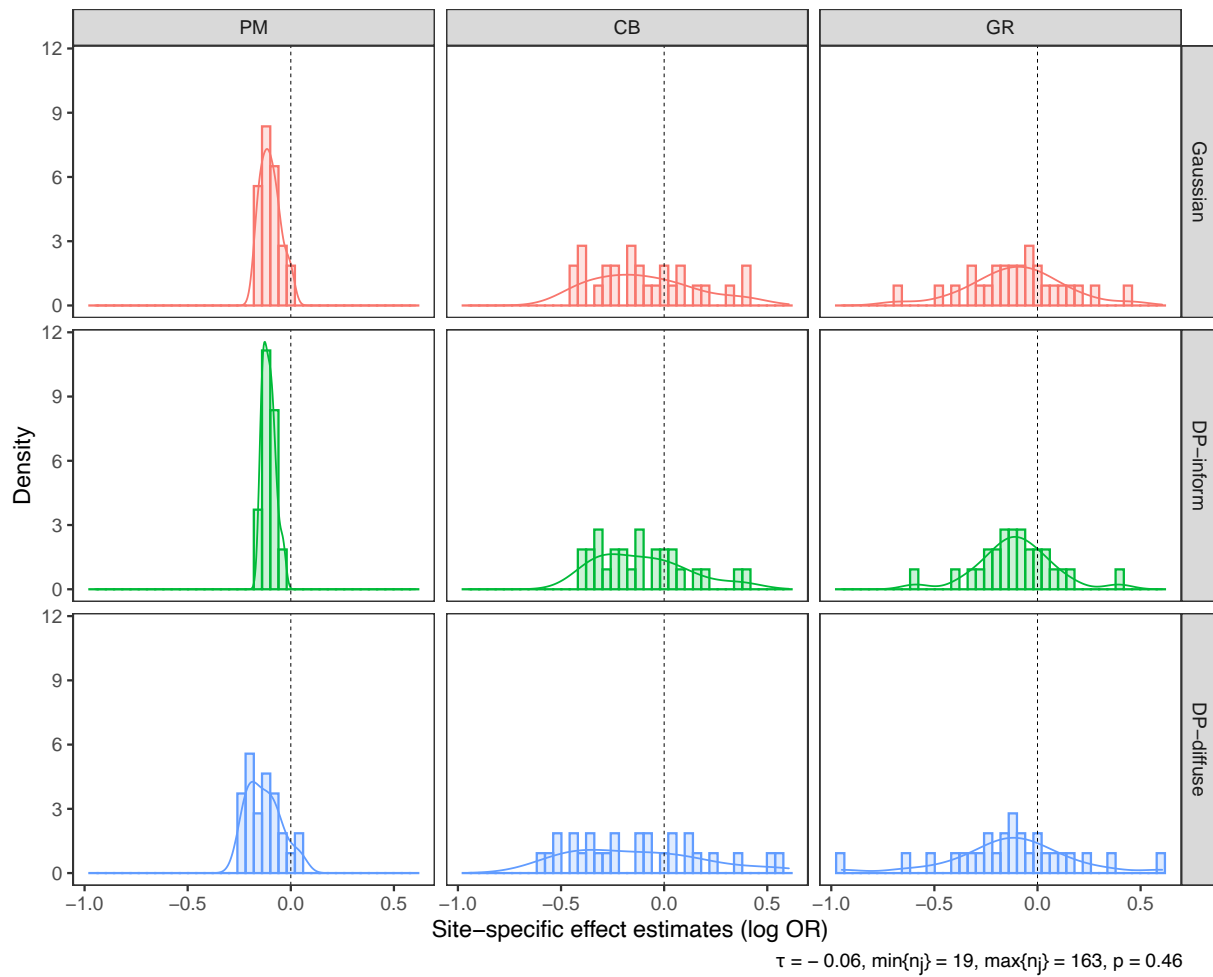


Figure D.9: Distribution of site-specific treatment effect estimates on tertiary enrollment in universities in Suba district

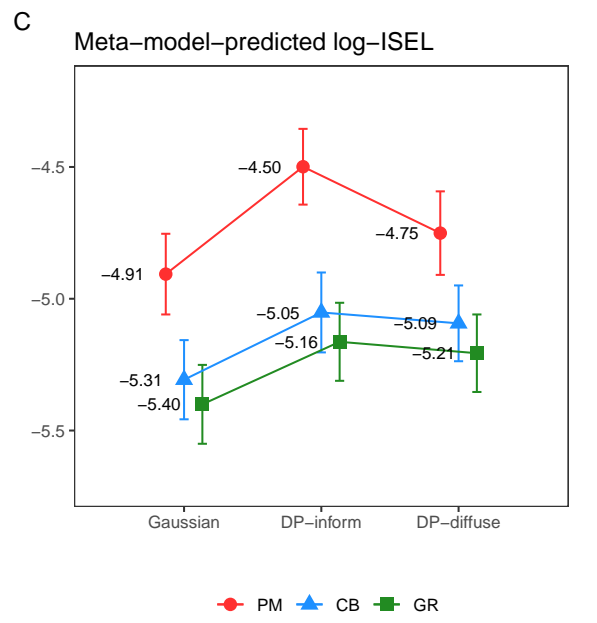
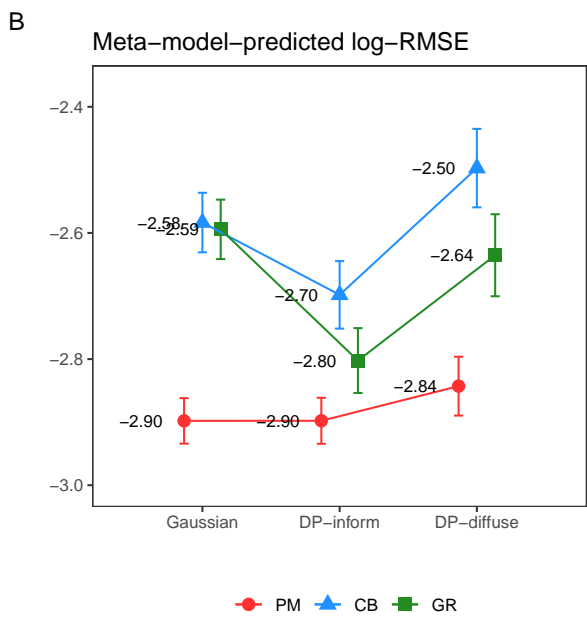
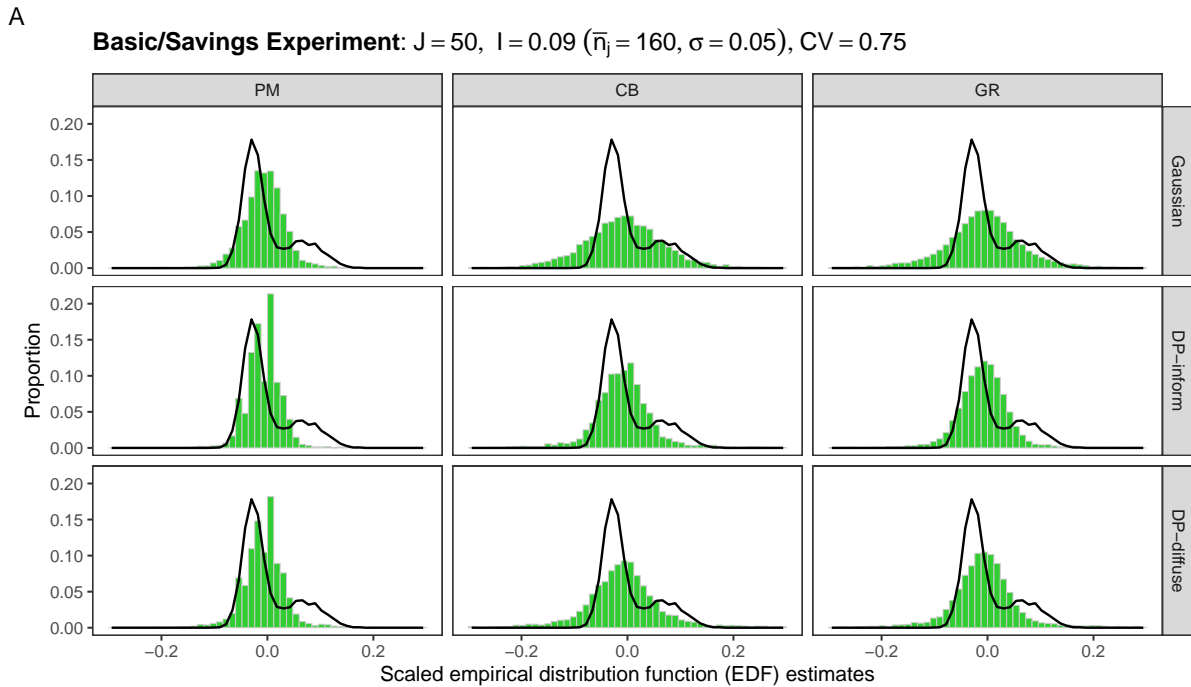


Figure D.10: Scaled EDF estimates and meta-model-predicted RMSE and ISEL on log-scale for each model-method combination, when the data-generation is based on the scenario simulating the Basic/Savings Experiment in San Christobal district ($J = 38$, $\bar{n}_j = 171.2$, $\sigma = 0.04$, and $CV = 0.67$ for the outcome, on-time secondary enrollment). True G is assumed to be Gaussian mixture. Plots include 95% prediction intervals around predicted values.

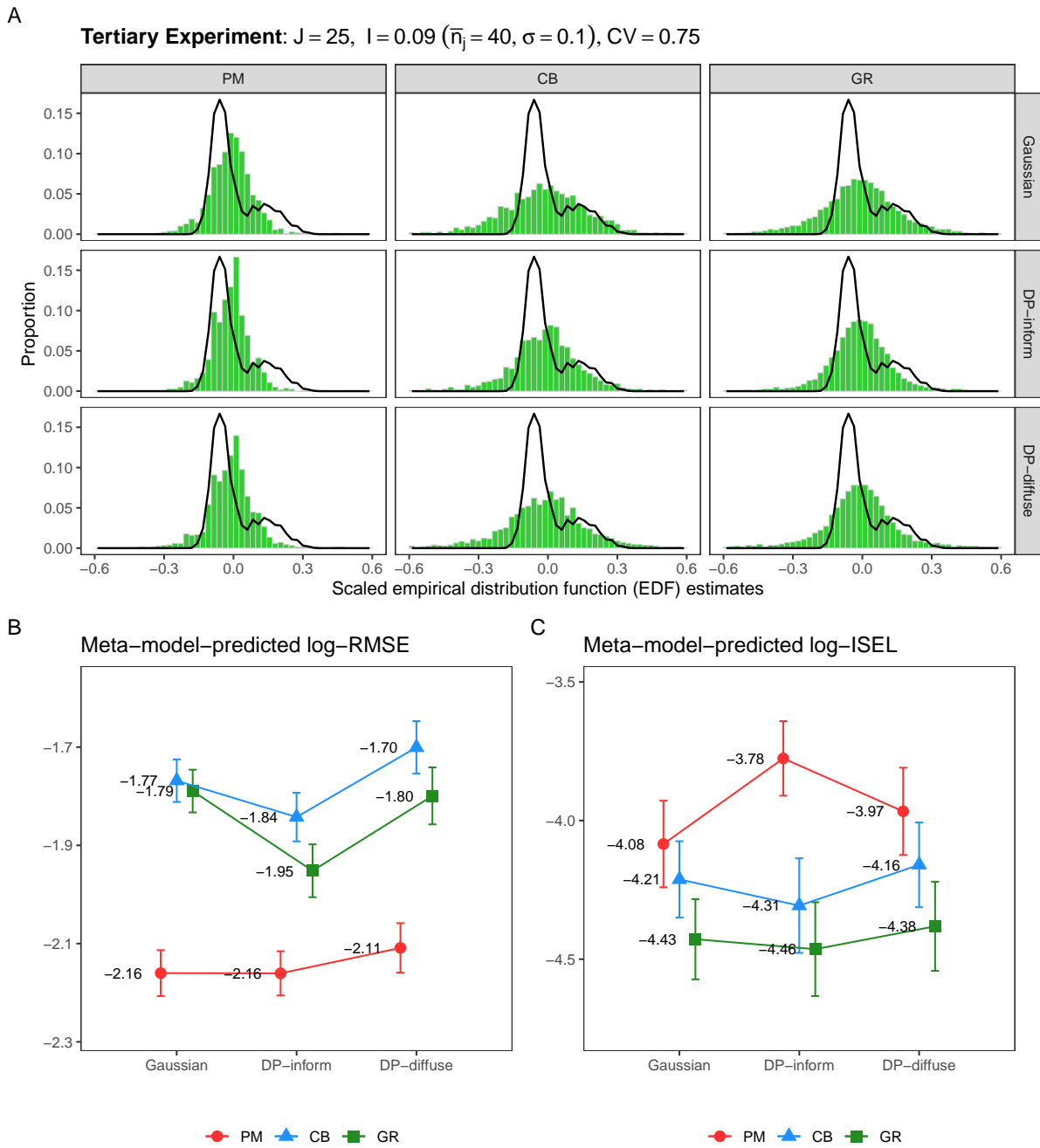


Figure D.11: Scaled EDF estimates and meta-model-predicted RMSE and ISEL on log-scale for each model-method combination, when the data-generation is based on the scenario simulating the Tertiary Experiment in Suba district ($J = 27$, $\bar{n}_j = 55.4$, $\sigma = 0.10$, and $CV = 0.63$ for the outcome, tertiary enrollment in universities). True G is assumed to be Gaussian mixture. Plots include 95% prediction intervals around predicted values.